DISSERTATION

UNCERTAINTY IN HYDROLOGICAL ESTIMATION

Submitted by

Douglas Michael Hultstrand

Department of Geosciences

In partial fulfillment of the requirements

For the Degree of Doctor of Philosophy

Colorado State University

Fort Collins, Colorado

Spring 2021

Doctoral Committee:

Advisor: Steven Fassnacht

Christopher Hiemstra
Melinda Laituri
John Stednick

ABSTRACT

UNCERTAINTY IN HYDROLOGICAL ESTIMATION

Detailed hydrometeorologic analyses and uncertainty assessments are needed to aid water resources decision-making, to account for upstream-downstream linkages and dominant process scale for integrated land and water resources management and planning. The water balance is a fundamental concept in hydrology that inspires many tools for predicting the specific components including precipitation, streamflow, soil moisture, and groundwater storage. A water balance is typically expressed as an equation that relates water inputs, outputs, and storage of a system. The water balance model is applied to analyze the allocation of water among components of the hydrologic system. Knowledge on the components composing inputs and outputs in a water balance are essential to understanding watershed processes. While methods to measure and model water balance components continue to improve, all components of the balance have substantial uncertainty.

Methods to analyze a water balance should acknowledge these uncertainties and consider how they propagate through water balance calculations in order to better assist water resources decisions. This research investigated four water balance components: (1) snowpack sublimation, (2) precipitation as snow, (3) precipitation as rain, and (4) stream discharge in mountainous watersheds in order to examine and build our knowledge of uncertainty in the water balance for mountainous environments. The research presented in this dissertation supports a theme that hydrology is a highly uncertain science, where uncertainty is a result of the hydrologic community's knowledge gap to accurately model physics of atmospheric and hydrologic

processes. A finding of this work is that no component of the water balance can be quantified at watershed scale without estimating he associated uncertainty. Results highlight that mean cumulative snowpack sublimation uncertainty is 41% with individual input variable uncertainties in the range of 1 to 29%; simulated to observed basin mean snow depth was estimated within 15% for 10-years while extreme dry and wet years were within 5%; and forcing precipitation datasets used in hydrologic models to estimate streamflow have cumulative uncertainties in the range of 30 to 60%. Results of this dissertation identify the importance to account for uncertainty in water resources, i.e., Monte Carlo methods, to properly account for and quantify associated risks in water management and design infrastructure decisions.

ACKNOWLEDGMENTS

I am grateful to have had the opportunity to learn from and work with my advisor, Dr. Steven Fassnacht, throughout my M.S. and Ph.D. programs at Colorado State University. He is my mentor and friend, and provided exceptional guidance, advice, and inspiration that has played an important role in my life. Similarly, I would like to thank the members of my Advisory Committee, Dr. Christopher Hiemstra, Dr. Melinda Laituri, and Dr. John Stednick whom provided valuable insight and time that strengthened this research.

This research would not have been possible without the support of Robert Musselman and John Korfmacher of the Rocky Mountain Research Station (US Forest Service) and everyone that contributed to the field data collection in the Glacier Lakes Ecosystem Experiments Site (GLEES). I wish to express thanks to all who assisted in field work and data collection in the GLEES over the years.

Lastly, I would like to thank my wife, Magdalena Hultstrand, for inspiring me to complete this dissertation and supporting me through its challenges. I would like to thank my daughter Winter and my son August, for reminding me to bring joy and laughter to all occasions in life. I would also like to thank my father, Dennis Hultstrand, and my mother, Dawn Hultstrand, and the rest of my family for their love and support in my personal and academic endeavors.

TABLE OF CONTENTS

LIST OF KEYWORDS

sublimation, uncertainty, snow depth distribution, winter season index, precipitation, radar, interpolation methods

1.0 INTRODUCTION

1.1 Rationale

The validity of hydrologic research is largely determined by the accuracy of observed and estimated variables. It is accepted that there are errors in instrumentation, measurement, and modelling, so the question is what the relative magnitude and nature of errors might be. Thus to properly test hydrologic hypotheses, it is essential to make estimates of uncertainty in the reliability of measured, sampled, and modelled quantities.

The problem is a balance of ensuring precise spatial and temporal measurements, and objectively estimating the accuracy of measurements already collected. For a set of measurements, precision refers to the closeness of two or more measurements to each other, while accuracy refers to the closeness of a measured value to a standard or known value. Precision refers to the sampling method and technique, while accuracy involves the degree of closeness between a measurement result and the true value of the quantity. The estimation of accuracy requires an understanding of the potential sources of uncertainty and knowledge of the relative magnitudes of uncertainty.

In hydrologic measurements, accuracy and precision are dependent on the measurement and model scales (Blöschl, 1999). Since larger regional hydrologic processes are to a great degree the resultant of processes at smaller scales, models representing these physical processes can in complexity considerably from one scale to another (Heuvelink, 1998; Blöschl, 1999). Blöschl (1999) addressed measurement scale and the relevance to sampling pattern with the scale triplet: spacing, extent, and support (Figure 1.1). Spacing is termed the distance between samples; extent is referred to the overall region of the data; and support, is defined as the size or

area represented by the sample (Blöschl et al., 1991; Blöschl, 1999). The model scale consists of a similar scale triplet, but depends on the spatial properties of the model (Blöschl et al., 1991; Blöschl, 1999). Heuvelink (1998) listed three reasons in which models representing physical processes can change scale: (i) different processes dominate and at different scales, different processes are ignored in simplification for model development; (ii) input data are often absent or of much lower quality at large scales which results in a tendency to use simpler, empirical models at larger scales; and (iii) the support of the inputs and outputs of a model vary with change of scale, and this affects the correlation between them. Issues of scale are inherent in all hydrologic processes. Sampling and modelling techniques need to consider the natural variability of the measured process and account for the measurement scales and model scales in order to accurately interpret the data, and model the physical processes.

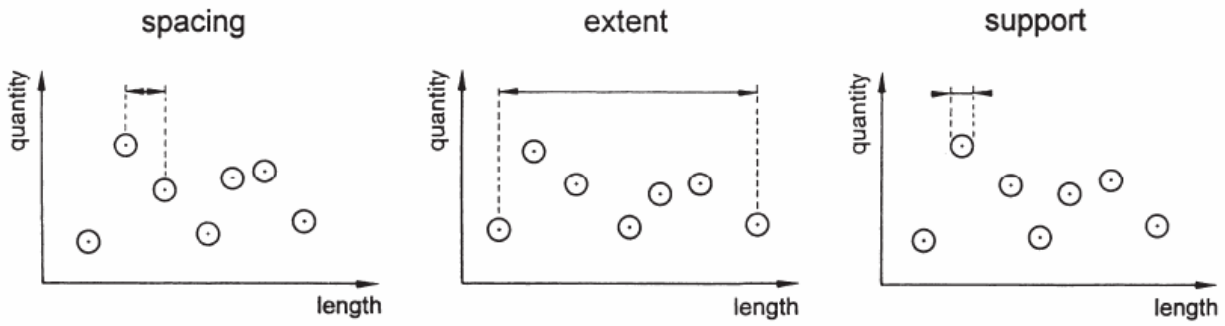

Figure 1.1. Definition of the scale triplet: spacing, extent, and support (Figure from Blöschl, 1999).

To investigate hydrologic errors, two basic approaches can be taken: (i) an analytical approach that considers in detail the potential sources of error and analyzes the nature of the component errors making use of available data, research results, and theoretical considerations, and (ii) an experimental approach that involves extensive comparative field studies (Dickinson,

1967; Montanari, 2007). A combination of the analytical and experimental approaches would provide the best information on measurement and model errors of the hydrologic system. It is important that every hydrologic study consider at least one approach for studying uncertainty and the effect of uncertainty in that study.

1.2 Water Balance Components

As hydrologic processes are affected by increasing climate variability and climate change, the need for detailed hydrometeorologic analyses and uncertainty measures are needed to aid climate-influenced water resources decisions. Water balance models are used to analyze the allocation of water among components of the hydrologic system. Knowledge on the components composing inputs and outputs in a water balance are essential to understanding watershed processes. The main components of a water balance are precipitation, streamflow, evaporation, transpiration, sublimation, and storage. Precipitation, as rain and/or snow, is the primary input to a watershed. Streamflow, evapotranspiration, and sublimation are the main outputs from a watershed. Storage within the watershed are in soil water, groundwater, lakes, and icefields, glaciers and permafrost. The most basic water balance equation is the continuity equation (Dingman, 2002), which states that over any time interval the difference in the volume of water entering a system, I, and leaving a system, O, must equal the change in the volume of water stored in the system, ΔS.

$$I - O = \Delta S, \qquad \text{equation 1.1}$$

An expanded and more detailed expression of the water balance equation for a region and time period is:

$$P_r + P_s + G_i + R_i - (Q + E_t + E_s + G_o + R_o) = \Delta S, \qquad \text{equation 1.2}$$

where P_r is precipitation as rain, P_s is precipitation as snow, Q is stream discharge, E_t is evapotranspiration, E_s is snowpack sublimation, G_i is groundwater in, G_o is groundwater out, R_i is snow redistribution in, R_o is snow redistribution out and S is storage. Quantifying water balance components, through measurement and estimation are crucial to understanding the hydrology of a watershed.

Accurate precipitation data are essential for quantifying input for water balance studies, therefore measurements need to be as accurate as possible. Rainfall, snowfall, and snowcover are not homogenous, are highly variable, and hard to estimate in complex terrain (Johnson and Hanson, 1994; Daly et al., 1994). In snow dominated watersheds, such as alpine and subalpine regions, it is extremely important to gain an understanding on solid precipitation quantity, variability, and distribution of snow water equivalent (SWE). Mountain topography creates complex patterns of snow distribution, controls snow accumulation, and snow ablation (Elder and Dozier, 1990; Balk and Elder, 2000; Erxleben et al., 2002; Erickson et al., 2005, Fassnacht et al., 2018). These interactions are critical for understanding basic alpine and subalpine hydrology and for modelling both the timing and magnitude of runoff. In general, precipitation and streamflow are the main water balance components measured in time and space.

1.2.1 Precipitation Gauges

Typical water balance studies measure both solid and liquid precipitation quantities with a standard precipitation gauge. Precipitation gauges, shielded and unshielded, inherently underestimate total precipitation due to local airflow, wind undercatch, wetting, and evaporation

loss (e.g., Larson and Peck, 1974; Goodison et al., 1998; Fassnacht, 2004; Roe, 2005). Wind-induced turbulence over the gauge orifice accounts for the greatest systematic error in precipitation measurements, this component accounts for 2–10 percent error for rain and 10-50 percent error for snow (Groisman and Easterling, 1994). Precipitation is not measured extensively across most watersheds, especially watershed in complex terrain with only a few or no gauge measurements available. To supplement limited measurements, regional observed datasets (National Weather Service, Global Historical Climatology Network, Snow Telemetry, Remote Automatic Weather Stations, …) and regional modeled datasets (PRISM, Livneh, Daymet, NARR, …) are available but often not representative of the quantity and distribution within a small-scale.

In addition, based on accessibility most precipitation gauges are located at lower elevations, do not account for variable orographic influences, and often record less precipitation than occurs in higher elevations (Groisman and Easterling, 1994; Roe, 2005). Precipitation gauge measurements need to be adjusted for wetting loss, evaporation loss, wind undercatch, and orographic influences before actual ground precipitation can be estimated (e.g. Daly et al., 1994; Goodison et al., 1998). Even after correction methods have been applied, large uncertainties and potential data errors can still be present. The most common and largest errors associated with precipitation gauges are those due to wind effects for both shielded and non-shielded gauges (Kochendorfer et al., 2017). Point measurement errors can be in the range of 5 to 15 percent for long-term data, and as high as 75 percent for individual storms (Winter, 1981).

1.2.2 Evapotranspiration

Evaporation is the process by which water changes from a liquid to a vapor. Transpiration is the loss of water from plant leaves by evaporation through the leaf stomata. Combined, evaporation and transpiration are termed evapotranspiration. Evapotranspiration rates are dependent upon temperature, vapor pressure, wind velocity, and the nature of the surface (Viessman and Lewis, 2003). Evapotranspiration is an important process within watershed studies because it can be a source of significant water loss to the atmosphere. Methods for estimating evapotranspiration include budget methods, such as energy budget and water budget; comparative methods such as evaporation pans; and aerodynamic methods, such as eddy correlation, gradient, and mass transfer (Winter, 1981). Previous research in western mountain watersheds has documented annual evapotranspiration values between 100-800 mm (Kattelmann and Elder, 1991; Hasfurther et al., 1994; Ruess et al., 1995). Antal et al., (1973) compared five evaporation methods (Penmans's formula, Meyer's formula, Daltons Law, adjusted Meyer's formula, and formula-based Lake Ferto in Hungary) to the energy balance evaporation method and showed that annual evaporation values deviate 5 percent from the energy balance method, and that monthly values deviate 10 to 15 percent from the energy balance method.

1.2.3 Snowpack Sublimation

Sublimation is the conversion between the solid phase and vapor phase, with no intermediate liquid stage. Sublimation of snow in windswept alpine/subalpine regions is an important hydrological process because snowpack sublimation can account for significant water losses to the atmosphere. Methods for estimating sublimation from a snowpack are energy

budget methods, snow evaporation pans, and aerodynamic profile methods, such as the latent heat flux and sensible heat flux.

Sublimation losses from the snowpack have been estimated for various environments and can constitute a significant component of the water balance, with net sublimation losses estimated between 10-35% of the seasonal snow accumulation, specifically: 12-33% in the Canadian prairies (Woo et al., 2000), 19% in the Wyoming Rocky Mountains (Hultstrand, 2006), 15% in the Colorado Rocky Mountains (Hood et al., 1999), 28% in north central Colorado Rocky Mountains (Sextone et al., 2018), and 18% in the Sierra Nevada Mountains (Kattelmann and Elder, 1991). Over a 40-day period in the Colorado Rocky Mountains, total snowpack sublimation was greater than measured precipitation (Molotch et al., 2007).

At regional macroscales, land surface models (LSM) use a resolution of 5 to 30 km to simulate cold season processes. LSM generate large variability in net sublimation: 0-15% based on twenty-one LSM in a grassland catchment Valdai, Russia (Slater et al., 2001), 10-35% based on the Variable Infiltration Capacity (VIC) model for Imnavait Creek, Alaska (Bowling et al., 2004), and 8-20% based on the MOSAIC, Noah, VIC models over the Northwest River Forecast Center's domain (Oregon, Washington, Idaho) (Sheffield et al., 2003). The SnowModel (Liston et al., 2006) used in the Upper Colorado River Basin estimated sublimation that ranged from 0-4% in the low valleys to 20-30% in the high mountains, 28% in north central Colorado Rocky Mountains (Sextone et al., 2018), with isolated areas exceeding 30% of annual precipitation (Phillips, 2013). Differences in regional sublimation estimates are attributed to coarse model scale, representation of small scale variability, and snowpack model algorithms (Sheffield et al., 2003; Pan et al., 2003; Bowling et al., 2004; Reba et al., 2012; Svoma, 2016; Sexstone et al., 2016).

1.2.4 Streamflow

Streamflow data are one the most important water balance components, the data are used to indicate the present hydrologic conditions and the discharge amounts of a watershed and to check methods for estimating present and future conditions. We tend to have the most confidence in streamflow measurements, as they represent an area that provides integrated process insight (Kampf et al., 2020). Streamflow has been studied extensively over the years (Stähli et al., 2011), and a number of devices and methods have been developed to measure streamflow (Chow, 1959; King and Brater, 1963; Henderson, 1966; Stähli et al., 2011). The most common stream gauging methods are direct measurement (volumetric, velocity-area, and dilution) and indirect measurement (empirical rating curves, theoretical rating curves from weirs and flumes) (Winter, 1981; Dingman, 2002). New technologies have resulted in alternatives to current meters. Acoustic velocity meters and acoustic Doppler current meters were designed to measure current velocities, depth, and area of a river along the water surface instantaneously to provide estimates of stream discharge (Duncker et al., 2006; Rehmel, 2007; Jongkook et al., 2016).

Water level or stage height is typically measured with a staff gauge or water level recorder. Stage height is converted to discharge either by stream gauging relationships or with calibrated structures such as flumes and weirs. Measurement error associated with stage readings and flumes are considered to be less than 5 percent (Winter, 1981). Errors associated with pygmy meter discharge measurements are +/-3.5 percent (Herschy, 1973). Errors associated with acoustic velocity meters and acoustic Doppler current meters are not statistically different from current meter measurements at a 95% confidence level (Duncker et al., 2006; Rehmel, 2007).

The largest errors tend to be with high flows, where the rating curve is less defined and the cross-section may change (McKerchar, 2003).

1.2.5 Groundwater

Groundwater is the part of hydrologic cycle that is infiltrated into the ground through the soil until it reaches impermeable layer that is saturated with water. Water in the ground is stored in the spaces between soil and/or rock particles. Groundwater moves through the sub-surface and can eventually seep into streams and lakes; it constitutes surface water baseflow (Dingman, 2002). Knowledge of groundwater conditions in a region provide and understanding in the fluctuations of streamflow and lake levels, particularly during dry periods. Quantifying groundwater is difficult because flow rates are determined largely by the underlying geology, which varies spatially and is under-sampled at the relevant process scales.

Based on field studies in mountainous areas, the percentage of groundwater contribution to streams, has been reported between 30-75% (Hood et al., 2006 and references therein), illustrating substantial variability in groundwater contribution. Groundwater was considered negligible for two small lakes in the Flattops Wilderness Area (Michel et al., 2002), and Winter (2003) stated that Loch Vale, Colorado and Emerald Lake, California were strongly dominated by surface flows. Typically, groundwater inflow and outflow are not measured, most often an assumption is made that these terms are negligible (Istanbulluoglu et al., 2012; Kampf et al., 2020). This assumption is a simplification to the water balance equation in that groundwater is accounted for in the residual error term.

1.2.6 Storage

Water storage is an essential part of the hydrologic cycle, especially for deep soils, groundwater, lakes, annual snowpack, glaciers, and vegetation. Storage in vegetation is small in total volume (compared to that stored elsewhere) but can have a significant impact, in the short-term, specifically on vegetation water use. For example, diurnal changes in stem storage of water in trees have a role to play in diurnal patterns of water use by woodlands and forests. Hood et al. (2006) used the change in lake storage as part of the water balance to quantify the importance of groundwater. The Thornthwaite monthly water balance applies the change in the storage component to represent soil moisture change and to estimate actual evapotranspiration (Thornthwaite, 1948).

Storage is generally assumed to be the residual in water balance studies, due to discrepancy in the water balance measurement or computation errors, components not considered, or unknown errors. A small residual value can indicate that the components used in the design water balance are in fact in balance.

1.3 Uncertainty, Calibration and Evaluation of Water Balance Components

Research on water balance components can be highly uncertain, the main reason being that we still do not understand the fundamental dynamics of many hydrological processes and cannot measure and model them accurately (Kampf et al., 2020). Most hydrological processes are not observed in detail, consequently accurate mathematical representation of hydrologic volumes, initial boundary layer conditions and physical processes cannot be represented accurately. Mantovan and Todini (2006) have identified sources of water balance uncertainties

as: (i) data uncertainty, (ii) model parameter uncertainty, (iii) model structure uncertainty, and (iv) natural uncertainty.

1.3.1 Data Uncertainty

The performance of hydrological models is mainly affected by data uncertainty. This uncertainty arises from errors in the observed data, particularly data used for model calibration. The errors may be linked to the quality of the data which depends on the type and conditions of measuring instruments as well as data handling and processing. Precipitation and streamflow are usually the major sources of input and output data that are used to calibrate and evaluate model uncertainty with the spatial and temporal precipitation uncertainty being large.

1.3.2 Model Parameter Uncertainty

Model parameter uncertainty is also known as model specification uncertainty. This relates to the inability to converge to a single best parameter set using available data, which leads to parameter identifiability problems (Beven, 2001; Wagener et al., 2004). The parameters are optimized so that the model results are as good as possible (Beven, 2001; Scharffenberg et al., 2018). Uncertainty then depends on how parameters are optimized (peak flow, volume, residuals) and results are applied (Scharffenberg *et al.*, 2018; Pokorny et al., 2021).

1.3.3 Model Structure Uncertainty

Model structure uncertainty is introduced through simplifications and/or inadequacies in the representation of physical processes in a given model. It also originates from inappropriate assumptions within the modelling procedure, inappropriate mathematical description of these processes (Beven, 2001), and the scale at which processes are represented in the model (Heuvelink, 1998; Blöschl, 1999; Koren et al., 1999). However, no matter how exact the model is calibrated, there always exists discrepancy between model outcome and observed data (Chiang et al., 2007; Beven, 2006). Hydrologic models typically give attention only to the dominant processes perceived to be important by the modeler, typically precipitation and streamflow, thereby possibly ignoring other processes, which may nevertheless affect model simulation results. This type of uncertainty is usually identified through assessing the model's ability to represent properties of the hydrograph (Butts et al., 2004) and can be quantified using goodness-of-fit methods during model calibration, such as the Nash-Sutcliffe model efficiency (NSME) (Nash and Sutcliffe, 1970; Chiang et al., 2007) and the Kling-Gupta efficiency (KGE) (Gupta et al., 2009).

1.3.4 Natural Uncertainty

Natural uncertainty arises due to the randomness of natural processes (Beven, 2001). This uncertainty can therefore be linked to data uncertainty, where by the quality and type of data plays a significant role in determining the amount of uncertainty. For example, the spatial and temporal randomness of rainfall can somewhat be represented explicitly when using good rain gauge networks and radar rainfall data (Segond, 2006). In addition, scaling issues, spatial

representativity and interpolation methods are typically represented within natural uncertainty (Heuvelink, 1998; Blöschl, 1999).

1.3.5 Uncertainty Estimation Techniques

The most common uncertainty estimation technique used in the literature is the generalized likelihood uncertainty estimation (GLUE) (Beven, 2001). GLUE is based on the estimation of probabilities of different outcomes using likelihood measure. In the GLUE methodology, a prior distribution of parameter values is used to generate random parameter sets. Each sampled set is used to drive the model to produce a sample result, such as, a Monte Carlo simulation (Melching and Singh, 1995). Each result is compared with the available calibration data using a quantitative likelihood measure of performance.

A likelihood measure in the GLUE approach can be any measure of performance as long as better performing models attain higher values and the sum taken over all sampled parameter sets is unity (Wagener et al., 2004), such that non-behavioral parameter sets have a likelihood of zero, i.e., for those parameter sets that fall below a given threshold value. Only the simulations with a likelihood measures greater than zero are used for predictions, and these predictions are weighed by the likelihood measure associated with that simulation (Beven, 2001; Wagener et al., 2004).

Uncertainty in the parameter values and input data are propagated and represented in the model output in the form of confidence limits at specified percentiles (Wagener et al., 2004). The GLUE methodology thus requires sets of decisions to be made, i.e. (i) the model or models to be

included in the analysis, (ii) a feasible range for each parameter, (iii) a sampling strategy for the parameter sets, and (iv) an appropriate likelihood measure.

As a GLUE model explores how model performance varies over the parameter, results may be used for parameter sensitivity analysis. This seeks to identify sensitive parameters or those which determine whether a model result has a high-likelihood or low likelihood. A quantitative measure such as the nonparametric Kolmagorov-Smirnov (KS, or d) statistic is often used to assess the significance of the differences between the likelihood or non- likelihood of the parameter values.

The main criticism of GLUE is that the selection of the threshold used in separating acceptable and unacceptable simulations is purely subjective. In addition, GLUE use an informal likelihood estimate as compared to applying a true maximum likelihood estimate of the parameters to benchmark model performance (Mantovan and Todini, 2006; Vrugt et al., 2009).

Monte Carlo simulation uses algorithmically generated pseudo-random numbers which are forced to follow a predetermined probability distribution (Hastings, 1970; Farrance and Frenkel, 2014). With input variations simulated by random numbers, the functional relationship provides the corresponding variations in the output in a manner which provides its probability distribution. Summary of the Monte Carlo simulation output can provide uncertainty estimates.

Other uncertainly methods used in literature include those based on formal Bayesian theory such as Markov Chain Monte Carlo (MCMC), which are a slight deviation from the GLUE methodology. One such method is the DiffeRential Evolution Adaptive Metropolis (MCMC-DREAM) (Vrugt et al., 2009). Unlike GLUE, MCMC DREAM simulation uses a formal likelihood function based on maximum likelihood theory, appropriately samples the high-

probability-density region of the parameter space, and separates likelihood from non-likelihood solutions using a cut-off threshold that is based on the sampled probability mass, and thus underlying probability distribution (Vrugt et al., 2009).

Another technique based on the Bayesian theory is the particle filter algorithm (Smith et al., 2008). In this approach, the model parameters are assumed to vary in time, and a filtering process is used to identify a unique parameter distribution needed at each time to reproduce the observed data in an iterative way. The treatment of model parameters as varying in time is another difference between this and other approaches such as GLUE mentioned above.

1.3.6 Calibration

Since most of the parameters used in conceptual models do not have a direct physical interpretation, they must be estimated through calibration with observed data, so as to improve the model fit (Wagener et al., 2004). Calibration is defined as the process of adjusting parameter values in order to optimize model performance according to predefined criteria. This is normally achieved by optimization of parameter values through comparing the results of repeated simulations with available data. The parameter values are adjusted between each run of the model, either manually by the modeler or by computerized optimization scheme until some best fit parameter set has been found (Beven, 2001). These optimization schemes involve measures of goodness of fit or objective functions.

1.3.7 Validation

In the literature, model validation, verification, or evaluation, depending on the author, is a process of demonstrating that a given site-specific model is capable of making acceptable predictions for periods outside a calibration period. This is usually in the form of a split-sampling test where a data set is divided into two periods of calibration and validation, etc. (Klemes, 1986, Wagener et al., 2004).

1.3.8 Stationarity

Stationary means that hydrological variables fluctuate randomly whose probability distribution does not change when shifted in time (Milly et al., 2008; Bayazit, 2015), i.e. parameters such as mean and variance do not change over time. Non-stationary means that hydrological variables probability distribution does change when shifted in time, non-stationarity has been attributed to climate change, climate variability, and land use changes (Milly et al., 2008; Bayazit, 2015).

Montanari and Koutsoyiannis (2014) stated all hydrological systems are time-invariant because the data analyses and results are interpreted on the basis of past experience and data. Addressing non-stationarity in the hydrologic system is a somewhat new concept, but addressing it will benefit planning, design, and management strategies for water resources projects making them more flexible, adaptable, and robust (Matter, 2010).

1.3.9 Objective Functions

Objective functions are measures of model performance, and often based on either measures derived from statistics or based on hydrological aspects of the model performance (Wagener et al., 2004). This is usually done in combination with visual inspection of the calculated output. There are several objective functions used in hydrology. These include the mean absolute error (MAE) method, the Root Mean Square Error (RMSE) method, Willmott's index of agreement (D), the NSME, and the KGE (Table 1.1). The aim of these objective functions is to minimize the magnitude of the residuals.

Table 1.1. Typical objective functions used to test goodness-of-fit between observed and simulated data. Where $\boldsymbol{z(x_i)}$ is the observed value at location *i*, $\boldsymbol{\hat{z}(x_i)}$ is the predicted value at location *i*, $\boldsymbol{\overline{z(x_i)}}$ is the mean observed value at location *i*, $\boldsymbol{\sigma_{obs}}$ is standard deviation in observations, $\boldsymbol{\sigma_{sim}}$ is standard deviation in estimates, $\boldsymbol{\mu_{obs}}$ is observation mean, $\boldsymbol{\mu_{sim}}$ is estimate mean, and *n* is the number of samples.

$RMSE = \sqrt{\frac{1}{n}\sum_{i=1}^{n}[z(x_i) - \hat{z}(x_i)]^2}$
$MAE = \frac{1}{n}\sum_{i=1}^{n}[\lvert z(x_i) - \hat{z}(x_i)\rvert]$
$D = 1 - \frac{\sum_{i=1}^{n}\sum_{i=1}^{n}\left(z(x_i) - \hat{z}(x_i)\right)^2}{\sum_{i=1}^{n}\left(\lvert z(x_i) - \overline{z(x_i)}\rvert + \lvert \hat{z}(x_i) - \overline{z(x_i)}\rvert\right)^2}$
$NSME = 1 - \frac{\sum_{i=1}^{n}\left(z(x_i) - \hat{z}(x_i)\right)^2}{\sum_{i=1}^{n}\left(z(x_i) - \overline{\hat{z}(x_i)}\right)^2}$
$KGE = 1 - \sqrt{(r-1)^2 + (\frac{\sigma_{sim}}{\sigma_{obs}} - 1)^2 + (\frac{\mu_{sim}}{\mu_{obs}} - 1)^2}$

The above objective functions have some limitations. By using the squared residuals or variance, they tend to exaggerate the influence of larger errors, which tends to be equivalent to exaggerating the influence of higher events, and putting relatively little weight on lower events (Perrin et al., 2001, Wagener et al., 2004).

Some investigators suggest the importance of studying the characteristics of the residual distribution in evaluating the suitability of a model structure, e.g. (Yapo et al., 1996; Mroczkowski et al., 1997; Wagener et al., 2004). This is based on the fact that if a fit produces residuals consistent with the random error assumptions, then the model has extracted all useful information from the data leaving only noise in the residuals (Wagener et al., 2004). This includes assessing: (i) whether the variance of the residuals increase with increasing values (which is known as heteroscedasticity) or increase with decreasing values (homoscedastic), (ii) whether the residuals reveal long term effects (trends) or dependency in time, (iii) how close the residual distribution is to a normal distribution, and (iv) how the residuals are correlated in time.

The question of which objective function to use normally depends on the objective of the study. However, it is evident from the literature that using only one objective function to validate the calibration of a model is not suitable, instead the use of several objective functions to validate the model and its performance is recommended (Littlewood, 2002).

1.4 Hypothesis & Objectives

This research intends to broaden the understanding of uncertainty in hydrological estimation by presenting the components that create uncertainty, and quantifying uncertainty associated with specific water balance components and the techniques used to estimate these

quantities. More specifically, the research objectives will focus on the uncertainty associated with calculating snowpack sublimation (E_s), the accuracy of sampling design methods for quantifying spatial snow distribution (P_s), and the uncertainty and sensitivity that spatial rainfall data (P_r) have on streamflow(Q). This research will use scientific methods to build upon and advance the current knowledge of water balance studies in mountainous environments and strive to improve the hydrologic communities view of water resources in terms of hydrologic error and uncertainty.

1.5 Research Overview

In recent years, the hydrological community has expanded studying the function and dynamics of individual basins to develop an integrated approach to understand interactions different hydrological processes have over various scales. In large river basins, processes that influence the hydrology in the headwater areas can have a profound impact on downstream hydrology hundreds of kilometers away. Thus, resource management practices in headwater areas can have both beneficial and adverse effects on downstream communities. Understanding these upstream-downstream linkages and the dominant process scales is an essential basis for integrated land and water resources management and planning in a river basin. It is particularly critical in basins with substantial elevation differences, where the climatic and topographic conditions at the source of the river are quite different to those downstream. Understanding such linkages and the scale of the processes is a challenge, especially across much of the mountainous Western United States.

The research objectives and hypotheses outlined above are investigated through three separate research papers. First, a Monte Carlo analysis is used to evaluate the sensitivity of

modeled sublimation to uncertainties of the input variables and parameters for three (average snowpack in 2005, deep snowpack in 2011, and shallow snowpack in 2012) winters. Second, ten years of surveyed snow depth data were combined with physiographic variables and were used to a derived statistical snow depth model to assess snow depth variability and uncertainties in derived spatial snow depth estimates. Third, four spatial precipitation estimates are used to generate high spatial and temporal resolution precipitation estimates for input into a hydrologic model to assess streamflow variability from the different precipitation inputs.

While methods to measure and model water balance components continue to improve, all components of the balance have substantial uncertainty at the watershed scale. Approaches for analyzing the water balance should acknowledge these uncertainties and consider how they propagate through water balance calculations in order to better assist water resources decisions. This research focused on the four water balance components (Figure 1.2): i) snowpack sublimation (E_s), ii) precipitation as snow (P_s), iii) precipitation as rain (P_r), and iv) stream discharge (Q) in order to examine the uncertainty associated with calculating snowpack sublimation; to examine the uncertainty associated with estimated snow depth distribution; and to examine the uncertainty different precipitation estimates have on streamflow to assess streamflow variability to build knowledge on the uncertainty in water balance studies.

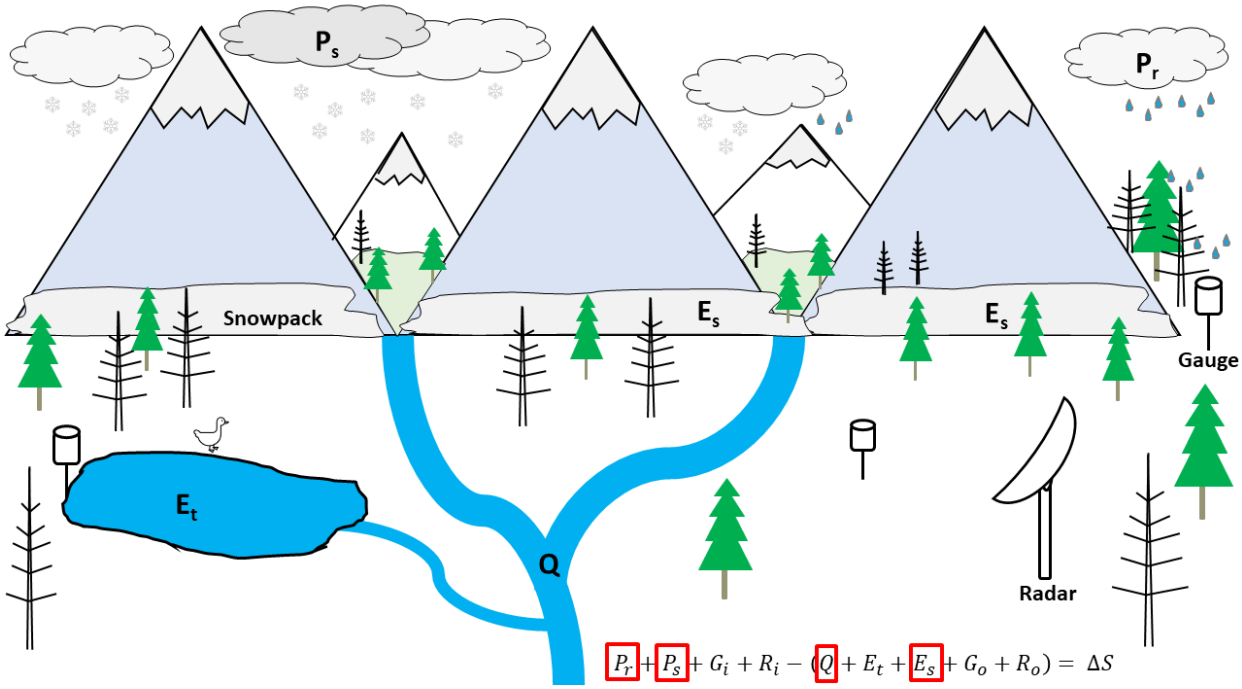

Figure 1.2. Graphical representation of water balance components and measurement instrumentation investigated in this dissertation. Where *P*r is precipitation as rain, P_s is precipitation as snow, G_i is ground water input, R_i snow redistribution input, Q is stream discharge, E_t is evapotranspiration, E_s is snowpack sublimation, G_o is groundwater out, R_o is snow redistribution out and S is storage.

REFERENCES

Antal, E., S. Baranyi, and E. Toth, 1973. Comparison of calculation methods for evaporation using lake Balaton as an example. In *Hydrology of Lakes,* Helsinki Symposium*, IAHS Publication* no. 109, 220-224.

Balk, B., and K. Elder, 2000. Combining binary decision tree and geostatistical methods to estimate snow distribution in a mountain watershed. *Water Resources Research*, 36(1): 13–26

Bayazit, M., 2015. Nonstationarity of Hydrological Records and Recent Trends in Trend Analysis: A State-of-the-art Review. *Environmental Processes*, 2, 527–542. https://doi.org/10.1007/s40710-015-0081-7

Beven, K.J., 2001. *Rainfall-runoff modelling: The Primer*. John Willey and Sons, Chichester, UK. pp 360.

Beven, K.J., 2006. A manifesto for the equifinality thesis. *Journal of Hydrology,* 320, 18-36.

Blösch, G., 1999. Scaling Issues in Snow Hydrology. *Hydrological Processes*, 13, 2149- 2175.

Blöschl, G., R. Kirnbauer, and D. Gutknecht, 1991. Distributed Snowmelt Simulations in an Alpine Catchment 1. Model Validation on the basis of Snow Cover Patterns. *Water Resources Research*, 27 (12), 3171-3179.

Bowling, L.C., J.W. Pomeroy, D.P. Lettenmaier, 2004. Parameterization of Blowing-Snow Sublimation in a Macroscale Hydrology Model. Journal of Hydrometeorology, 5, 745-762.

Butts, M.B., J.T. Payne, M. Kristensen, and H. Madsen, 2004. An evaluation of the impact of model structure on hydrological modelling uncertainty for streamflow simulation. *Journal of Hydrology*, 298, 242-266.

Chaing, S., Y. Tachikawa, and K. Takara, 2007. Hydrological model performance comparison through uncertainty recognition and quantification. *Hydrological Processes*, 21, 1179-1195.

Chow, V.T., 1959. *Open Channel Hydraulics*, McGraw-Hill, New York, New York, 680 pp.

Daly, C., R.P. Neilson, D.L. Phillips, 1994. A statistical-topographic model for mapping climatological precipitation over mountainous terrain. *Journal of Applied Meteorology*, 33, 140-158.

Dickinson, W.T., 1967. *Accuracy of Discharge Measurements*. Hydrology Paper No. 20, Colorado State University, Fort Collins.

Dingman, S.L., 2002. *Physical Hydrology*. Second edition, Prentice Hall, Upper Saddle River, New Jersey, 646 pp.

Dunker, J.J., T.M. Over, and J.A. Gonzalez, 2006. *Computation and Error Analysis of Discharge for Lake Michigan Diversion Project in Illinois: 1997-99 Water Years*. USGS Scientific Investigations Report 2006-5018.

Elder, K., and J. Dozier, 1990. Improving methods for measurement and estimation of snow storage in alpine watersheds. In *Hydrology in Mountain Regions. I - Hydrological Measurements, Water Cycle, IAHS Publ*. no. 193, 147-156.

Erickson T, M. Williams, and A. Winstral, 2005. Persistence of topographic controls on the spatial distribution of snow in rugged mountain terrain, Colorado, United States. *Water Resources Research*, 41(4), W04014

Erxleben J, K. Elder, and R. Davis, 2002. Comparison of spatial interpolation methods for estimating snow distribution in the Colorado Rocky Mountains. *Hydrological Processes*, 16(18), 3627–3649

Fassnacht, S.R., 2004. Estimating Alter-shielded gauge snowfall undercatch, snowpack sublimation, and blowing snow transport at six sites in the coterminous USA. *Hydrological Processes*, 18, 3481-3492.

Fassnacht, S.R., et al., 2018. Distribution of snow depth variability. *Frontiers of Earth Science* 12, 683–692. https://doi.org/10.1007/s11707-018-0714-z

Farrance, I., and R. Frenkel, 2014. Uncertainty in Measurement: A Review of Monte Carlo Simulation Using Microsoft Excel for the Calculation of Uncertainties Through Functional Relationships, Including Uncertainties in Empirically Derived Constants. *The Clinical Biochemist Reviews,* 35.1, 37–61.

Goodison, B.E., P.Y.T Louie, and D. Yang, 1998. *WMO solid precipitation measurement intercomparison final report*. WMO Instruments and Observing Methods Report No. 67, WMO/TD No. 872.

Groisman, P.Y, and D.R. Easterling, 1994. Variability and trends of total precipitation and snowfall over the United States and Canada,. *Journal of Climate*, 7, 184-205.

Gupta, H. V., H. Kling, K.K. Yilmaz, and G.F. Martinez, 2009. Decomposition of the mean squared error and NSE performance criteria: Implications for improving hydrological modelling. *Journal of hydrology*, 377(1-2), 80-91. https://doi.org/10.1016/j.jhydrol.2009.08.003

Hasfurther, V.C., G.L. Kerr, G. Parks, and J. Wetstein, 1994. Chapter 9 "*Hydrology*" in *The Glacier Lakes Ecosystem Experiments Site*, R.C. Musselman (editor), General Technical Report RM-249.

Hastings, W.K., 1970. Monte Carlo sampling methods using Markov chains and their applications. *Biometrika*, Vol 57(1), 97-109.

Henderson, F.M., 1966. *Open Channel Flow*. MacMillan, New York, New York, 544 pp.

Herschy, R.W., 1973. The magnitude of errors at flow measurement stations: Hydrometry. Proceedings of the Koblenz Symposium, 1970, UNESCO, *World Meteorological Organization, International Association of Hydrological Sciences*, 1:109-131.

Heuvelink, G., 1998. *Error Propagation in Environmental Modelling with GIS*. CRC Press, 150 pp.

Hood, E., M. N. Gooseff, and S. L. Johnson. 2006. Changes in the character of stream water dissolved organic carbon during flushing in three small watersheds, Oregon. *Journal of Geophysical Research,* 111, G01007, doi:10.1029/2005JG000082.

Hood, E., M. Williams, and D. Cline, 1999. Sublimation from a seasonal snowpack at a continental mid-latitude alpine site. *Hydrological Processes*, 13, 1781-1797.

Hultstrand, D.M., 2006. *Geostatistical Methods for Estimating Snowmelt Contribution to the Seasonal Water Balance in an Alpine Watershed*. Master of Science Thesis, Watershed Science Program, Colorado State University, 130 pp.

Istanbulluoglu, E. et al., 2012. Interpretation of hydrologic trends from a water balance perspective: The role of groundwater storage in the Budyko hypothesis. *Water Resources Research*, 48(3). https://doi.org/10.1029/2010WR010100

Johnson, G. L., and C. L. Hanson, 1993. Topographic and Atmospheric Influences on Precipitation Variability over a Mountainous Watershed. *Journal of Applied Meteorology*, 34, 68-87.

Jongkook L, S. Hongjoon, A. Jeonghwan, and J. Changsam, 2016. Accuracy Improvement of Discharge Measurement with Modification of Distance Made Good Heading. *Advances in Meteorology*, 1-9. https://doi.org/10.1155/2016/9437401

Kampf, S.K., et al., 2020. The case for an open water balance: Re-envisioning network design and data analysis for a complex, uncertain world. *Water Resources Research*, 56(6), e2019WR026699. https://doi.org/10.1029/2019WR026699

Kattelmann, R., and K. Elder, 1991. Hydrologic characteristics and water balance of an alpine basin in the Sierra Nevada. *Water Resources Research*, 27(7), 1553-1562.

King, H.W. and E.F. Brater, 1963. *Handbook of Hydraulics*. Fifth edition, McGraw-Hill, New York, New York, 582 pp.

Klemes, V., 1986. Operational testing of hydrological simulation models. *Hydrological Sciences Journal*, 31, 13-24.

Kochendorfer, J., et al., 2017. Analysis of single-Alter-shielded and unshielded measurements of mixed and solid precipitation from WMO-SPICE, *Hydrology and Earth System Science*, 21, 3525–3542. https://doi.org/10.5194/hess-21-3525-2017, 2017

Koren, V.I., B.D. Finnerty, J.C. Schaake, M.B. Smith, D.J. Seo, and Q. Duan, 1999. Scale dependencies of hydrologic models to spatial variability of precipitation. *Journal of Hydrology*, 217, 285-302.

Larson, L.E, and E.L. Peck, 1974. Accuracy of precipitation measurements for hydrologic modeling. *Water Resources Research*, 10(4) 587-863. https://doi.org/10.1029/WR010i004p00857

Liston, G.E., and K. Elder, 2006. A distributed snow-evolution modeling system (snowmodel), *Journal of Hydrometeorology*, 7(6), 1259–1276.

Littlewood, I.G., 2002. Improved unit hydrograph characterisation of the daily flow regime (including low flows) for the River Teifi, Wales: towards better rainfall-streamflow models for regionalisation. *Hydrology ad Earth Systems Science,* 6(5), 899-911.

Mantovan, P., and E. Tondini, 2006. Hydrological forecasting uncertainty assessment: Incoherences of the GLUE methodology. *Journal of Hydrology*, 330(1-2), 368-381.

Matter, M.A., 2010. Nonstationarity: Another 'Inconvenient Truth'. Colorado Water, 27(2), 10-11.

McKerchar, A.I., 2003. Encyclopedia of Physical Science and Technology (Third Edition), Streamflow, Academic Press, 129-142. https://doi.org/10.1016/B0-12-227410-5/00741-9

Melching, C.S, and V.P. Singh, 1995. Reliability estimation in Computer models of watershed hydrology. In Reliability estimation in Computer models of watershed hydrology. *Water Resources*, 69-118.

Michel, R. L., J. T. Turk, D. H. Campbell, and M. A. Mast, 2002. Use of natural 35S to trace sulphate cycling in small lakes, Flattops Wilderness Area, Colorado, U.S.A. *Water Air Soil Pollut. Focus*, 2, 5 –18.

Milly, P.C. et al., 2008. Stationarity is Dead: Whither Water Management?, Science, 319(5863), 573-574. DOI: 10.1126/science.1151915

Molotch N.P., P.D. Blanken, M.W. Williams, A.A. Turnispeed, R.K. Monson, and S.A. Margulis, 2007. Estimating sublimation of intercepted and sub-canopy snow using eddy covariance systems. *Hydrological Processes*, 21, 1567-1575. https://doi.org/10.1002/hyp.6719

Montanari, A., 2007. What do we mean by uncertainty? The need for a consistent wording about uncertainty assessment in hydrology. *Hydrological Processes*, 21, 841-845.

Montanari A, and D. Koutsoyiannis, 2014. Modeling and mitigating natural hazards: stationarity is immortal! Water Resources Research, 50, 9748-9756. https://doi.org/10.1002/2014WR016092

Mroczowski, M., G.P. Raper, and G. Kuczera, 1997. The quest for more powerful validation of conceptual catchment models. *Water Resources Research*, 33, 2325-2335.

Nash J.E., and J.V. Sutcliffe, 1970. River flow forecasting through conceptual models part I — A discussion of principles. *Journal of Hydrology*, 10(3), 282-290. https://doi.org/10.1016/0022-1694(70)90255-6

Pan, M., et al., 2003. Snow process modeling in the North American Land Data Assimilation System (NLDAS): 2. Evaluation of model-simulated snow water equivalent. *Journal of Geophysical Research*, 108(D22), 8850. https://doi.org/10.1029/2003JD003994

Perrin, C.., C. Michael, and V. Anderson, 2001. Does large number of parameters enhance model performance? Comparative assessment of common catchment model structures on 429 catchments. *Journal of Hydrology*, 242, 275-301.

Phillips, M., 2013. *Estimates of sublimation in the upper Colorado river basin*. Master of Science Thesis, Department of Atmospheric Science, Colorado State University, 57pp.

Pokorny S. et al., 2021. Cumulative Effects of Uncertainty on Simulated Streamflow in a Hydrologic Modeling Environment. Elementa: Science of the Anthropocene 9(1) 431. https://doi.org/10.1525/elementa.431

Reba, M.L., J. Pomeroy, D. Marks, and T.E. Link, 2012. Estimating surface sublimation losses from snowpacks in a mountain catchment using eddy covariance and turbulent transfer calculations. *Hydrological Processes*, 26, 3699–3711.

Rehmel, M., 2007. Application of Acoustic Doppler Velocimeters for Streamflow Measurements. *Journal of Hydraulic Engineering*, 133, 1433–1438. doi:10.1061/ ASCE 0733-9429 2007 133:12 1433

Roe, G.H, 2005. Orographic Precipitation., *Annual Review, Earth Planet Science,* 33, 645-67.

Ruess, J.O., F.A. Vertucci, R.C. Musselman, and R.A. Sommerfeld, 1995. Chemical fluxes and sensitivity to acidification of two high-elevation catchments in southern Wyoming, *Journal of Hydrology*, 173, 165-189.

Scharffenberg, B., Bartles, M., Brauer, T., Fleming, M., Karlovits, G. 2018. Hydrologic Modeling System HEC-HMS – User's Manual, Version 4.3. U.S. Army Corps of Engineers, Institute for Water Resources, Hydrologic Engineering Center (CEIWR-HEC), Davis, CA, USA.

Segond, M.L., C. Onof, and H.S. Wheater, 2006. Spatial-temporal disaggregation of daily rainfall from a generalized linear model. *Journal of Hydrology*, 331, 674-689.

Sexstone GA, D.W. Clow, D.I. Stannard, and S.R. Fassnacht, 2016. Comparison of methods for quantifying surface sublimation over seasonally snow-covered terrain. *Hydrological Processes*, 30, 3373-3389. https://doi.org/10.1002/hyp.10864

Sexstone, G. A., Clow, D. W., Fassnacht, S. R., Liston, G. E., Hiemstra, C. A., Knowles, J. F., and Penn, C. A., 2018. Snow sublimation in mountain environments and its sensitivity to forest disturbance and climate warming. Water Resources Research, 54: 1191–1211, https://doi.org/10.1002/2017WR021172

Sheffield, J. et al., 2003. Snow process modeling in the North American Land Data Assimilation System (NLDAS): 1. Evaluation of model-simulated snow cover extent. *Journal of Geophysical Research*, 108(D22), 8849, doi:10.1029/2002JD003274.

Slater, A.G., et al., 2001. The Representation of Snow in Land Surface Schemes: Results from PILPS 2(d). *Journal of Hydrometeorology*, 2, 7-24.

Smith, P. J., K. J. Beven, *and* J. A. Tawn, 2008. Detection of structural inadequacy in process-based hydrological models: A particle-filtering approach. *Water Resource Research,* 44*, W01410. https://doi.org/10.1029/2006WR005205*

Stähli, M., et al., 2011. One century of hydrological monitoring in two small catchments with different forest coverage. Environmental Monitoring and Assessment, 174, 91–106. https://doi.org/10.1007/s10661-010-1757-0

Svoma, B.M., 2016. Difficulties in Determining Snowpack Sublimation in Complex Terrain at the Macroscale. *Advances in Meteorology*, vol. 2016, Article ID 9695757. https://doi.org/10.1155/2016/9695757

Thornthwaite, C. W., 1948. An approach towards a rational classification of climate. *Geographical Review*. 38, 55–94.

Viessman, W., and G.L. Lewis, 2003. *Introduction to Hydrology*, Fifth edition. Prentice Hall, Upper Saddle River, New Jersey, 612 pp.

Vrugt, J. A., C. J. F. ter Braak, H. V. Gupta, and B. A. Robinson, 2009. Equifinality of formal (DREAM) and informal (GLUE) Bayesian approaches in hydrologic modeling? *Stochastic Environmental Research and Risk Assessment*, 23(7), 1011–1026. doi:10.1007/s00477-008-0274-y.

Wagener, T., H.S. Wheather, and H.V. Gupta, 2004. *Rainfall-runoff modelling in gauged and ungauged catchments*. Imperial College Press, London pp 306.

Winter, T.C., 1981. Uncertainties in estimating the water balance of lakes, *Water Resources Bulletin*, 17(1): 82-115.

Winter, T.C., 2003. The hydrology of Lakes. In *The Lakes Handbook*, vol. 1, Limnology and Limnetic Ecology, edited by P. E. O'Sullivan and C. S. Reynolds, pp. 61– 78, Blackwell Sci., Oxford, U. K.

Woo, M, P. Marsh, and W. P. Pomeroy, 2000. Snow, frozen soils and permafrost hydrology in Canada, 1995 – 1998. *Hydrological Processes*, 14, 1591– 1611.

Yapo, P.O., H.V. Gupta, and S. Sorooshian, 1996. Automatic calibration of conceptual rainfall-runoff models: Sensitivity to calibration data. *Journal of Hydrology*, 181, 23-48.

CHAPTER 2.0 - THE SENSITIVITY OF SNOWPACK SUBLIMATION ESTIMATES TO INSTRUMENT AND MEASUREMENT UNCERTAINTY PERTURBED IN A MONTE CARLO FRAMEWORK

2.1 Summary

The bulk aerodynamic flux equation is often used to estimate snowpack sublimation since it requires meteorological measurements at only one height above the snow surface. However, to date the uncertainty of these estimates and the individual input variables and input parameters uncertainty have not been quantified. We modeled sublimation for three (average snowpack in 2005, deep snowpack in 2011, and shallow snowpack in 2012) different water years (October 1 to September 30) at West Glacier Lake watershed within the Glacier Lakes Ecosystem Experiments Site in Wyoming. We performed a Monte Carlo analysis to evaluate the sensitivity of modeled sublimation to uncertainties of the input variables and parameters from the bulk aerodynamic flux equation. Input variable time series were uniformly adjusted by a normally distributed random variable with a standard deviation given as follows: 1) the manufacturer's stated instrument accuracy of 0.3 °C for temperature (T), 0.3 m/s for wind speed (U_z), 2% for relative humidity (RH), and 1 mb for pressure (P); 2) 0.0093 m for the aerodynamic roughness length (z_0) based on z_0 profiles calculations from multiple heights; and 3) 0.08 m for measurement height (z). Often z is held constant; here we used a constant z compared to the ground surface, and subsequently altered z to account for the change in snow depth (d_s). The most important source of uncertainty was z_0, then RH. Accounting for measurement height as it changed due to snowpack accumulation/ablation was also relevant for deeper snow. Snow surface sublimation uncertainties, from this study, are in the range of 1 to 29% for individual input parameter perturbations. The mean cumulative uncertainty was 41% for the three water

years with 55%, 37%, and 32% occurring for the wet, average, and low water years. The top three variables (z varying with d_s, z_0, and RH) accounted for 74% to 84% of the cumulative sublimation uncertainty.

2.2 Introduction

In mountainous regions, such as the western United States, most of annual precipitation falls as snow and is stored in high-elevation mountain snowpacks. Snowpack sublimation is an important hydrologic process which can account for significant water losses to the atmosphere (Hood et al., 1999; Liston et al., 2006a; Liston et al., 2006b; Molotch et al., 2007; Sexstone et al., 2016). However, the amount of water that is exchanged between seasonal snowpacks and the atmosphere through sublimation is still poorly understood (Lang, 1981; Hood et al., 1999; Molotch et al., 2007). The large degree of uncertainty can have significant consequences on hydrologic studies, water supply forecasting, and water supply modelling.

Sublimation losses from the snowpack have been estimated for various environments and can constitute a significant component of the water balance, with net sublimation losses estimated between 10-35% of the seasonal snow accumulation, specifically: 12-33% in the Canadian prairies (Woo et al., 2000), 19% in the Wyoming Rocky Mountains (Hultstrand, 2006), 15% in the Colorado Rocky Mountains (Hood et al., 1999), and 18% in the Sierra Nevada Mountains (Kattelmann and Elder, 1991). Over a 40-day period in the Colorado Rocky Mountains, total snowpack sublimation was greater than measured precipitation (Molotch et al., 2007).

Sublimation occurs more readily under certain weather conditions, such as low relative humidity (RH) and increased wind speed (U_z). Vapour pressure (e) gradients (Δe) between the

snowpack and the atmosphere, snow surface roughness length (z_0), wind speed, and atmospheric stability all have a significant contribution to sublimation magnitude and direction (upward as a loss or downward as vapour deposition). Methods for estimating sublimation from a snowpack include the bulk aerodynamic flux (BF) calculation, Bowen ratio-energy balance, snow evaporation pans, and aerodynamic profile (AP) methods. Newer techniques that directly measure atmospheric flux (eddy covariance, EC) have also been tested for use in snowpack sublimation monitoring in alpine and sub-alpine environments (Hood et al., 1999; Molotch et al., 2007; Marks et al., 2008; Reba et al., 2012; Sexstone et al., 2016).

Sublimation losses from the snowpack are typically calculated from a mass transfer equation, as per Dingman (2002) and Fassnacht (2004). The latent heat flux (Q_E in kJ/s/m^2) is equal to the product of the latent heat of sublimation (L_S as 2838 kJ/kg at a temperature (T) of 0 ^{o}C; Datt, 2011) and the rate of latent mass transfer (E in kg/s/m^2). The most common method for estimating snowpack sublimation is measuring snowpack Q_E using the BF equation (Moore, 1983). This method has the advantage of requiring meteorological measurements at only one height above the snow surface. However, a primary assumption applied to the BF method is that the snow surface temperature follows the air temperature for the estimation of saturation vapour pressure (e_{sat}). This assumption is often inaccurate at temperatures colder than 0 °C (Raleigh et al., 2013) and can lead to an over-estimation of sublimation (Bernier and Edwards, 1989; Marks et al., 2008). In addition, this method also assumes the snow surface is saturated with respect to ice or water (i.e., 100% relative humidity), which may not always be the case (Box and Steffen, 2001). With the surface temperature and humidity assumptions, the estimated sublimation loss (upward flux) is a function of the difference in vapour pressure between the measurement height and the surface (Fassnacht, 2004) and can never be downward, such as in the form of frost

deposition (Sexstone et al., 2016). In reality, the snow surface temperature is limited to 0°C but the air temperature can be warmer and vapour deposition can occur depending on the relative humidity of the air, i.e., the vapour gradient.

A more accurate method for calculating the snowpack Q_E and snowpack turbulent fluxes as compared to the BF method is the AP method which requires the measurement of U_z, T, and RH at multiple heights above the snowpack (Cline, 1997a; Hood et al., 1999; Sexstone et al., 2016). Both the BF and AP methods require an estimate of z_0 to define the U_z profile. Using z_0 as a variable rather than a constant parameter will alter the computed snowpack sublimation loss estimates (Fassnacht, 2010); z_0 has been seen to vary by almost three orders of magnitude (2 x 10^{-5} to 9.76 x 10^{-3} m) (Brock et al., 2006). Previous research has used z_0 as a parameter with values of 1 x 10^{-3} m (Hultstrand, 2006), 5 x 10^{-2} m (Fassnacht, 2004) and 5 x 10^{-4} m (Box and Steffen, 2001).

The EC method is considered the most accurate/direct method for calculating snowpack Q_E (Molotch et al., 2007; Sexstone et al., 2016). A two-tower approach (two eddy covariance sensors) 35 miles north of Bangor, ME was used to test the EC method uncertainties in Q_E measurements, results from the study state thata Q_E measurement uncertainty of 0.005 kJ/s/m^2 was reported for an entire calendar year (Hollinger and Richardson, 2005). This method is considered a direct atmospheric flux measurement technique to determine the vertical turbulent fluxes within the atmospheric boundary layer. While EC systems are fairly robust, the EC procedure requires adequate site conditions, such as long fetches, and a high frequency sonic anemometer that can be cost and energy prohibitive. Sublimation measurements that require extensive meteorological measurements and equipment for the EC and AP methods are relatively limited in complex mountain regions (Sexstone et al., 2016), typically limited to research

facilities, which makes the BF calculation the most common method used to estimate snowpack sublimation at local and regional scales.

The objectives of this research for one seasonally snow-covered alpine environment are (i) to quantify the sensitivity of sublimation estimates using the BF method from the uncertainty of the input measurements; ii) to quantify snow sublimation uncertainty as a function of peak snow water equivalent and total precipitation; and (iii) to provide guidance to account for instrumentation errors and what input variables need the greatest attention while quantifying snowpack sublimation. This study provides an evaluation of the sensitivity of snow sublimation calculations and possible uncertainties which can improve our understanding of water resources, water supply forecasting, and water supply modelling.

2.3 Study Site

For this study, sublimation estimates were conducted in West Glacier Lake watershed (WGLW) within the Snowy Range Mountains, Wyoming (41°22’30" N latitude and 106°15’30" W longitude) (Figure 2.1). WGLW is part of the US Forest Service’s Glacier Lakes Ecosystem Experiments Site (GLEES) developed to conduct research on the effects of atmospheric deposition on alpine and subalpine ecosystems (Musselman, 1994). Approximately 575 ha in size, GLEES consists of three small watersheds, beneath a northeast-southwest ridge, and WGLW ranges in elevation from 3,277 m at the lake outlet to 3,493 m at the top. Mean annual temperature is -1 °C at the outlet and -2.5 °C at the top of the basin (Korfmacher and Hultstrand, 2006). Mean annual precipitation is 1200 mm, with approximately 75 to 85 % falling as snow, which remains from late November to early June (Wooldridge et al., 1996; Korfmacher and

Hultstrand, 2006). This region is dominated by high westerly winds that range between 0 and 26 m/s with an average of 8 m/s (Korfmacher and Hultstrand, 2006). These climatic conditions combine to create an environment where snow accumulation, snow redistribution, and snowpack sublimation can have significant impacts on the watershed hydrology.

2.4 Methodology

2.4.1 Bulk Aerodynamic Flux

The meteorological variables needed for the BF equation are T (in ºC), RH (in %), U_z (in m/s), and station pressure (P in mb). For the BF method, the latent mass flux is calculated as:

$$E = \frac{0.622 \cdot \rho_a}{P \cdot \emptyset_m \cdot \emptyset_v} \cdot U_z \cdot \frac{k^2 (q_a - q_o)}{ln\left(\frac{Z_a + Z_d}{Z_o}\right)^2} \qquad \text{Equation 2.1}$$

where ρ_a is the density of air (kg/m^3), ϕ_m is the stability function for momentum calculated as a function of the Richardson number (unitless), ϕ_v is the stability function for water vapour calculated as a function of the Richardson number (Ri, unitless), k is von Karman's constant (0.4), q_o is the specific humidity (kg/kg) at the surface of the snow, q_a is the specific humidity at measurement height Z_a (in m), and Z_d is the zero-plane displacement (in m). A value of zero is used for Z_d.

The q_o at each level in the profile is determined by (Saucier, 1983):

$$q_o = \frac{0.622e}{P - 0.378e} \qquad \text{Equation 2.2}$$

where e is the vapour pressure (in mb), calculated from the equation:

$$e = \frac{e_{sat}(RH)}{100} \qquad \text{Equation 2.3}$$

where e_{sat} is the saturation vapour pressure over water (in mb), estimated from the equation:

$$e_{sat} = 6.11 * exp\left(\frac{17.3*T}{T+237.3}\right) \quad \text{Equation 2.4}$$

with T in °C. Stability functions are calculated as a function of the Ri as described by Ohmura (1981) The Richardson number is determined by:

$$Ri = \frac{g}{\overline{\theta}}\left(\frac{\delta\theta/\delta z}{(\delta U/\delta z)^2}\right) \quad \text{Equation 2.5}$$

where g is the acceleration due to gravity (9.81 m/s^2) and $\overline{\theta}$ is the mean potential temperature of the levels (in ºC) (Andreas, 2002). The stability factors (Φ_m and Φ_v) are estimated as a function of the calculated Ri, based on the value of Ri, as per Cline (1997a).

Air density ρ_a is calculated from the equation:

$$\rho_a = \frac{P}{R \cdot T} \quad \text{Equation 2.6}$$

where P is air pressure (mb *100), R is the specific gas constant (287.05 J/kg/K), and T is the air temperature in degrees Kelvin.

2.4.2 Data

The GLEES maintains an 18-meter tower equipped with standard meteorological sensors located at 3286 m elevation between east and west Glacier Lakes (Figure 2.1). T, RH, U_z, wind Direction (W_d), solar radiation (Q_h), and soil temperature (T_{soil}) are measured every 15 minutes. For this study, we utilized the quality controlled hourly meteorological data (T, RH, U_z, P) from the GLEES tower for the water years (October 1 to September 30) 2005, 2011, and 2012 (data are available at <*https://www.fs.usda.gov/rds/archive/Product/RDS-2006-0003-2/*>. These years were selected because they represent an average snow season (2005), a wet snow season with cooler T, higher RH and above average precipitation (2011), and a drier snow season that melted

out early with warmer *T*, lower *RH*, and below average precipitation (2012) (Figure 2.2 and Table 2.1). Snow depth (d_s) and snow water equivalent (SWE) were obtained from the Natural Resources Conservation Service Snow Telemetry (SNOTEL) site Brooklyn Lake, Wyoming located approximately 1 km to the southeast at an elevation of 3115 m (Figure 2.2; data are available at <*https://www.wcc.nrcs.usda.gov/*>). Snow depth data were only available since water year 2004. The SNOTEL data were used to determine the snow-cover period for the three water years and the snowpack and average meteorological conditions were computed (Table 2.1).

The z_0 parameter was empirically derived from a nearby research site, Niwot Ridge Subnivean Lab Colorado that measures meteorological variables at multiple heights allowing for AP calculations. Niwot Ridge is similar in elevation and meteorology as West Glacier Lake region and is assumed that the Niwot Ridge z_0 parameter was transposable to West Glacier Lake. The z_0 parameter estimates were computed during the snowcover season (Cline, 1997b) using U_z measurements at two different heights, z_a and z_b:

$$Z_o = \exp \frac{(U_a * LN(z_b) - U_b * LN(z_a))}{(z_a - z_b)} \qquad \text{Equation 2.7}$$

An average z_0 value of 0.0043 m and a standard deviation to 0.0013 m were computed from sub-hourly wind measurements that were at 0.5 and 2.0 m above the snowpack for water years 1994 and 1995. These are similar to values (0.0022 m to 0.0050 m) presented in Brock et al. (2006).

2.4.3 Monte Carlo Simulations

To evaluate the sensitivity of simulated sublimation using the BF method to uncertainties of the input variables and parameters data, we performed a Monte Carlo analysis. Monte Carlo

methods utilize computational algorithms to model the probability of different outcomes in a process that cannot easily be predicted due to the intervention of random variables and/or uncertainty (Hastings, 1970). Only one variable or parameter was perturbed at a time to determine which one was most sensitive in the sublimation calculation; we did not examine joint-uncertainties (Graham et al., 2010 and Sexstone et al., 2016). Cumulative sublimation uncertainty was quantified by the addition of individual variable/parameter uncertainties (Bliss et al., 2011). Seven numerical experiments were performed (Table 2.2) by individually changing four meteorological variables (*T, RH, Uz, P*) that had an hourly time step, two parameters (z_0 and z) that are usually assumed to be constant, and one parameter (z) that was used as a variable. For each hourly time step, the variable or parameter was adjusted using a random number that was selected from a normal distribution with a mean of zero and a standard deviation based on the instrumentation measurement error range which was set to the manufacturer's stated instrument accuracy (Table 2.2). The perturbed *RH* values were constrained to a maximum of 100%. For z_0, a standard deviation was calculated from field data, as presented above (equation 7). For the Monte Carlo analysis, sublimation was computed for each year 1000 times, each of the 1000 times using the randomly selected perturbation to the individual input variable or parameter to assess the sensitivity of the sources of uncertainty. The measurement height changes as snow accumulates or ablates, but z is often held constant (Fassnacht, 2004). Therefore, z was used as constant of 3.0 m with a standard deviation of 0.08 m based on stated instrument accuracy (Judd snow depth sensor < juddcom.com>) (Ryan et al., 2008). The value of z was also adjusted to account for the change in d_s (Figure 2.2); the Monte Carlo approach was not used in this last test (Table 2.2).

2.4.4 Surface Temperature Estimates

We evaluated the use of dewpoint temperature to represent the snow surface temperature, as shown in Raleigh et al. (2013). Sublimation was computed using air temperature and relative humidity to estimate the dewpoint temperature (equation 4), without perturbations. These sublimation estimates were compared to the base case scenarios for the three years.

2.5 Results

For the three different snow years, the estimated sublimation for the non-perturbed base case (Table 2.1 and lines in Figure 2.2c) was inversely related with the amount of snow (Figures 2.2a and 2.2b), which is in part a function of the other meteorological conditions. The simulated sublimation was somewhat consistent over the winter of 2011, as seen by approximately constant slope of cumulative sublimation (Figure 2.2c). In 2012, the change in cumulative sublimation rate decreased after February while in 2011 it started to increase then (Figure 2.2c).

Using the Monte Carlo approach with input variable/parameter perturbations yielded a range of results (Table 2.3), which were consistent for some variables, such as RH, U_z, and z_0. The range of variability from the perturbations became larger in mid-February 2011, mid-March 2012, and early April 2011 (Figure 2.2c). The shape of the z_0 simulation was similar for each year (Figure 2.3 and the standard deviation in Table 2.2) and coefficient of variation was the same (Table 2.3). Sublimation sensitivity based on the perturbed input variables/parameters with the Monte Carlo simulations show consistent inter-annual variability in the simulations for *RH*, U_z, and z_0, but not for *T* or the two *z* tests (Figure 2.4 and Table 2.3). Since the instrument accuracy of *P* was so high (~0.1%), the *P* perturbations has a negligible effect on sublimation estimates.

Calculated sublimation was most sensitive to the perturbations of z_0, RH, z (in 2011 due to deep snow; Figure 2.4b), U_z and finally T (Table 2.3 and Figure 2.4). Temperature perturbation yielded the most noticeable sublimation variability in 2005, about four to five as much as in the other years due to (Figure 2.4); this likely occurred since 2005 had the most freezing days. However, this variation in temperature was small compared to the other years. When the snowpack is shallower, such as in 2005 and 2012 (Figure 2.2a), z has less of an influence on the sensitivity of the calculated sublimation (Figures 2.3a and 2.3c).

The range of variability in calculated sublimation using the Monte Carlo approach was most for 2011 and least for 2005 (Figure 2.2c). However, the variation in simulated sublimation (Table 2.4) was much greater for the lower snow years when taken as a percentage of peak SWE (Figure 2.2b) and annual precipitation (Table 2.1). The range of simulated sublimation to peak SWE and to annual total precipitation was greater by a factor of two for both 2005 and 2012 (Table 2.4). More importantly, sublimation was estimated to be at least half of the peak SWE in 2012, and a third of peak SWE in 2005 (Table 2.4). The maximum simulated sublimation was more than two-thirds for 2005 and almost 100% for 2012 (Table 2.4). These values can be considered scaled when subsequently compared to the annual precipitation total, since peak SWE was 67% of annual precipitation in both 2005 and 2012; it was 83% in 2011 (Table 2.1). For the base case, sublimation was computed to be 37, 21, and 52% of the annual precipitation in 2005, 2011, and 2012, respectively (Table 2.4).

The average daytime dewpoint temperature has a negative bias (Raleigh et al., 2013). This use of dewpoint temperature (T_d) for the surface temperature (T_s) yielded a negative cumulative sublimation estimate throughout the winter for each year (Figure 2.5), which is not correct. Interestingly, this assumption yielded the most deposition (negative cumulative

sublimation in Figure 2.5) and were somewhat of a translation of the base case (Figure 2.2c). The computed mean hourly sublimation rate is also negative every hour and smaller in magnitude than when the surface air temperature is used, as stated above (Figure 2.6). Therefore, using dewpoint temperature for surface temperature was not evaluated further.

2.6 Discussion

The three snow seasons represent a range of snow conditions within the available period of record. Given the large variability in the amount of snowfall (Figure 2.2 and Table 2.1), the importance of sublimation to the seasonal water balance varied widely (Hultstrand, 2006; Table 4). There were large variations in calculated sublimation were due to z_0 (Figure 2.3) and there is much uncertainty in estimating the value of z_0 (Andreas, 2002; Fassnacht et al., 2015), as it varies spatially and temporally (Brock et al., 2006). Only for deep snow (2011; Figure 2.2a) was perturbation in z relevant (Figure 2.4c). When using the BF method, the actual measurement height should be estimated from snow depth (e.g., Figure 2.2a; Fassnacht, 2010).

There was some sensitivity to U_z, but much less to T (mostly in 2005), and essentially none to P (Figure 2.4). The calculated sublimation sensitivity due to RH and U_z is based on instrumentation accuracy. More advanced methods, such as the EC method (Box and Steffen, 2001; Reba et al., 2012; Sexstone et al., 2016), could improve accuracy. However, such more accurate sensors may not be as robust in the field (Sexstone et al., 2016).

The mean BF cumulative sublimation uncertainty was 41% for the three water years with 55%, 37%, and 32% occurring for the wet, average, and low water years (Table 2.3). The mean uncertainty for each input parameter in order from largest to smallest uncertainty is z varying

with d_s (15.8%), z_0 (9.6%), *RH* (7.1%), U_z (4.9%), *z* at constant height (2.0%), and *T* (1.9%) (Table 2.3). The uncertainty for top three variables account for 74% to 84% of the cumulative sublimation uncertainty (Table 2.3).

Latent heat flux estimates over snow covered surfaces are highly correlated for the EC and BF methods, but with some discrepancies (e.g., Marks et al., 2008), such as a positive bias in estimating sublimation using the BF method (Box and Steffen, 2001; Marks et al., 2008). The BF sublimation estimates calculated here (Table 2.1 and Figure 2.2c) are larger than those presented in the literature (e.g., Hood et al., 1999). The EC and AP methods were shown to compare well (Reba et al., 2012), and both are considered better than BF (Sexstone et al., 2016). However, the BF method provided reasonable snowpack sublimation estimates when EC instrumentation were not available (Sexstone et al., 2016), which is often the case (Fassnacht, 2004).

For the average and deep snowpack, there was limited inter-annual year variability whereas the drier and shallower snowpack had larger inter-annual variability of total modeled snow sublimation from the snow surface using the base case (Figure 2.2c). This was also observed by Sexstone et al. (2016) and Reba et al. (2012) suggesting snow sublimation is largely dependent on the amount of snowfall. Sexstone et al. (2016) stated that snow sublimation rates do not scale with snowpack depth or SWE, i.e. during a low snow season a larger percentage of the snowpack is lost to sublimation and hence less total snow is available for melt. The results of this study confirm the statements made by Reba et al. (2012) and Sexstone et al. (2016). It should be noted that blowing snow (Fassnacht, 2004) and blowing snow sublimation were not considered (Sexstone et al., 2018). The variability in the BF-based sublimation estimates were a function of the amount of snow (Figure 2.2c), specifically how the snow depth is represented (Figure 2.4).

The contribution from turbulent transfer to the ablation of the snow cover has been shown to vary between 5% and 60% (Stewart, 1982; Kattleman and Elder, 1991; Cline, 1997a, 1997b; Hunsaker et al., 2012), with sublimation losses ranging from 20% of the snowpack in the alpine of the California Sierra Nevada (Marks and Dozier, 1992; Marks et al.,1992; Marks et al., 1998) to 45% of the snowpack in a subalpine forest in the Rocky Mountains (Hood et al., 1999; Pomeroy and Essery, 1999; Marks et al., 2001; Pomeroy et al., 2006; Molotch et al., 2007; Reba et al., 2012; Sexstone et al., 2016). This analysis shows sublimation losses generally greater than this range (21 to 52% of the snowpack for the base case in Table 2.4), but it was largely dependent on the amount of snow that accumulated (Figure 2.2a). It should be noted that the reported percentages could be lower if direct measurements of SWE and d_s were made in the GLEES basin where a deeper snowpack maybe present.

The understanding of sublimation is not well established at regional macroscales, where land surface models (LSM) have been used to simulate cold season processes. LSM have a coarse resolution (5-30 km), usually larger than the scale of many cold season processes, which restricts how a LSM represents the variability of elevation, vegetation, and meteorology in complex terrain, due in part to a lack of reliable data. Model generated net sublimation has shown large variability based on the model and domain, small scale variability, and snowpack model algorithms (Sheffield et al., 2003; Pan et al., 2003; Bowling et al., 2004; Reba et al., 2012; Svoma, 2016). For example, snowpack sublimation as a percent of precipitation was estimated from 0-15% using various LSMs for a grassland catchment Russia (Slater et al., 2001), 10-35% in Alaska using the Variable Infiltration Capacity (VIC) model (Bowling et al., 2004), 8-20% using various models over the Pacific Northwest of the United States (Sheffield et al., 2003), and from 0-4% in low valleys to 20-30% in the high mountains of the Upper Colorado River Basin

(UCRB) using SnowModel (Liston et al., 2006b). Sublimation in isolated areas of the UCRB has been modeled to exceed 30% of the annual precipitation (Phillips, 2013). This study focused on site specific calculations representing a small localized region, and showed some large variability (Tables 2.3 and 2.4, Figures 2.1, 2.2 and 2.3). Thus, without accurate measurements of sublimation at the localized scale, it is more difficult to evaluate large scale estimates of sublimation (Svoma, 2016). Advancing the understanding of how localized variability affects large scale sublimation can still be achieved through careful model experiments, especially if the sensitivity of results is examined through variable/parameter adjustment and model simulations (Strasser et al., 2011; Phillips, 2013).

One of the simplistic assumptions of applying the BF method is that the snow surface temperature tracks the air temperature measurement, and is thus likely a major uncertainty in the experimental setup and can lead to substantial overestimations of sublimation (Bernier and Edwards, 1989; Marks et al., 2008). Recent experimental studies have used outgoing longwave radiation measurements to measure snow surface temperature and highlight that the snow surface tends to be consistently colder than the air temperature, especially at night (Reba et al., 2012; Sexstone et al., 2016). Most models that utilize the BF equation do not assume that snow surface temperature tracks air temperature but rather solve the snow energy balance equation for snow surface temperature (e.g., Liston and Elder, 2006). We tested using dewpoint temperature to estimate the snow surface temperature and this yielded a negative (downward) sublimation (Figures 2.5 and 2.6). Downward sublimation or deposition as frost does occur some nights and into the early morning, so an improvement is necessary to the assumption for the snow surface temperature.

2.7 Conclusion

Surface sublimation sensitivity was evaluated and quantified in an alpine environment based on the BF method over three water years (average snow season, a wet snow season, and a low snow season). The magnitude and range of perturbed snow sublimation estimates show considerable uncertainty with perturbed input variables. Of the factors affecting the calculated snow sublimation estimates, z_0 and RH are the most significant. For deep snow conditions, where the distance between the instrument and the snow surface can be small, z is important. Wind speed uncertainty caused sensitivity in the sublimation estimates. Temperature perturbation only yielded noticeable sublimation variability in 2005.

Sublimation calculations are derived from a rather large array of parameters, many of which have rather high degrees of uncertainty. As a result, snowpack sublimation is, often reported as a single number, but can be better characterized as a range of values. Snow surface sublimation uncertainties, from this study, are in the range of 1 to 29% for individual input parameter perturbations, with the top three variables (z_0, RH, and z) accounting for 74% to 84% of the cumulative sublimation uncertainty. Surface sublimation uncertainties from this study provide a means to properly account for instrumentation errors and what variables need the greatest attention while performing snowpack sublimation estimates in high elevation regions.

Data Availability

The meteorological data used in this paper are available from the United States Forest Service Rocky Mountain Research Station <here>. The snow data are available from the Natural Resources Conservation Service Water and Climate Center <here>.

2.8 Tables and Figures

Table 2.1. Snowpack and mean meteorological conditions for October-May, the period when temperatures are below 0°C and conducive for sublimation, plus the unperturbed sublimation estimated from the BF method.

	WY 2005	WY 2011	WY 2012
temperature; T (°C)	-4.78	-6.18	-4.82
relative humidity; RH (%)	67.8	72.3	62.4
wind speed; U_z (m/s)	4.99	5.42	5.28
saturation vapor pressure; e_s (mb)	4.71	4.36	4.85
station pressure; P (mb)	684	685	687
vapour pressure; e (mb)	2.92	2.89	2.66
momentum stability function; $\emptyset_m$	0.94	1.01	0.98
water vapour stability function; $\emptyset_v$	0.99	1.05	1.01
total precipitation (mm)	777	1303	671
peak snow water equivalent; SWE (mm)	521	1087	450
snow cover period (days)	234	249	220
unperturbed sublimation (mm)	290	276	350

Table 2.2. Summary of the seven numerical tests that were performed in the sensitivity analysis for sublimation calculations. The mean and standard deviation used in the perturbations for the variables and parameters is listed.

test #	variable / parameter	mean	standard deviation
1	temperature (°C)	time series	0.3
2	relative humidity (%)	time series	2
3	wind speed (m/s)	time series	0.3
4	station pressure (mb)	time series	1
5	aerodynamic roughness length (m)	0.0043	0.0013
6	measurement height (z) is constant (m)	3	0.08
7	z varies with d_s (m)	time series	not used

Table 2.3. Uncertainty summary statistics by Water Year based on Monte Carlo simulation from uniformly perturbing input sublimation variables/parameters: T is air temperature, RH is relative humidity, U_z is wind speed, z_0 is the aerodynamic roughness length, z = 3, is a constant measurement height of 3.0 m, and z is the height of the instrumentation above the snow surface that varies as a function of the snow depth. The variable z was not perturbed (Table 2) so no range is available. The P perturbations are not included as they did not impact the calculated sublimation.

variable / year	T	RH	U_z	z_0	z = 3	z = f(d_s)
standard deviation (mm)						
2005	10.3	21.7	14.7	28.0	3.9	33.5
2011	1.7	21.9	12.8	26.6	14.4	112
2012	5.7	20.3	17.9	33.8	4.1	31.9
coefficient of variation (%)						
2005	3.6	7.5	5.0	9.6	1.2	10.3
2011	0.6	8.0	4.6	9.6	3.8	28.8
2012	1.6	5.8	5.1	9.6	1.1	8.3
maximum range (mm)						
2005	45	110	80	130	21	34
2011	15	112	65	123	139	112
2012	36	105	88	156	22	32
difference from the base value for standard deviation (%)						
2005	5.4	9.7	6.4	12	1.7	-
2011	0.9	9.8	5.8	11.4	6.6	-
2012	1.3	9.0	8.4	14.5	1.8	-
difference from the base value for maximum range (%)						
2005	15.4	38	27.5	44.7	7.2	11.5
2011	2.5	38.6	22.5	42.5	47.6	38.6
2012	12.4	36.3	30.4	53.9	7.6	11

Table 2.4. The amount of sublimation for the minimum, base and maximum computed values compared to peak SWE and annual total precipitation, given as a percent.

	% of peak SWE			% of annual total precipitation		
year	minimum	base	maximum	minimum	base	maximum
2005	37	56	70	25	37	47
2011	17	25	47	14	21	39
2012	52	78	96	35	52	65

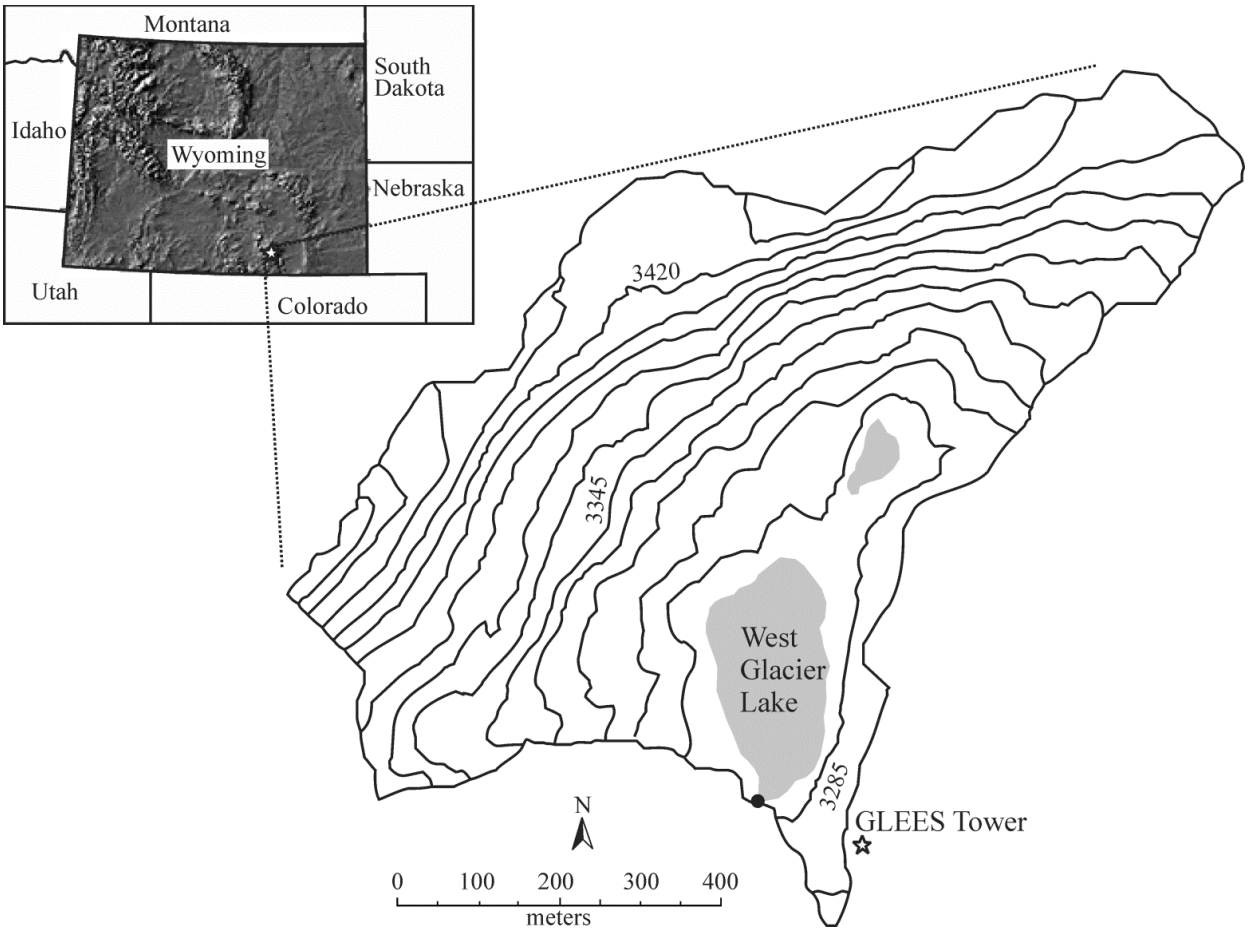

Figure 2.1. Topographic map of West Glacier Lake watershed, located in the Snowy Range of the Medicine Bow Mountains of southern Wyoming. Contour interval is 15 m. Solid dot shows location of lake outlet. The star shows the location of GLEES meteorological station used in this study. Data from the GLEES tower were used in the study.

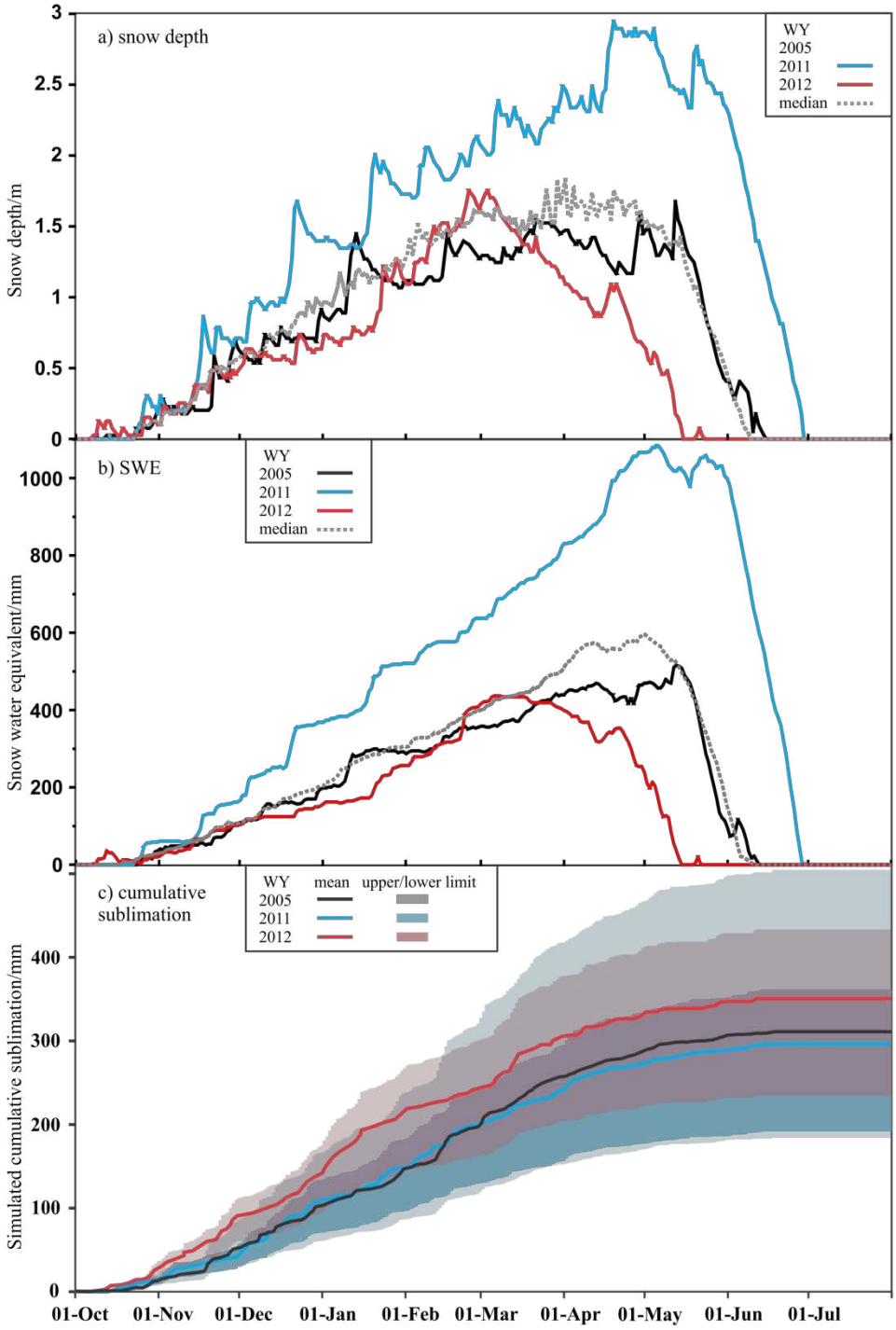

Figure 2.2. Brooklyn Lake SNOTEL a) snow depth and b) snow water equivalent, and c) the calculated unperturbed and range of perturbed cumulative sublimation for water year 2005, 2011, and 2012. The median ds (2004 to 2017) and SWE (1981-2017) are included. In c), the shaded zones are the upper and lower limits of the perturbed computations.

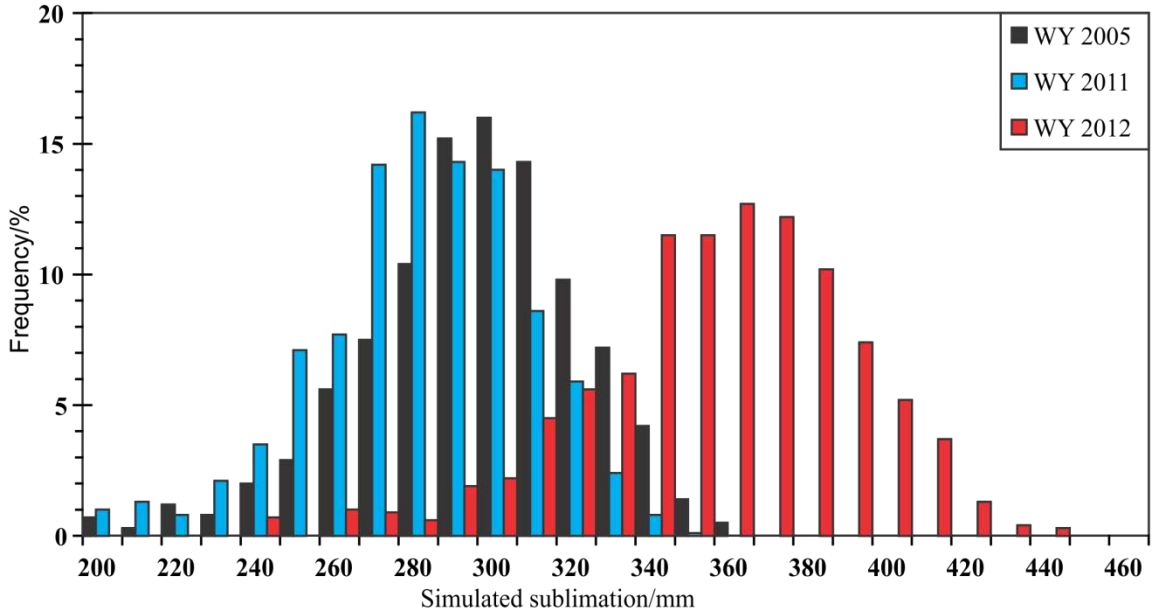

Figure 2.3. Histogram of 1000 modeled sublimation simulations for z_0 perturbations for water year 2005 (unperturbed 290 mm), 2011 (unperturbed 276 mm), and 2012 (unperturbed 350 mm).

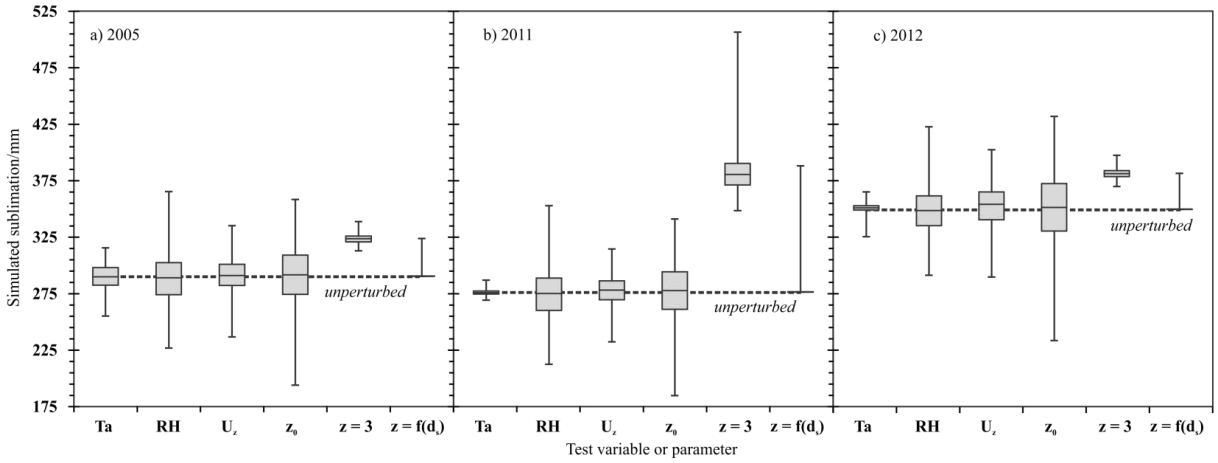

Figure 2.4. Sensitivity statistics by water year a) 2005, b) 2011, and c) 2012 for the Monte Carlo simulation from uniformly perturbing input sublimation variables and parameters (see Table 2). The unperturbed sublimation is shown as a dotted line for each water year.

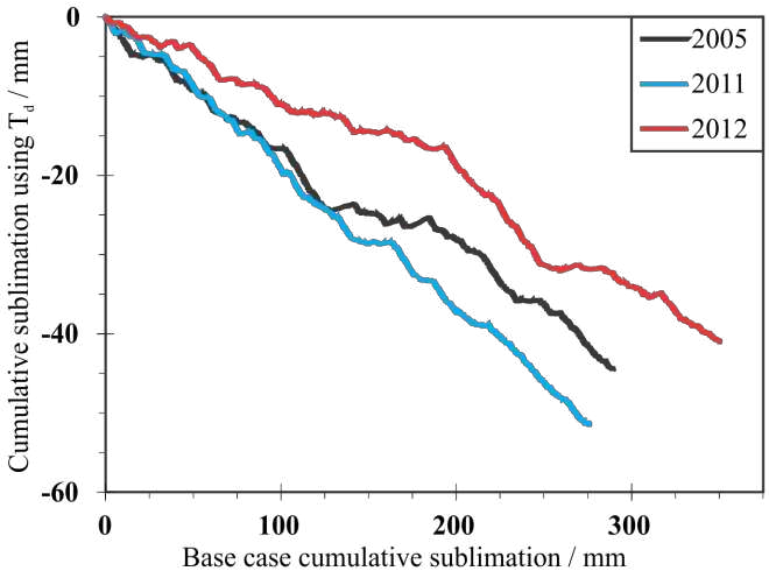

Figure 2.5. Comparison of the estimated cumulative sublimation using dewpoint temperature as the surface temperature (T_s) versus the base case, using air temperature to estimate T_s for the study winters of 2005, 2011, and 2012.

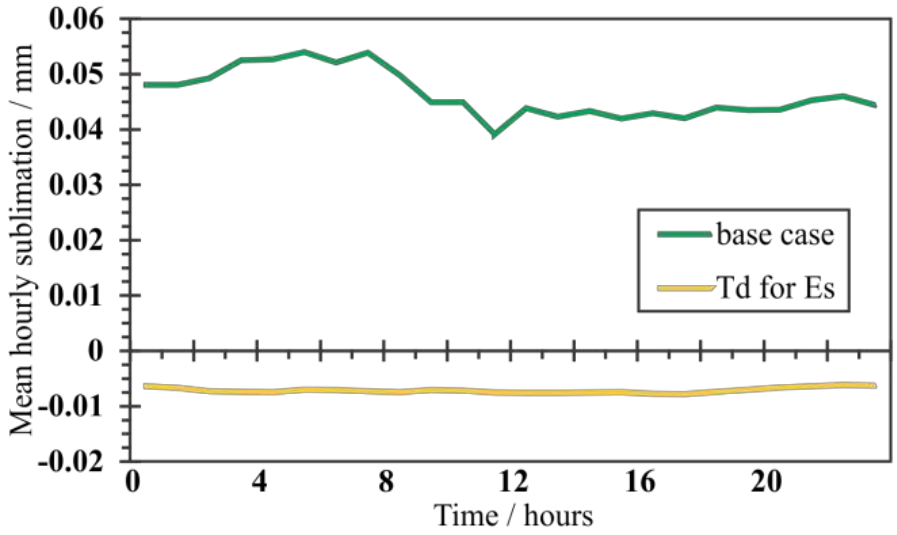

Figure 2.6. Mean hourly computed sublimation for the base case with air temperature (see x-axis in Figure 2.5) and using the dewpoint temperature (see y-axis in Figure 2.5).

REFERENCES

Andreas EL (2002). Parameterizing Scalar Transfer over Snow and Ice: A Review. Journal of Hydrometeorology, 3: 417-432

Bernier P, Edwards GC (1989). Differences between air and snow surface temperatures during snow evaporation. Eastern Snow Conference Proceedings, 46: 117-120

Bliss A, Cuffey K, Kavanaugh J (2011). Sublimation and surface energy budget of Taylor Glacier, Antarctica. Journal of Glaciology, 57(204), 684-696, doi:10.3189/002214311797409767

Bowling LC, Pomeroy JW, Lettenmaier DP (2004). Parameterization of Blowing-Snow Sublimation in a Macroscale Hydrology Model, Journal of Hydrometeorology, 5: 745-762

Box JE, Steffen K (2001). Sublimation estimates for the Greenland ice sheet using automated weather station observations. Journal of Geophysical Research, 106(D24): 33965-33982

Brock BW, Willis IC, Sharp MJ (2006). Measurement and parameterization of aerodynamic roughness length variations at Haut Glacier d'Arolla, Switzerland. Journal of Glaciology, 52(177): 281-297, doi: 10.3189/172756506781828746

Cline D (1997a). Snow surface energy exchange at a continental, mid-latitude alpine site. Water Resources Research, 33: 689-701

Cline D (1997b). Effect of seasonality of snow accumulation and melt on snow surface energy exchanges at a continental alpine site. Journal of Applied Meteorology, 36(1): 32-51

Datt P (2011). Latent Heat of Sublimation. In: (eds., Singh V.P., Singh P., Haritashya U.K.) Encyclopedia of Snow, Ice and Glaciers, Encyclopedia of Earth Sciences Series, Springer, Dordrecht

Dingman, SL, (2002). Physical Hydrology. Second edition, Prentice Hall, Upper Saddle River, New Jersey, 646 pp.

Fassnacht SR (2004). Estimating Alter-shielded gauge snowfall undercatch, snowpack sublimation, and blowing snow transport at six sites in the coterminous USA. Hydrological Processes, 18: 3481-3492, doi:10.1002/hyp.1408

Fassnacht SR (2010). Temporal changes in small scale snowpack surface roughness length for sublimation estimates in hydrological modeling. Cuadernos de Investigación Geográfica (Journal of Geographical Research), 36(1): 43-57, doi: 10.18172/cig.1226

Graham CB, Verseveld W, Barnard HR, McDonnell JJ (2010). Estimating the deep seepage component of the hillslope and catchment water balance within a measurement uncertainty framework, Hydrological Processes, 24, 3631-3647

Hastings WK (1970) Monte Carlo sampling methods using Markov chains and their applications. Biometrika, 57(1): 97-109

Hollinger DY, Richardson AD (2005). Uncertainty in eddy covariance measurements and its application to physiological models. Tree Physiology, 25: 873-885

Hood E, Williams M, Cline D (1999). Sublimation from a seasonal snowpack at a continental mid-latitude alpine site. Hydrological Processes, 13: 1781-1797

Hultstrand DM (2006). Geostatistical Methods for Estimating Snowmelt Contribution to the Seasonal Water Balance in an Alpine Watershed. Unpublished Master of Science Thesis, Watershed Science Program, Colorado State University, 130 pp

Hunsaker CT, Whitaker TW, Bales RC (2012). Snowmelt runoff and water yield along elevation and temperature gradients in California's Southern Sierra Nevada. Journal of the American Water Resource Association, 48: 667-678, doi:10.1111/j.1752- 1688.2012.00641.x

Kattelmann R, Elder K (1991). Hydrologic characteristics and water balance of an alpine basin in the Sierra Nevada. Water Resources Research, 27(7): 1553-1562

Korfmacher JL, Hultstrand DM (2006). Glacier Lakes Ecosystem Experiments Site (GLEES) hourly meteorological tower data: 1989-2005. U.S. Department of Agriculture, Forest Service, Rocky Mountain Research Station, Fort Collins, CO

Lang H (1981). Is evaporation an important component in high alpine hydrology? Nordic Hydrology, 12: 217-224

Liston GE, Elder K (2006a). A meteorological distribution system for high-resolution terrestrial modeling (MicroMet). Journal of Hydrometeorology, 7(2): 217-234

Liston GE, Elder K (2006b). A distributed snow-evolution modeling system (snowmodel). Journal of Hydrometeorology, 7(6): 1259-1276

Marks D, Dozier J (1992). Climate and energy exchange at the snow surface in the alpine region of the Sierra Nevada. Water Resources Research, 28(11): 3043-3054

Marks D, Dozier J, Davis RE (1992). Climate and energy exchange at the snow surface in the alpine region of the Sierra Nevada: Meteorological measurements and monitoring. Water Resources Research, 28(11): 3029-3042

Marks D, Kimball J, Tingey D, Link T (1998). The sensitivity of snowmelt processes to climate conditions and forest cover during rain-on-snow: A study of the 1996 Pacific Northwest flood. Hydrological Processes, 12: 1569-1587

Marks D, Cooley KR, Robertson DC, Winstral A (2001). Long-term snow database, Reynolds Creek Experimental Watershed, Idaho, USA. Water Resources Research, 37: 2835-2838

Marks D, Reba M, Pomeroy J, Link T, Winstral A, Flerchinger G, Elder K (2008). Comparing simulated and measured sensible and latent heat fluxes over snow under a pine canopy. Journal of Hydrometeorology, 8: 1506-1522, doi: 10.1175/2008JHM874.1

Molotch NP, Blanken PD, Williams MW, Turnipseed AA, Monson RK, Margulis SA (2007). Estimating sublimation of intercepted and sub-canopy snow using eddy covariance systems. Hydrological Processes, 21: 1567-1575, doi: 10.1002/hyp.6719

Moore RD (1983). On the use of the bulk aerodynamic formulae over melting snow. Nordic Hydrology, 14: 193-206

Musselman RC (1994). The Glacier Lakes Ecosystem Experiments Site. Rocky Mountain Forest and Range Experiment Station, General Technical Report RM-249, 94 pp

Ohmura A (1981). Climate and energy balance on arctic tundra, Axel Heiberg Island, Canadian Arctic Archipelago, Spring and Summer 1969, 1970 and 1972. Zürcher Geographische

Schriften, 3, Dept. of Geography, Swiss Federal Institute of Technology (ETH), Zürich, 447 pp

Pan M., et al. (2003). Snow process modeling in the North American Land Data Assimilation System (NLDAS): 2. Evaluation of model-simulated snow water equivalent. Journal of Geophysical Research, 108(D22): 8850, doi:10.1029/2003JD003994

Phillips M (2013). Estimates of sublimation in the Upper Colorado River basin. Unpublished Master of Science Thesis, Department of Atmospheric Science, Colorado State University, 57pp, < http://hdl.handle.net/10217/81052>

Pomeroy JW, Essery RLH (1999). Turbulent fluxes during blowing snow: field tests of model sublimation predictions. Hydrological Processes, 13: 2963-2975

Pomeroy JW, Bewley D, Essery RH, Hedstrom N, Link T, Granger R, Sicart J, Ellis C, Janowicz JR (2006). Shrub tundra snowmelt. Hydrological Processes, 20: 923-941

Raleigh MS, Landry CC, Hayashi M, Quinton WL, Lundquist JD (2013). Approximating snow surface temperature from standard temperature and humidity data: New possibilities for snow model and remote sensing evaluation. Water Resources Research, 49: 8053-8069

Reba ML, Pomeroy J, Marks D, Link TE (2012). Estimating surface sublimation losses from snowpacks in a mountain catchment using eddy covariance and turbulent transfer calculations. Hydrological Processes, 26: 3699-3711

Ryan WA, Doesken NJ, Fassnacht SR (2008). Evaluation of ultrasonic snow depth sensors for U.S. snow measurements. Journal of Atmospheric and Oceanic Technology, 25(5): 667-684

Saucier WJ (1983). Principles of Meteorological Analysis. Dover Earth Science, Mineola, N.Y., 464pp

Sexstone GA, Clow DW, Stannard DI, Fassnacht SR (2016). Comparison of methods for quantifying surface sublimation over seasonally snow-covered terrain. Hydrological Processes, 30: 3373-3389, doi: 10.1002/hyp.10864

Sexstone, G. A., Clow, D. W., Fassnacht, S. R., Liston, G. E., Hiemstra, C. A., Knowles, J. F., and Penn, C. A., 2018. Snow sublimation in mountain environments and its sensitivity to forest disturbance and climate warming. Water Resources Research, 54: 1191–1211, https://doi.org/10.1002/2017WR021172

Sheffield J, et al. (2003). Snow process modeling in the North American Land Data Assimilation System (NLDAS): 1. Evaluation of model-simulated snow cover extent. Journal of Geophysical Research, 108(D22): 8849, doi:10.1029/2002JD003274

Slater AG, et al. (2001). The Representation of Snow in Land Surface Schemes: Results from PILPS 2(d). Journal of Hydrometeorology, 2: 7-24

Stewart BJ (1982). Sensitivity and Significance of Turbulent Energy Exchange over an Alpine Snow Surface. Unpublished Master of Arts thesis, University of California, Santa Barbara, CA

Strasser U, Warscher M, Liston GE (2011). Modeling snow canopy processes on an idealized mountain. Journal of Hydrometeorology, 12(4): 663-677

Svoma BM (2016). Difficulties in Determining Snowpack Sublimation in Complex Terrain at the Macroscale. Advances in Meteorology, 2016, 9695757, doi:10.1155/2016/9695757

Woo M, Marsh P, Pomeroy JW (2000). Snow, frozen soils and permafrost hydrology in Canada, 1995-1998. Hydrological Processes, 14: 1591-1611

Wooldridge GL, Musselman RC, Sommerfeld RA, Fow DG, Connell BH (1996). Mean wind patterns and snow depth in an alpine-subalpine ecosystem as measured by damage to coniferous trees. Journal of Applied Ecology, 33: 100-108

CHAPTER 3.0 - SIMULATED SNOWPACK BASED ON A CLIMATOLOGICAL SNOW DISTRIBUTION PATTERN AND WINTER SEASON INDEX

3.1 Summary

In mountainous regions of the western United States, the majority of annual precipitation falls as snow and is stored in high-elevation snowpacks. Mountain snowfall can be stored on the surface for time periods ranging from hours to months before melting and continuing through the hydrologic cycle. In high-elevation seasonally snow-covered basins, obtaining accurate estimates of the amount of water contained within the snowpack is important for the purposes of river and flood forecasting, and in terms of correctly representing the inputs into a snow-dominated system. In snow dominated regions it is important to gain an understanding of precipitation quantity, variability, and the distribution. Mountain topography can produce complex patterns of snow distribution, controls snow accumulation, and snow ablation. Accurate estimates of winter precipitation, distribution, and ablation are fundamental toward understanding watershed processes in mountainous regions.

The interaction of topography and consistent meteorological patterns tend to generate similar snow depth distribution patterns form year to year. As a result of these interactions, it is hypothesized that deep and shallow regions of snow depth are repeatable and scalable. In this study, we question whether snow depth patterns near peak accumulation are consistent for a 10-year time frame and whether limited snow depth measurement years can be used to accurately represent snow depth distribution and basin mean snow depth. We use 10 years of snow depth measurements collected near peak accumulation in West Glacier Lake watershed, Wyoming to analyze snow depth patterns controlled by meteorologic and topographic interactions. Generalized Additive Models (GAMs) combined with topographic variables and snow depth

measurements were used to estimate snow depth distribution and a snow depth climatological pattern with high levels of accuracy. The near peak snow depth patterns were identified as repeatable with an average annual correlation estimate equal to 0.83; the winter season index provide a method to scale and quantify annual snow depth within West Glacier Lake watershed.

3.2 Introduction

In snow-dominated watersheds, it is important to understand the quantity, variability, and distribution of snow, as the snow is an important water storage for downstream purposes (Doesken and Judson, 1997). In mountainous terrain, one of the most apparent characteristics of the snowpack is its spatial heterogeneity (McKay and Gray, 1981; Pomeroy and Gray, 1995; Elder et al., 1991; Molotch et al., 2005; Elder et al., 2009; Fassnacht et al., 2018; Mott et al., 2018). Mountain topography can produce complex patterns of snow distribution, control snow accumulation, and snow ablation (Elder and Dozier, 1990). The snowfall deposition and snowmelt patterns are a result of consistent interactions between the localized meteorology and terrain (Pflug and Lundquist, 2020). The resultant distribution of snow often has a similar pattern from year to year (Grayson et al., 2002; Sturm and Wagner, 2010) based on topography, canopy, if present, and wind characteristics, i.e., speed and direction (Winstral et al., 2002; Erickson et al., 2005). These distribution patterns and the associated topography (and canopy) dictate further distribution and ablation processes (Revuelto et al., 2014) that dictate peak streamflow out of the basin (Fassnacht et al., 2014), baseflow characteristics (Godsey et al., 2014), and groundwater recharge (Carroll et al., 2019).

Various studies have focused on identifying the correlation between snow distribution and surrogate topographic variables (Meiman, 1968; Elder et al., 1998; Erxleben et al., 2002;

Winstral et al., 2002; Erickson et al., 2005; Molotch et al., 2005; Fassnacht et al., 2012; Grünewald et al., 2013; Revuelto et al., 2014; Pflug and Lundquist, 2020). These studies identify topography, solar radiation, wind redistribution, slope, aspect, and vegetation as the primary components that control snow depth and snow water equivalent (SWE) variability. Consistent snow patterns are found where fixed controls such as vegetation and topography dominate the region (Sturm and Wagner, 2010).

Grayson et al. (2002) identified the following three distinct ways to identify patterns: (i) "lots of points" (LOP) where there is a sufficiently dense array of point measurements to be interpolated to a pattern, (ii) "binary data" such as remote sensing of snow cover; and (iii) "surrogate data" used to create correlations between the snow and easily established patterns such as topography and vegetation. Where topographic parameters are used to explain the spatial heterogeneity of snow depth, various statistical approaches have been evaluated. The statistical modelling methods include linear regression models (Fassnacht, et al., 2003; Zheng, et al., 2016), multiple linear regression models (Grünewald et al., 2013; Revuelto et al., 2014), binary regression trees (Erxleben et al., 2002; Gleason et al., 2017; Molotch et al., 2005; Winstral et al., 2002), general additive models (López-Moreno, Latron, & Lehmann, 2010; López-Moreno & Nogués-Bravo, 2005), and geostatistical models (Erickson et al., 2005; Molotch et al., 2005; Hultstand, 2006; Fassnacht et al., 2012).

The character of a winter season can be defined by features, including temperature averages and extremes, snowfall totals, snow depth, and the duration winter (Cerruti and Decker, 2011; Mayes Boustead et al., 2015; Vögeli, 2016). A snowfall index (Vögeli, 2016), a snow drift factor (Tarboton and Luce, 2006), a winter season severity index (Mayes Boustead et al., 2015), and a climatological grid index (Sturm and Wagner, 2010) have been used to evaluate and

improve distributed snow models (Grayson and Blöschl, 2001; Hiemstra et al., 2006; Tarboton and Luce, 2006) and suggested that these indices can be applied to consistent snow patterns (Grayson et al., 2002; Erickson et al., 2005; Sturm and Wagner, 2010). Winter season indices allow quantities such as averages, percentiles, and extremes to be calculated to establish a baseline year which individual years can be compared (Mayes Boustead et al., 2015).

Studies have hypothesized that snow accumulation and distribution patterns are consistent over time (Elder er al., 1991; Woolridge et al., 1996; Grayson et al., 2002, Erickson et al., 2005; Deems et al., 2008; Sturm and Wagner, 2010; López Moreno et al., 2015; Pflug and Lundquist, 2020). In this study, we test whether snow depth distribution patterns are consistent over a 10-year period within a sub-alpine basin, West Glacier Lake, in Wyoming and whether limited snow depth measurement years can be used to accurately represent snow depth distribution and basin mean snow depth. The specific questions for this study are the following: (1) do snow depth measurements reveal a consistent snow depth distribution over time, (2) can a snow depth model be developed, (3) what snow depth interpolation model provides the best representation of snow depth distribution, (4) what are the dominant topographic parameters that control snow distribution and do they vary over time, and (5) can a winter season index be developed to quantify basin snow depth.

3.3 Study Site

For this study, snow depth measurements were collected in West Glacier Lake watershed (WGLW) within the Snowy Range Mountains, Wyoming (41°22’30" N latitude and 106°15’30" W longitude) (Figure 3.1a). WGLW is part of the US Forest Service’s Glacier Lakes Ecosystem

Experiments Site (GLEES) developed to conduct research on the effects of atmospheric deposition on alpine and subalpine ecosystems (Musselman, 1994). Approximately 5.75 km^2 in size, GLEES consists of three small watersheds, beneath a northeast-southwest ridge. WGLW is 0.61 km^2 in size, ranges in elevation from 3,277 m at the lake outlet to 3,493 m at the top. The mean annual temperature is -1 °C at the outlet and -2.5 °C at the top of the basin (Korfmacher and Hultstrand, 2006). Mean annual precipitation is 1200 mm, with approximately 75 to 85 % falling as snow, which typically remains from late October to early June (Wooldridge et al., 1996; Korfmacher and Hultstrand, 2006). Large inter-annual and spatial station variability exists between measured precipitation quantities (Hultstrand, 2006), as seen at the five precipitation monitoring stations within 4 km of GLEES: National Atmospheric Deposition Program (NADP) WY00 and WY95, Clean Air Status and Trends Network (CASTNET), GLEES Tower, and Brooklyn Snowpack Telemetry (SNOTEL). This region is dominated by strong westerly winds that range between 0 and 26 m/s with an average of 8 m/s (Korfmacher and Hultstrand, 2006). The topographic and consistent climatic conditions within the region create an optimal environment to evaluate whether snow distributions are consistent over time (Hiemstra et al., 2006).

3.4 DATA and METHODS

3.4.1 Survey Data

Snow depth data were collected across the WGLW from 2005 through 2014, during or close to peak snow accumulation each year (generally late April to early- May) (Figure 3.2) on an approximate 50 m measurement grid similar to the protocol of Hultstrand et al., (2006) (Figure 3.1). Snowpack in the WGLW usually exhibits large spatial variability, and topographic

variables apply a strong control on its distribution. At each snow depth measurement location, either five measurements or three measurements were collected, the snow depth measurements were recorded to the nearest 0.01 m, and the locations recorded with Global Positioning System (GPS) with an approximate accuracy of 5 m. Multiple snow depth measurements were taken to limit the effect of local anomalies related to microtopography, rocks, or other limitations of reaching the ground surface (Fassnacht et al., 2013) and to account for grid size scale uncertainty (Molotch et al., 2005; Fassnacht et al., 2018). The final snow depths values were obtained by averaging the measurements.

The advantage of analyzing a multiyear data set is that it allows for the identification of topographic controls that are significant across years. From measurement years 2005 through 2009, between 400 and 500+ measurement locations were collected; the measured snow depth data contained similar sampling spatial distributions across the entire watershed and measurements had similar summary statistics (mean, standard deviation, and coefficient of variation) for these five years (Figure 3.1; Table 3.1). Compared to the 2005 through 2009 snow depth survey data, the 2010 through 2014 years were limited in the number of measurements recorded with only 100 to 300 measured and the measured locations were not as consistent across the basin, with focus in the lower elevations and flatter terrain (Figure 3.1; Table 3.1). Therefore, the snow depth measurement years were split into two groups for modelling and verification: 1) measurement years 2005 through 2009 were used to test our first objective determine whether a consistent snow depth distribution can be identified and if this snow depth distribution can be quantified and 2) the remaining measurement years 2010 through 2014 were used as verification for limited measurement location years.

3.4.2 Topographic Parameters

The topographic parameters of elevation, solar radiation, slope, northness, aspect, ponding, and maximum upwind slope were considered as an independent variable in snow depth models to improve interpolated estimates (Elder et al., 1998; Lapen and Martz, 1996; Balk and Elder, 2000; Erxleben et al., 2002; Molotch et al., 2005; López-Moreno and Nogués-Bravo, 2006). Vegetation was not used as a predictor due to the limited vegetation within WGLW.

3.4.2.1 Elevation

Precipitation generally increases with elevation due topographic precipitation enhancements (Meiman, 1968; Gray and Male, 1981; Barry, 1992; Roe, 2005). Even in low relief basins, small changes in elevation can alter snow distribution processes through wind scour and deposition. A 5 m DEM was generated by the US Forest Service (USFS) based on infrared and aerial photographs. The 5 m DEM was used to derive all WGLW topographic variables.

3.4.2.2 Slope

Slope is considered to be an important terrain feature affecting the snow depth distribution (McClung and Schaerer, 1993). In topographically similar terrain, snow depth can be exposed to high wind shear forces, a slope that is oriented toward the mean wind direction tends to have a decrease in snow depth (Gray and Male, 1981). Slope was calculated within ArcGIS® (ESRI, 2020), using the Spatial Analyst Tool based on the 5 m DEM. The slope function calculates the maximum rate of change between each cell and its neighbors, every cell in the

output raster has a slope value. The lower the slope value, the flatter the terrain; the higher the slope value, the steeper the terrain.

3.4.2.3 Northness

Northness is commonly considered a substitute for solar (Molotch et al., 2005). Northness was used in this study and was calculated as the product of the cosine of the aspect and the sine of the slope (Molotch et al., 2005). Northness is also considered to be a stable variable over long periods of time.

3.4.2.4 Aspect

Aspect has been attributed with melt effect (Meiman, 1968). The exposure of the slope aspect to the sun can affect solar radiation inputs, which in turn controls snowpack temperature and stability (Barry, 1992; Deems, 2002). Aspect is also considered to be a stable variable over long periods of time. Aspect was calculated within ArcGIS® (ESRI, 2020), using the Spatial Analyst Tool based on the 5 m DEM. The aspect function identifies the steepest downslope direction from each cell to its neighbors, the value of each indicates the direction the cell's slope faces.

3.4.2.5 Solar Radiation

An index of daily incoming direct solar radiation was modelled for each pixel in WGLW. Solar Analyst, an ArcGIS® GIS extension, computes direct, diffuse, global radiation, and direct radiation duration, sunmaps and skymaps, and viewsheds was used for the modelling solar radiation following Fu and Rich (2000). The required inputs for Solar Analyst were elevation, slope, and aspect grids.

Solar radiation was calculated for the basin for the 15th of each month from December to April. The average monthly value for the five dates was used as an index of direct solar radiation during the accumulation season. Previous research has calculated a solar radiation index using similar methods (Elder et al., 1998; Erxleben, 2002; Molotch et al. 2005).

3.4.2.6 Ponding

Water ponding depths, a variable used to delimit drainage paths and depressions, can be significant for snow accumulation in windswept landscapes (Whiting and Kiss, 1987; Lapen et al., 1996). Water ponding represents the depth (m) of surface depression on the surface in regards to the surrounds in elevation (Lapen et al., 1996).

3.4.2.7 Maximum Upslope Wind

Strong winds interact with local topography and are critical to the creation of heterogeneous snow depth distribution, often cited as one of the dominant influences on snow accumulation and distribution (Elder et al., 1991; Luce et al. 1998; Winstral et al., 2002; Molotch

et al., 2005; Hiemstra et al., 2006; Revuelto et al., 2014). Accounting for wind interactions is a crucial process to aid in the understanding of snow distribution and snow variability. In order to capture this process, a wind shelter index (Winstral and Marks, 2002) was used to aid in the modelling of snow depth distribution. The maximum upwind slope parameter (S*x*), defined by Winstral and Marks (2002) is:

$$Sx_{A,dmax}(x_i y_i) = \max\left(tan^{-1}\left[\frac{ELEV(x_v y_v) - ELEV(x_i y_i)}{((x_v - x_i)^2 + (y_v - y_i)^2)^{0.5}}\right]\right), \qquad \text{equation 3.1}$$

where *A* is the Azimuth of the search direction, *dmax* is lateral search distance, (x_i,y_i) are the coordinates of the cell of interest, and (x_v,y_v) are the set of cell coordinates located along the line segment defined by (x_i,y_i), *A*, and *dmax*. Negative *Sx* values indicate exposure relative to the shelter-defining pixel (i.e. the cell of interest is higher than the shelter defining pixel).

Averaging the Sx value across the upwind direction is shown to be more robust to both natural and systematic deviations (Winstral and Marks, 2002). The mean maximum upwind slope parameter ($\overline{Sx}$), defined by Winstral and Marks (2002) is:

$$\overline{Sx}_{\overline{A},dmax}(x_i, y_i)|_{A_1}^{A_2} = \frac{1}{n_v}\sum_{A=A_1}^{A_2} Sx_{A,dmax}(x_i, y_i), \qquad \text{equation 3.2}$$

where A_1 and A_2 define the outer limits of the upwind directions, $\overline{A}$ bisects A_1 and A_2, and n_v is the number of search vectors in the window defined by A_1 and A_2.

3.4.3 Interpolation Methods

In this study, we compare three commonly used interpolation methods (Binary Regression Tree, Multiple Linear Regression, and Generalized Additive) that are applied in snow depth distribution research to assess their capacity to estimate the snow depth distribution. The calibration measurement years 2005 through 2009 were used to assess the three interpolation methods (Table 3.1). To assess the accuracy of the interpolation methods, cross-validation was used to compare the estimated values with the observed. The predicted snow depth values were used to calculate error estimates (Willmott, 1982), such as mean absolute error (MAE), root mean squared error (RMSE), and Willmott's index of agreement (D) statistics.

3.4.3.1 Binary Regression Tree

Binary regression tree method was selected for the ease of calculation, interpretation of results, and due to previous success in snow distribution studies (Balk and Elder, 2000; Erxleben et al., 2002; Molotch et al., 2005, Fassnacht et al., 2013; Fassnacht et al., 2018). Binary regression tree models predict dependent variables from a group of independent variables in a non-linear hierarchical manner through a series of binary decisions (Breiman et al., 1984). Snow depth data are often related to independent variables in a non-linear and hierarchical manner, thus binary regression trees provide an alternative to linear and non-additive models (Erxleben et al., 2002; Molotch et al., 2005). Increasing homogenous subsets of data were binned together through binary recursive partitioning. Detailed explanation of binary regression tree fitting, pruning, and cross-validation can be found in Breiman et al., (1984), Elder et al., (1995), and Balk and Elder (2000). The tree model with the lowest deviance and highest coefficient of determination (r^2) using a combination of topographic variables was selected.

3.4.3.2 Multiple Linear Regression

Multiple Linear Regression (MLR) models were selected for the ease of calculation and interpretation and due to previous success in snow distribution studies (Fassnacht et al., 2003; Yang et al. 2003; Razi and Athappilly 2005, Marofi et al., 2011; Grünewald et al., 2013; Revuelto et al., 2014). MLR models model non-linear relationship between a dependent variable and one or more independent variables. Unlike traditional linear regression, which is restricted to estimating linear models, MLR can estimate models with arbitrary relationships between independent and dependent. A MLR model was used between physiographic variables and snow depth. Initially, each variable was assessed with respect to its relationship to snow depth and the variable with the largest correlation selected. A stepwise procedure following the protocol of Fassnacht et al. (2003) was repeated until the addition/removal of new variables no longer increased the correlation coefficient. The MLR model with the lowest deviance and highest coefficient of determination (r^2) using a combination of topographic variables was selected.

3.4.3.3 Generalize Additive Model

Generalized Additive Model (GAM) methods were selected for the ease of calculation, the ability to capture non-linear interactions, and due to previous success in snow distribution studies (López-Moreno and Nogués-Bravo, 2005; López-Moreno and Nogués-Bravo, 2006; López-Moreno et al., 2010; Björk, 2016). GAMs are non-parametric extensions of linear model regressions that apply non-parametric smoothing functions to each predictor and additively calculate the component response (Hastie and Tibshirani, 1987; López-Moreno and Nogués-Bravo, 2005). GAM regression supports non-Gaussian error distributions and non-linear relationships between response and predictor variables.

3.4.4 Standardized Snow Depth Distribution

Our study focused on the repeatability of snow depth distribution using the modeled snow depth distributions and observed snow depth measurement locations across WGLW from different years. We examined the modeled snow depth distributions to the observations snow depth data in order to correlate snow depth patterns from different years. The modeled snow distributions for different measurement years with different snow depth magnitudes were standardized by the snow depth measurement locations snow depth mean. The standardized snow depth values (SDV) were calculated based on methods in Sturm and Wagner (2010):

$$SDV_i = \frac{d_i}{\mu_{d,y}}, \qquad \text{equation 3.3}$$

where d_i is the modeled snow depth at grid cell i, μ_d is the survey snow depth measurement locations mean snow depth for year y. From the 2005 through 2009 SDV patterns we developed a climatological snow distribution pattern (CSDP) by calculating the arithmetic mean of five survey patterns (Sturm and Wagner, 2010).

3.4.5 Climatological Snow Distribution Pattern Uncertainty

To quantify the uncertainty due to grid-scale variability of the estimated SDV grids that were used to estimate the CSDP, we conducted a Monte Carlo analysis that used repeated random sampling of input variables to calculate a distribution of output variables. Monte Carlo methods utilize computational algorithms to model the probability of different outcomes in a process that cannot easily be predicted due to the intervention of random variables and/or uncertainty (Hastings, 1970). We repeat the random sampling process 2000 times, resulting in a

distribution of CSDP values based on the mean and standard deviation of the scaled snow depth grids. The Monte Carlo analysis provided a range of uncertainty and confidence for the calculated CSDP.

3.4.6 SNOTEL Data And Winter Season Index

The Natural Resources Conservation Service (NRCS) operates a snow pillow sensor at the Brooklyn Lake SNOTEL site. Table 3.4 shows the SWE and snow depth measured at the SNOTEL site obtained from the USDA NRCS Web site (https://www.wcc.nrcs.usda.gov) during the snow depth measurement dates compared to the WGLW mean measurement depth. The WGLW measurements occurred near peak SWE date (Figure 3.2). The Brooklyn Lake SNOTEL site is within 2-km of WGLW, these data are investigated as an index to scale the SDV distribution within a WGLW.

A winter severity index was estimated based on the correlation between mean snow depth measurements by year to Brooklyn Lake SNOTEL SWE and snow depth data following methods discussed in Erickson et al. (2005) and Mayes Boustead et al. (2015). The winter snow depth severity index was applied to the CSDP to provide a direct scaling of snow depth distribution for WGLW. The scaled snow depth was calculated by:

$$SD_i = CSDP_i * WSD_{index,y}, \qquad \text{equation 3.4}$$

where SD_i is the normalized snow depth at grid point i, $CSDP_i$ is climatological snow distribution pattern snow depth at grid point i, and $WSD_{index,y}$ is the winter snow depth season index for year y. The modeled snow depth scaling method is similar to the lidar modeled snow depth scaling described by Pflug and Lundquist (2020).

3.5 Results

3.5.1 Survey Data

A multi-year data set of 3382 snow depth measurements (mean of 3 or 5 depth measurements per location) (Figure 3.1) was used to model snow depth distribution. This data set was large in terms of number of snow depth measurements and the number of years compared to other field surveys (Table 3.2). The number of snow depth measurement locations ranged from a low of 118 measurements in 2011 to a high of 538 measurements in 2005 (Table 3.1). Summary statistics for the ten years of snow depth measurements were calculated (Table 3.1). The spatial extent of field measurements varied from year to year as a function of the number and experience of field personnel, weather conditions and safety considerations. The snow depth mean sampling resolution was 50 m. The measured snow depth locations in a yearly data set ranged from 0 to 505 cm with the yearly mean snow depth between 173 to 285 cm (Table 3.1). The coefficient of variation for snow depth measurements in a yearly data set ranged from 0.37 to 0.62, which is within the range of 0.33 to 0.63 reported by Elder et al. (1991) for three snow depth surveys near maximum accumulation (1986–1988).

3.5.2 Model Selection

Three interpolation models were used to estimate the dependent variable of snow depth from a group of seven independent topographic variables. We used the 2006 snow depth data set to evaluate the performance and spatial accuracy of the three interpolation methods. The cross-validation error estimates indicate the high predictive ability of non-linear relationships in snow

depth distribution for the GAM, the MAE, RMSE, and D were 68 cm, 86 cm, and 0.72 respectively with a basin mean snow depth of 197 cm (Figure 3.3a, Table 3.3). The MLR model provided a decent estimation of the snow depth distribution, did not adequately represent wind redistribution in around the lake region but provided a good range of snow depth estimates, the MAE, RMSE, and D were 86 cm, 103 cm, and 0.396 respectively with a basin mean snow depth of 190 cm (Figure 3.3b; Table 3.3). The pruned ten node binary regression-tree model provided a poor estimation of the observed snow depth distribution, did not adequately represent wind redistribution and topographic variables in around the lake region, and provided limited range of snow depth estimates the MAE, RMSE, and D were 86 cm, 109 cm, and 0.552 respectively with a basin mean snow depth of 196 cm (Figure 3.3c; Table 3.3).

Results from the 2006 test case were similar to López-Moreno and Nogués-Bravo (2005), the binary regression tree model provided an accurate description of the basin mean data but show relatively low predictive capability of the observed spatial pattern, and using MLR and GAM provided more robust estimates. Based on our case study and results in the literature (López-Moreno and Nogués-Bravo, 2005; López-Moreno and Nogués-Bravo, 2006; López-Moreno et al., 2010; Björk, 2016), we applied GAM methodology with topographic variables to simulate snow depth distribution in WGLW.

All seven of the topographic variables were used to identify significant predictors of snow depth in the WGLW for the 2005 through 2009 calibration years (Table 3.4). Slope was statistically significant in all five calibration years, with elevation and aspect being significant in four and three years, respectively (Table 3.4). Ponding was somewhat significant ($p<0.1$) in three years and significant in one year (Table 3.4). The other variables were significant or somewhat significant in two years.

Topographic variables that were significant ($p < 0.05$) (Table 3.4) in two or more calibration years, elevation, slope, aspect, and maximum upwind slope (and all significant in 2006), were selected to model snow depth distribution independently for each of the five calibration years. To illustrate the ability of GAMs to capture non-linear correlations, the GAM response curves for measurement year 2006 and 2008 are shown to highlight the effects the topographic variables elevation, slope, aspect, and maximum upwind slope have on snow depth in WGLW (Figure 3.4).

3.5.3 Standardized Snow Depth And Pattern Repeatability

Similarity between the individual years model SDV is visually striking (Figure 3.5): the deepest snow was always on the east facing slopes, the shallowest snow on west facing slopes and across WGLW (Figure 3.5). The five years of SDV data (Figure 3.5) were used to develop the CSDP, (Figure 3.5f) by calculating the arithmetic mean of five SDV grids. The Monte Carlo analysis provided a sensitivity of the normalized basin mean snow depth (1.038), the Monte Carlo mean snow depth result was within 1% but estimated a larger range in SDV variability. The snow depth pattern repeatability (r) was calculated as the Pearson's correlation coefficient between the CSDP and induvial years SDV (Figure 3.6). The basin mean snow depth pattern repeatability (r) ranged from 0.78 to 0.88 with a mean of 0.83, which is within the range of 0.70 to 0.89 reported by Pflug and Lundquist (2020) (Figure 3.6). The highly correlated snow depth pattern repeatability (r) is critical because it means that estimated CSDP can be used to simulate snow depth distribution patterns with a reasonable degree of confidence (Sturm and Wagner, 2010; Pflug and Lundquist, 2020).

3.5.4 Snow Season Index

The WGLW survey dates are shown with the daily snow depth and SWE for March 1 through May 31 at Brooklyn Lake SNOTEL (Figure 3.2). In regard to snow depth, five of the survey dates occurred on above normal (median) years, five occurred on below normal years, one measured year (2011) was above the 90th percentile, and one measured year (2012) was below the 10th percentile (Figure 3.2a). In regard to SWE, six of the survey dates occurred on above normal (median) years, four occurred on below normal years, one measured year (2011) was above the 90th percentile, and one measured year (2012) was below the 10th percentile (Figure 3.2b).

Brooklyn Lake SWE and the WGLW snow depth measurement locations mean were correlated for (a) the ten measurement years ($r^2 = 0.64$) and (b) the five calibration measurement years (r^2 0.18) (Figure 3.7a; Table 3.5). Brooklyn Lake snow depth and the WGLW snow depth measurement locations mean snow were correlated for (a) the ten measurement years ($r^2 = 0.75$) and (b) the five calibration measurement years (r^2 0.69) (Figure 3.7b; Table 3.5). The Brooklyn Lake snow depth to the WGLW snow depth measurement locations mean correlation (Figure 3.7b) was used as the winter season index because it produced accurate and more robust estimations.

3.5.5 Snow Depth Simulation

The combined winter season index, the CSDP, and the WLGW snow depth measurements estimated the WGLW snow distribution (Figure 3.8; Table 3.5) with a high degree of accuracy. The mean simulated to observed basin snow depth difference and percent difference for the ten years were 8 cm and 5% respectively (Table 3.5). The snow depth simulation

estimates during extreme years, below normal year 2012 and above normal year 2011, were captured extremely well with the basin mean difference and percent difference within 10 cm and 5% respectively (Table 3.5).

The snow depth measurement locations distribution had larger snow depth variability that ranged from 0 to 500+ cm (Figure 3.9a), whereas the simulated snow depth distribution had less variability that ranged from 50 to 485 cm (Figure 3.9b). The basin mean snow depths were typically within 10% (Figure 3.9; Table 3.5).

Simulated basin mean snow depth was above the snow depth measurement mean for the five data intense years (Figure 3.10), and above the snow depth measurement mean for eight of the ten measurement years (Figure 3.10). For measurement years 2010 and 2012, the snow depth measurement location means were larger than the simulated mean snow depth. For these two years, the snow depth measurement locations where focused in the lower portion of the basin around Wet Glacier Lake (Figure 3.1g,i). Measurement year 2012 collected snow depth measurement locations in higher regions of WGLW (Figure 3.1i), this provided a better estimated measurement mean compared to the simulated basin mean (Figure 3.10). Results indicate a positive bias of the basin mean snow depth estimate when snow depth measurement locations are only measured in lower elevations around West Glacier Lake.

3.6 Discussion

In this study, snow depth sampling in WGLW followed Grayson et al. (2002) LOP sampling method to identify snow depth spatial patterns. Snow depth measurements in WGLW (Figure 3.1) were numerous with 3382 collected over 10 years (Table 3.1; Table 3.2). The snow

depth measurement periods captured normal snow depth years and record dry (2012) and wet years (2011) (Figure 3.2; Figure 3.8 and 3.9). The multi-year snow depth dataset had consistent standard deviations that ranged from 90 to 118 cm, and coefficient of variation that ranged from 0.33 to 0.63 by year, while the mean snow depth varied substantially between years (Table 3.1). Snow distribution within WGLW consisted of drifted and wind scoured patterns that were controlled by persistent westerly winds (Korfmacher and Hultstrand, 2006) and topographic influences (Erickson et al., 2005).

Although labor intensive, the LOP sampling method (Grayson et al., 2002) provided a robust dataset (Elder et al., 1998; Balk and Elder, 2000; Erxleben et al., 2002; Erickson et al., 2005) that was able to confirm consistent snow depth distribution and repeatability (Figure 3.6) with the same accuracy as Airborne Lidar Surveys (ALS) (Pflug and Lundquist, 2020). More advanced snow depth sampling methods, such as ALS (Deems et al. 2008; Deems et al. 2017; Pflug and Lundquist, 2020), may improve spatial sampling footprint (~ 1m) and temporal sampling frequency. However, the ALS survey methods may not be as robust in densely vegetated and high relief regions (Deems et al. 2017).

The complex topography (Figure 3.11) of WGLW plays a dominate role in snow distribution modelling. Spatial interpolation techniques such as binary regression tree models, MLR models, geostatistical models, and GAM methods have been used to estimate snow depth and SWE distribution in complex terrain with considerable results (Balk and Elder, 2000; López-Moreno and Nogués-Bravo, 2005; Molotch et al., 2005; Erickson et al., 2005; López-Moreno et al., 2010; Grünewald et al., 2013; Fassnacht et al., 2013; Revuelto et al., 2014; Björk, 2016). Spatial modelling results were similar to López-Moreno and Nogués-Bravo (2005) in that binary regression tree model provided an accurate description of the basin mean snow depth (Figure 3;

Table 3) but showed relatively low predictive capability, and MLR and GAMs provided more robust estimates (Figure 3.3). In this study, like recent studies (López-Moreno and Nogués-Bravo, 2005; López-Moreno and Nogués-Bravo, 2006; López-Moreno et al., 2010; Björk, 2016), snow depth distribution modelling was performed using GAMs with topographic variables to capture the nonlinear interactions controlling snow depth distribution.

Mountain snow depth distribution is highly variable and typically controlled by meteorologic and topographic variables (Elder and Dozier, 1990; Winstral et al., 2002; Erickson et al., 2005; Pflug and Lundquist, 2020). We identified four topographic variables that influenced snow depth distribution that were significant and consistent among years (Table 3.4); elevation, slope, aspect, and maximum upwind slope (Winstral and Marks, 2002; Winstral et al., 2002) were significant predictors and consistent among years for estimating snow depth distribution within WGLW (Elder et al., 1998; Erxleben et al., 2002; Erickson et al., 2005; Molotch et al., 2005; Revuelto et al., 2014). The slope variable has been found to largely explain the snow distribution in steep terrain related to snow redistribution, avalanches, and as a surrogate for solar radiation (McClung and Schaerer, 1993; Elder et al., 1998; Erxleben et al., 2002), in this study slope was identified as the most significant variable controlling snow depth distribution.

Elevation has been found to largely explain the snow distribution in areas having big elevational differences (Elder et al., 1998; Erxleben et al., 2002; Molotch et al., 2005), or in some cases limited elevational differences (Fassnacht et al., 2018). In this study elevation was the second most significant variable found between snow depth and elevation, with significant correlations occurring in four out of five years. Aspect has been attributed with melt effect (Meiman, 1968) and can influence snowpack temperature, stability and snow distribution (Barry, 1992; Deems, 2002; Erxleben et al., 2002; Fassnacht et al., 2018). Here, aspect was the third

significant variable found between snow depth and elevation. The maximum upwind slope has been found to largely explain the snow distribution in areas of topography that have consistent prevailing winds (Elder et al., 1991; Luce et al. 1998; Winstral et al., 2002; Molotch et al., 2005; Revuelto et al., 2014), as was found in this study.

We modeled snow depth distribution for years 2005 through 2009 with a high degree of accuracy (Figure 3.5; Table 3.3) and repeatability (r = 0.82; Figure 3.6) for the five calibration years. These five years were used to estimate a CSDP for WGLW. To characterize the winter season in regard to precipitation magnitude, we developed a winter season index (r = 0.75; Figure 3.7b) for WGLW based on the nearby Brooklyn Lake SNOTEL station data. Once established, the CSDP (Figure 3.5f) and winter season index (Figure 3.7b) were used to simulate snow depth information for near peak snow accumulation with relatively high confidence for measurement limited years (Figure 3.8 and 3.9; Table 3.5). Simulated mean snow depth to snow depth measurement mean was highly correlated (r^2 = 0.75; Figure 3.10), the simulated dataset did not capture the upper and lower range of snow depth measurement as well (Figure 3.9). This study investigated the assumption of pattern repeatability (Sturm and Wagner, 2010) and a winter season scaling index (Erickson et al., 2005; Mayes Boustead et al., 2015; Vögeli, 2016) to an alpine watershed based using 10 years of snow depth measurement locations with reported results slightly higher and within range of ALS in California (Pflug and Lundquist, 2020).

3.7 Conclusion

This study applied 10 years of near peak snow depth measurements, a general additive model interpolation method, combined with topographic variables to estimate a climatological consistent snow depth pattern that is scalable based on a winter season index. The utility of

GAM interpolation captured the nonlinear interaction of snow depth with topographic variables. The topographic variables of elevation, slope, aspect, and maximum upwind slope were significant predictors of snow depth distribution. The estimated climatological snow distribution pattern and winter season index were able to simulate WGLW snow depth with high accuracy both quantitatively and qualitatively comparable to previous studies.

3.8 Tables and Figures

Table 3.1. Summary of snow depth measurements and statistics for WGL snow surveys.

Sample Year	Number of Samples	Mean Depth, cm	Standard Deviation, cm	Coefficient of Variation
2005	538	182	98	0.54
2006	395	176	105	0.60
2007	520	198	107	0.54
2008	407	217	104	0.48
2009	408	204	90	0.44
2010	182	266	98	0.37
2011	118	285	118	0.42
2012	255	173	107	0.62
2013	294	195	102	0.52
2014	265	226	99	0.44

Table 3.2. Summary of snow depth measurements from selected snow distribution studies (modified from Erickson et al., 2005 and Clark et al., 2011).

Reference	Location	Basin Area (km^2)	Years Sampled	Depth Samples
Elder et al. (1991)	Emerald Lake Basin, California	1.2	3	2048
Elder et al. (1998)	Blacktop Basin, California	92.8	1	700
Balk and Elder (2000)	Loch Vale, Colorado	6.9	2	370
Erxleben et al. (2002)	three sites, Colorado	6.0	1	1650
Stähli et al. (2002)	Erlenbach, Switzerland	0.7	2	853
Erickson et al. (2005)	Green Lakes Valley, Colorado	2.3	7	3235
Sturm and Wagner (2010)	Imnavait Creek, Alaska	6.0	12*	21637
This study	*West Glacier Lake, Wyoming*	*0.6*	*10*	*3382*

* multiple sampling periods within a year; two intensive sampling years

Table 3.3. The mean absolute error (MAE), root-mean square error (RMSE) and Wilmott's index of agreement (D) cross validation estimates for sample year 2006 interpolation.

	GAM	Linear	Regression Tree
MAE	68	86	86
RMSE	86	103	109
D	0.715	0.396	0.552

Table 3.4. Summary of topographic variables for GAM snow depth model. WGL snow depth was modeled with the topographic variables of elevation, slope, aspect, and maximum upwind slope.

Sample Year	Elevation	Solar Radiation	Slope	Northness	Aspect	Ponding	Maximum Upwind Slope
2005	***	+	***			+	
2006	***		*		***	+	*
2007	*	*	**		***	**	
2008	***		**	+	***	+	
2009			*	+			**

*** is for $p \leq 0.001$; ** is for $p \leq 0.01$; * is for $p \leq 0.05$; + is for $p<0.1$

Table 3.5. Summary of snow depth measurements for WGL snow surveys, concurrent Brooklyn Lake SNOTEL snow depth and SWE measurements, and simulated snow depth statistics. The difference and percent difference are calculated from the sample basin mean depth to the simulated basin mean depth.

Sample Year	Sample Depth, cm	Brooklyn Lake SWE, mm	Brooklyn Lake Snow Depth, cm	Simulated Snow Depth, cm	Difference, cm	Percent Difference
2005	182	424	117	187	5	3%
2006	176	615	147	206	30	17%
2007	198	528	152	209	11	6%
2008	217	612	180	227	10	5%
2009	204	663	175	224	20	10%
2010	266	615	180	227	-39	-15%
2011	285	1067	287	295	10	4%
2012	173	351	91	170	-3	-2%
2013	195	516	157	212	17	9%
2014	226	792	208	245	19	8%

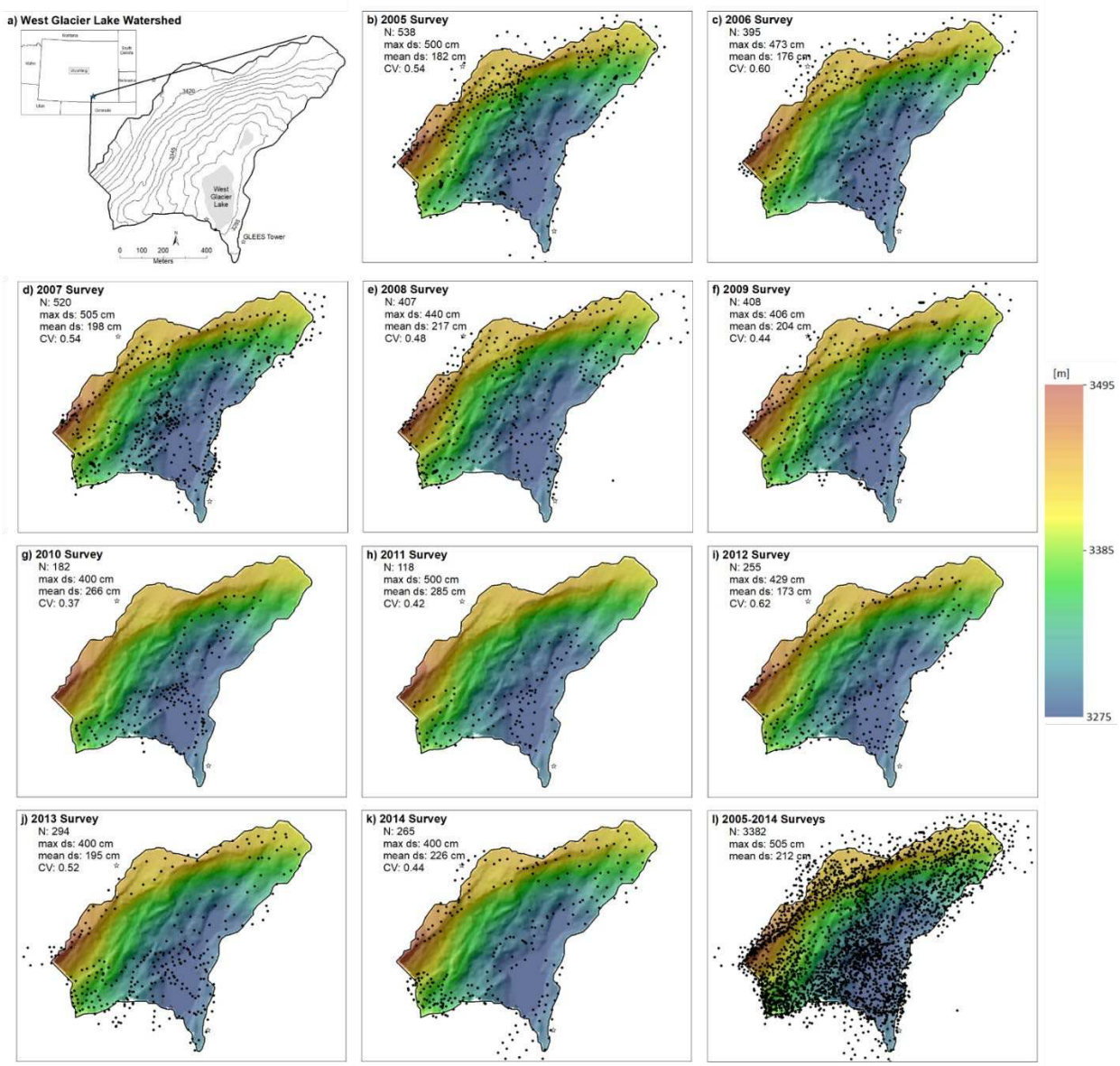

Figure 3.1. Topographic map of West Glacier Lake watershed (a). Snow depth sample locations and summary statistics for sample year (b) 2005, (c) 2006, (d) 2007, (e) 2008, (f) 2009, (g) 2010, (h) 2011, (i) 2012, (j) 2013, (k) 2014, and (l) all year locations (n=3382).

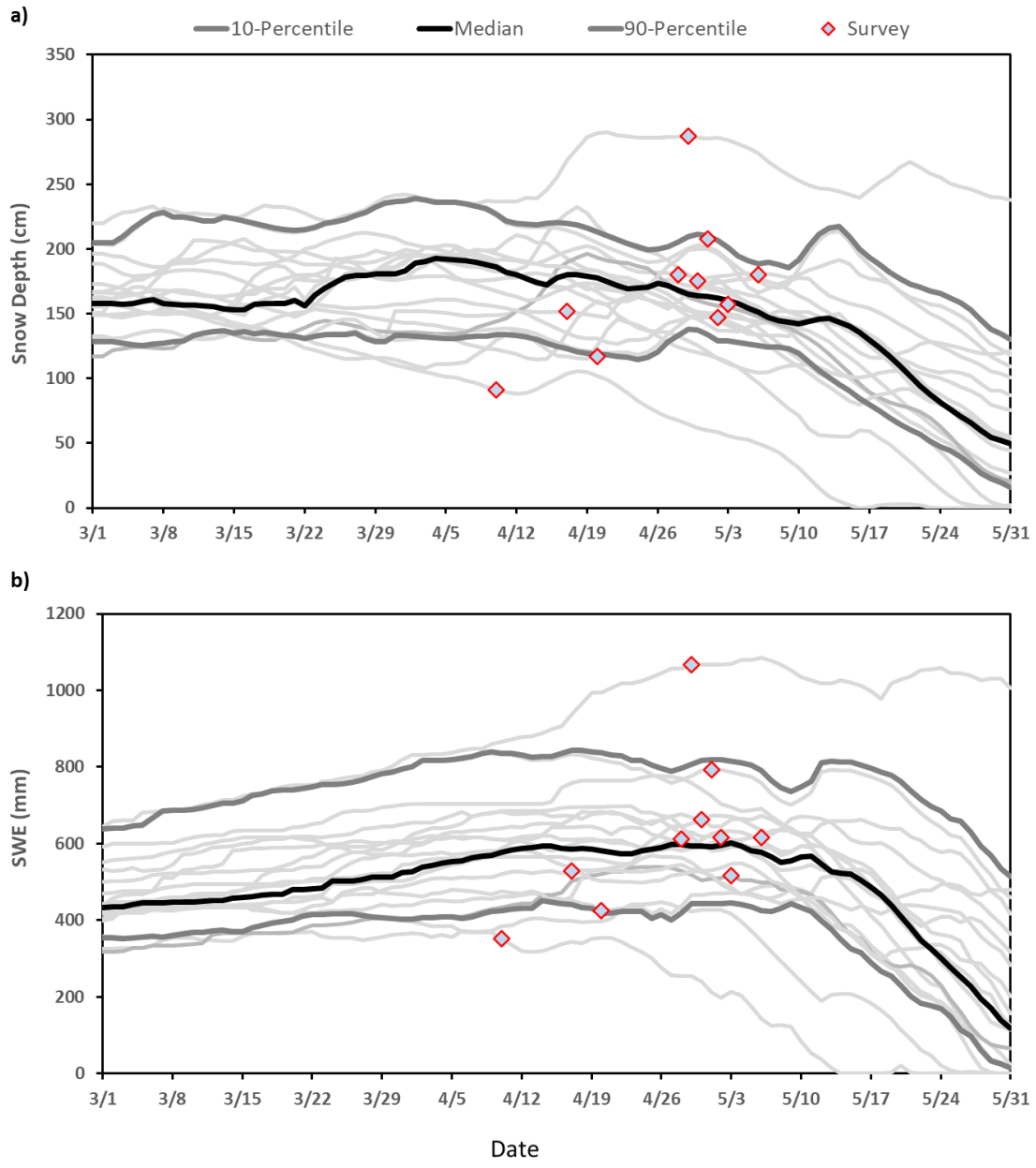

Figure 3.2. Snow survey dates plotted on top of a) snow depth and b) SWE data from the Brooklyn Lake SNOTEL site for years 2005 through 2020. The red symbols are the survey dates and associated SNOTEL date values.

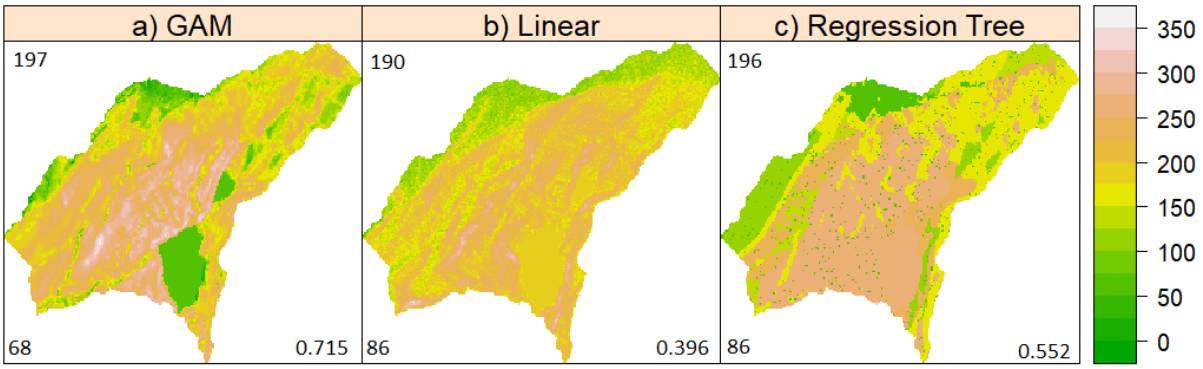

Figure 3.3. Snow depth distribution estimated for sample year 2006 using three statistical interpolation methods a) GAM, b) linear regression, and c) binary regression tree methods. The number in the top left corner represents the average snow depth in cm, the number in the bottom left corner is the mean absolute error (MAE), and the number in the bottom right corner is the Willmott's D.

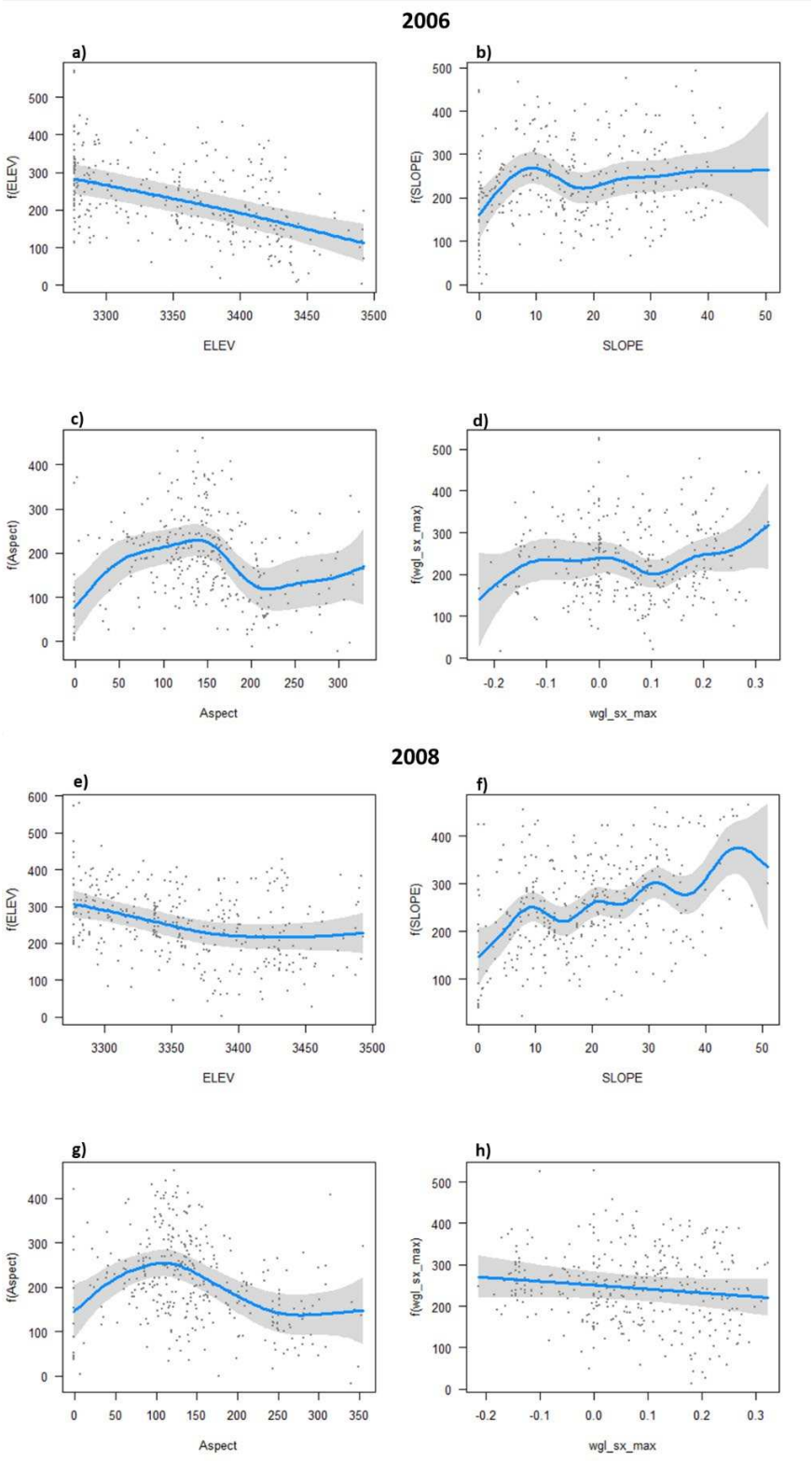

Figure 3.4. Significant topographic variables elevation (a and e); slope (b and f); aspect (c and g); and maximum upwind slope (d and h) non-linear relationships to snow depth for sample year 2006 and 2008.

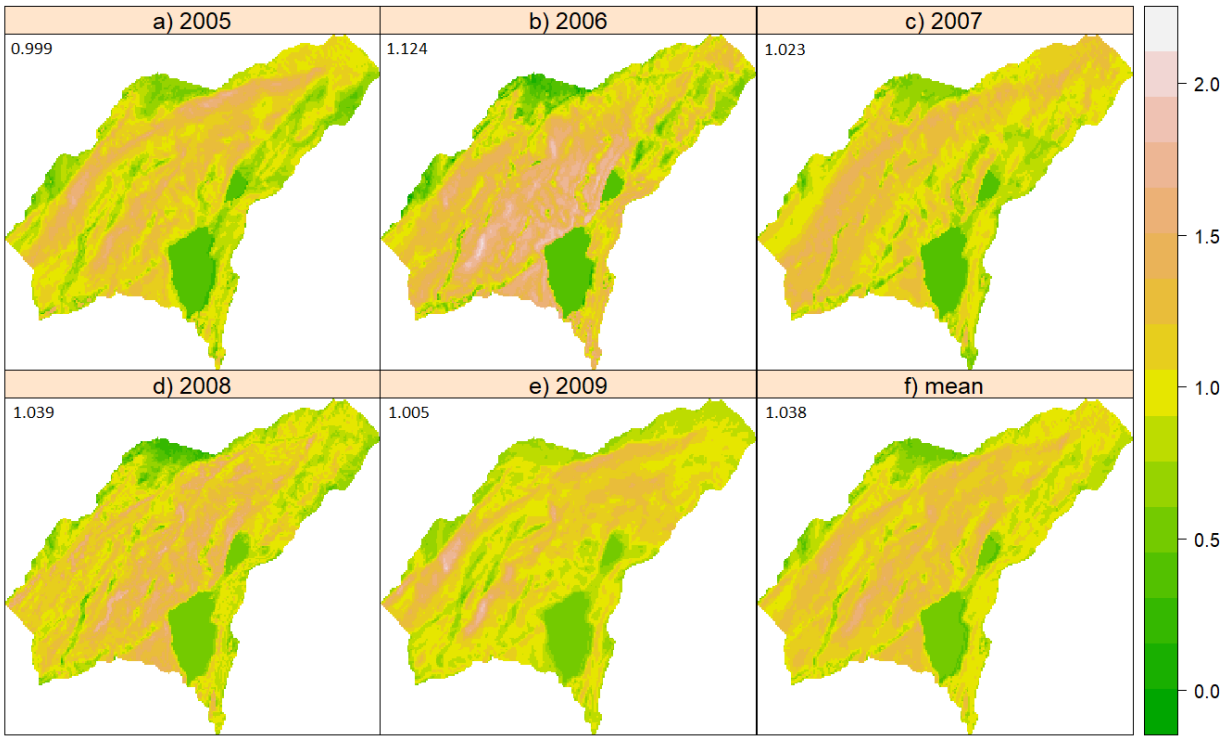

Figure 3.5. Plots of standardized snow depth values (SDV) and mean climatological snow depth distribution. The number in the top left corner represents the mean SDV.

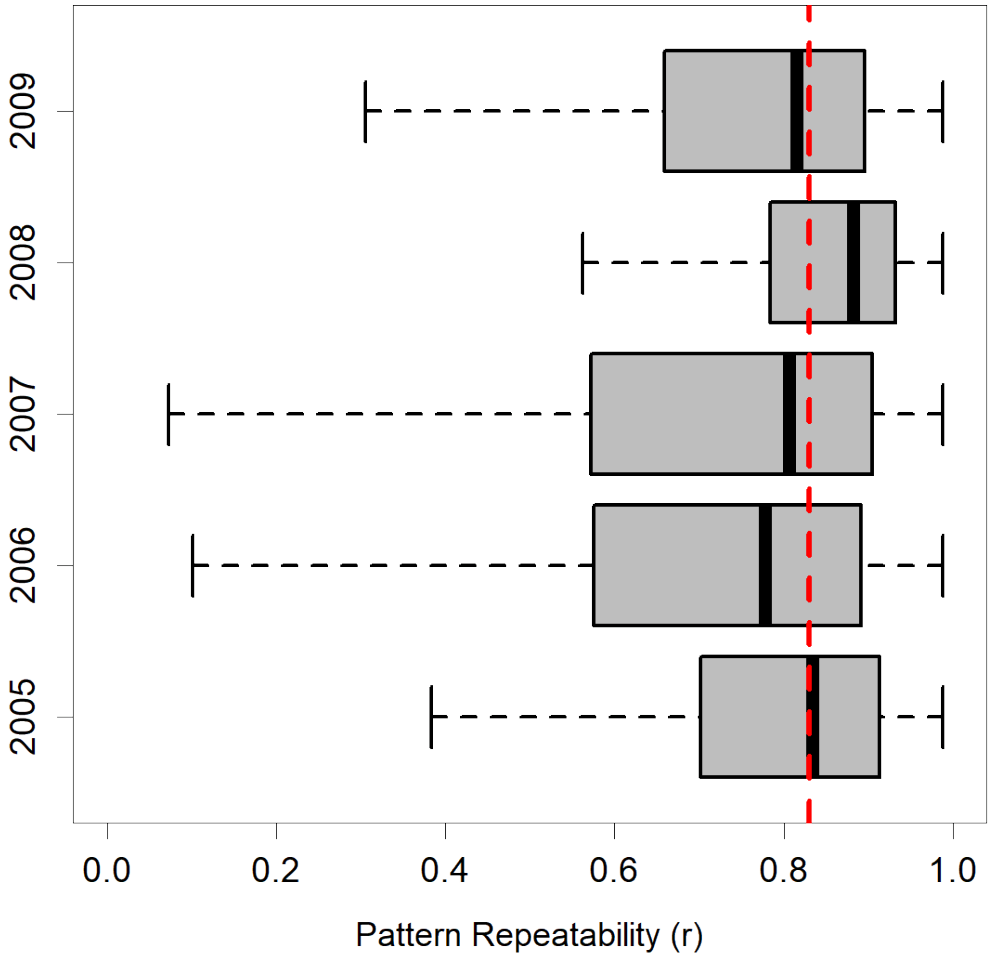

Figure 3.6. Pattern repeatability (Pearson correlation, r) between standardized climatological snow depth pattern and individual years SDV patten. The vertical red dashed line at 0.83 represents the mean r value for the five-year calibration period.

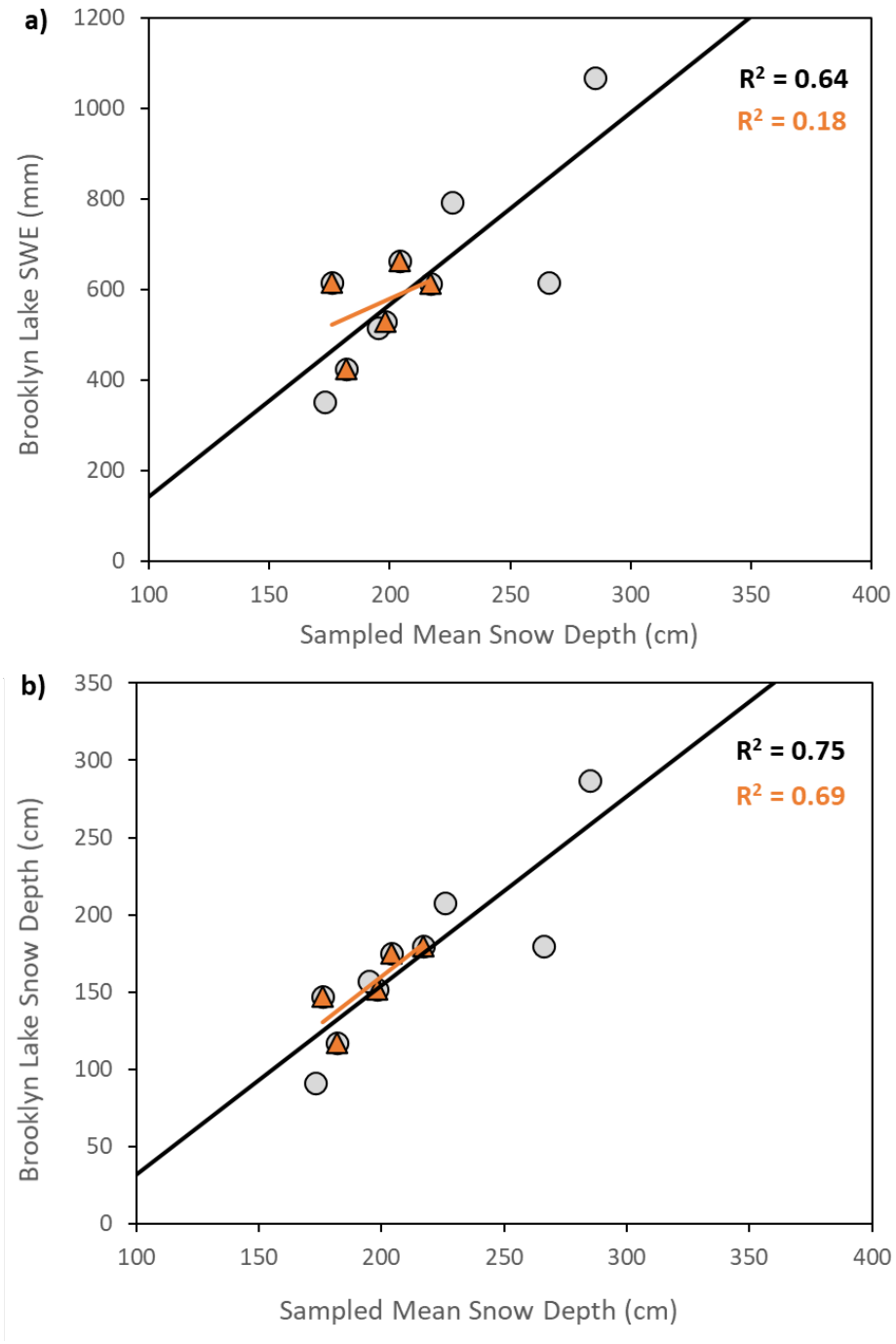

Figure 3.7. The sampled mean snow depth correlated to a) SWE and b) snow depth for 2005 to 2014 samples (grey circles) and the 2005 to 2009 calibration period samples (orange triangles).

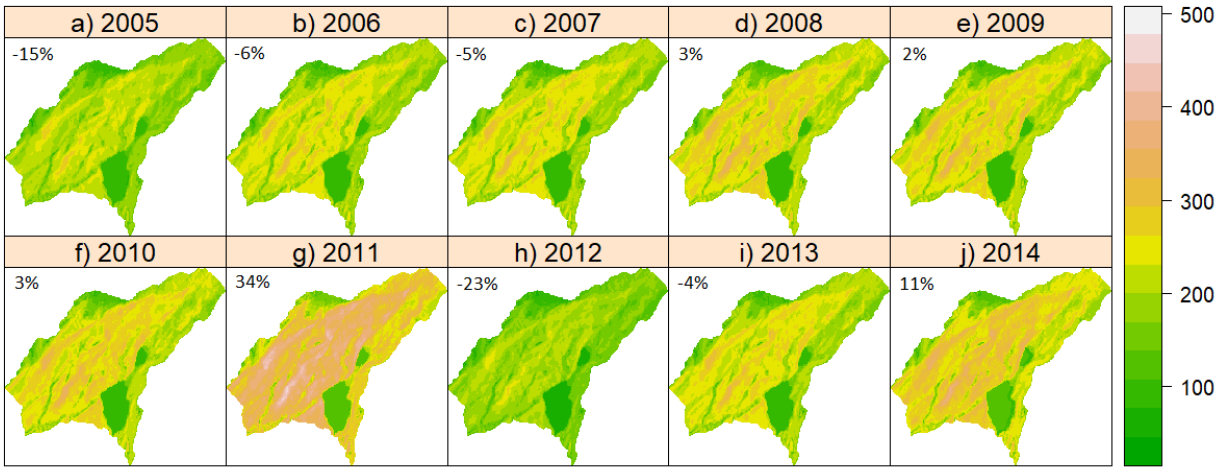

Figure 3.8. Estimates of snow depth distribution for years 2005 through 2014 at near peak snow depth accumulation. The number in the top left corner represents the percent difference from a mean snow depth of 169 cm, calculated from the Brooklyn Lake SNOTEL snow depth in Table 3.5.

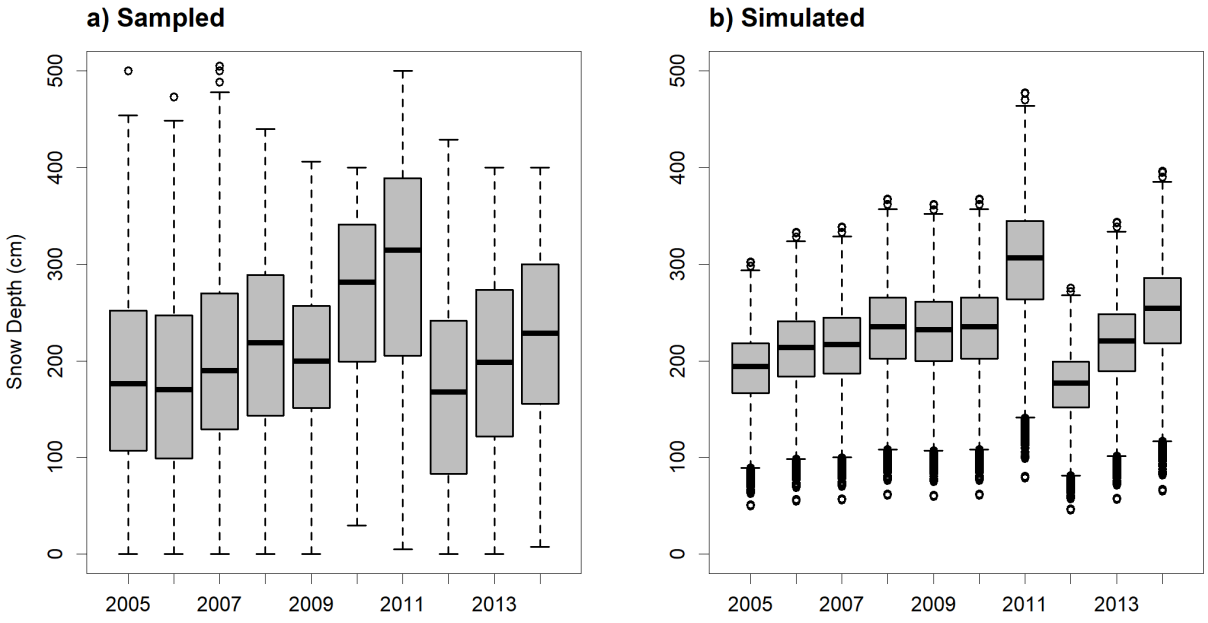

Figure 3.9. Comparison of annual a) sampled snow depth data and b) simulated snow depth.

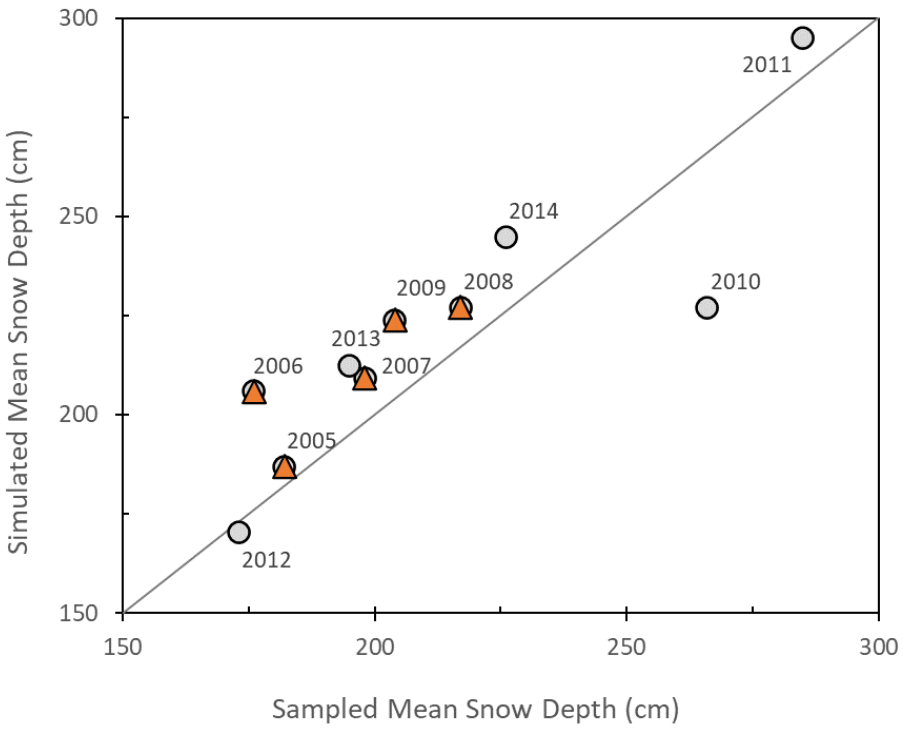

Figure 3.10. Estimates of sampled mean snow depth versus simulated mean WGLW snow depth for years 2005 through 2014 (grey circles) and the 2005 to 2009 calibration period (orange triangles).

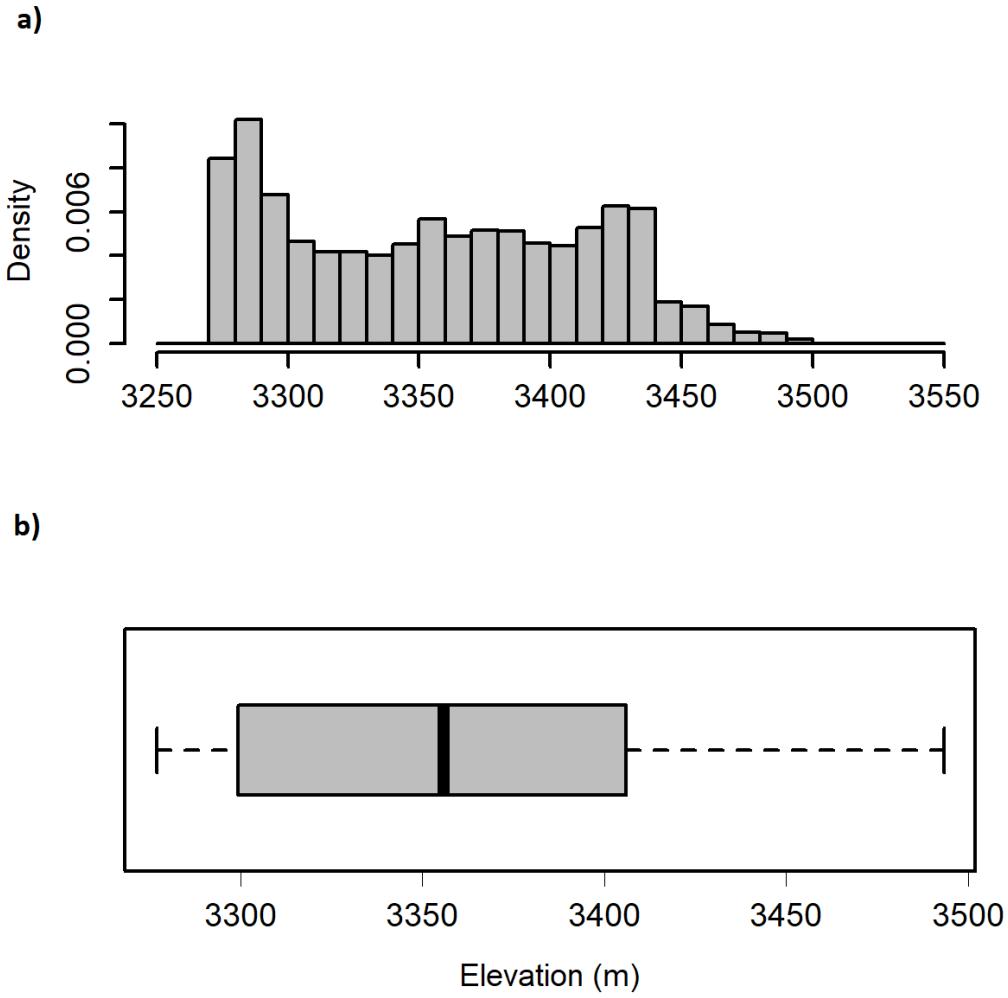

Figure 3.11. Elevation distribution of WGLW illustrated as a) histogram and b) boxplot.

REFERENCES

Anderton SP, S.M. White, and B. Alvera, 2004. Evaluation of spatial variability in snow water equivalent for a high mountain catchment. *Hydrological Processes*, 18, 435–453. https://doi.org/10.1002/hyp.1319

Balk B., and K. Elder, 2000. Combining binary regression tree and geostatistical methods to estimate snow distribution in a mountain watershed, *Water Resources Research*, 36 (1), 13-26.

Barry, R.G., 1992. *Mountain weather and climate*, Second edition, Routledge, New York, 402 pp.

Björk, P., 2016. Modelling the spatial variability of maximum mountain snow depth in Northern Norway. *Nordia Geographical Publications*, 45(2), 81-88. https://nordia.journal.fi/article/view/64932

Bloschl G, R. Kirnbauer, D. Gutknecht, 1991. Distribution snowmelt simulations in an alpine catchment's: 1. Model evaluation on the basis of snow cover patterns. *Water Resources Research*, 27, 3171–3179

Blösch, G., 1999. Scaling Issues in Snow Hydrology. *Hydrological Processes*, 13, 2149- 2175.

Breiman, L, J. Friedman, R. Olsen, and C. Stone, 1984. *Classification and Regression Trees*, Wadsworth and Brooks, Pacific Grove, Ca, 358 pp.

Carroll, R.W.H., J.S. Deems, R. Niswonger, R. Schumer, and K.H. Williams, 2019. The importance of interflow to groundwater recharge in a snowmelt-dominated headwater basin. *Geophysical Research Letters*, 46, 5899–5908. https://doi.org/10.1029/2019GL082447

Cerruti, B.J., and S.G. Decker, 2011. The local winter storm scale: A measure of the intrinsic ability of winter storms to disrupt society. *Bulletin of the American Meteorological Society*, 92(6), 721–737. https://doi.org/10.1175/2010BAMS3191.1

Clark et al., 2011. Representing spatial variability of snow water equivalent in hydrologic and land-surface models: A review. *Hydrological Processes*, 47(7), 1-23. https://doi.org/10.1029/2011WR010745

Currier et al., 2019. Comparing Aerial Lidar Observations With Terrestrial Lidar and Snow-Probe Transects From NASA's 2017 SnowEx Campaign. *Water Resources Research*, 55(7), 6285-6294. https://doi.org/10.1029/2018WR024533

Deems, J.S., 2002. *Topographic effects on the spatial and temporal patterns of snow temperature gradients in a mountain snowpack*. Master of Science Thesis, Department of Earth Sciences, Montana State University, 85 pp.

Deems, J.S., S.R. Fassnacht, and K.J. Elder, 2006. Fractal distribution of snow depth from LiDAR data, *Journal of Hydrometeorology*, 7(2), 285-297.

Deems, J.S., S.R. Fassnacht, and K.J. Elder, 2008. Interannual consistency in fractal snow depth patterns at two Colorado Mountain sites. *Journal of Hydrometeorology*, 9(5), 977–988. https://doi.org/10.1175/2008JHM901.1

Deems, J S., T.H. Painter, and D.C. Finnegan, 2017. Lidar measurement of snow depth: a review, *Journal of Glaciology*, 59(215), 467-479. https://doi.org/10.3189/2013JoG12J154

Doesken, N.J., A. Judson, 1996. *The Snow Booklet: A Guide to the Science, Climatology, and Measurement of Snow in the United States*. Colorado Climate Center, Department of Atmospheric Science, Colorado State University, Fort Collins, Colorado, 84 pp.

Elder, K. and J. Dozier, 1990. Improving methods for measurement and estimation of snow storage in an alpine watershed, *IAHS Publication* 193, 147-156.

Elder, K., J. Dozier, and J. Michaelsen, 1991. Snow accumulation and distribution in an alpine watershed, *Water Resources Research*, 27, 1541-1552.

Elder, K., W. Rosenthal, and R. Davis, 1998. Estimating the spatial distribution of snow water equivalent in a montane watershed, *Hydrological Processes*, 12, 1793-1808.

Elder, K., D. Cline, G.E. Liston, and R. Armstrong, 2019. NASA Cold Land Processes Experiment (CLPX 2002/03): Field Measurements of Snowpack Properties and Soil Moisture, *Journal of Hydrometeorology*, 10(1), 320-329. https://doi.org/10.1175/2008JHM877.1

Erickson, T.A., M.W. Williams, and A Winstral, 2005. Persistence of topographic controls on the spatial distribution of snow in rugged mountain terrain, Colorado, United States, *Water Resources Research*, 41 (4), 1-17, doi:10.1029/2003WR002973.

Erxleben, J., K. Elder, and R. Davis, 2002. Comparison of spatial interpolation methods for estimating snow distribution in the Colorado Rocky Mountains, *Hydrological Processes*, 16, 3627-3649.

ESRI, 2020. *ArcGIS Desktop: Release 10.8*. Redlands, CA: Environmental Systems Research Institute (ESRI).

Fassnacht, S.R., K.A. Dressler, and R.C. Bales, 2003.Snow water equivalent interpolation for the Colorado River Basin from snow telemetry (SNOTEL) data, *Water Resources Research*, 39(8), 1208. https://doi.org/10.1029/2002WR001512

Fassnacht, S.R., K.A. Dressler, D.M. Hultstrand, R.C. Bales, and G. Patterson, 2012. Temporal inconsistencies in coarse-scale snow water equivalent patterns: Colorado River basin snow telemetry-topography regressions, *Pirineos*, 167, 167-186, doi:10.3989/Pirineos.2011.166008.

Fassnacht, S.R., J. López-Moreno, M. Toro, and D.M. Hultstrand, 2013. Mapping snow cover and snow depth across the Lake Limnopolar watershed on Byers Peninsula, Livingston Island, Maritime Antarctica, *Antarctic Science*, 25(2), 157-166. https://doi.org/10.1017/S0954102012001216

Fassnacht, S.R., D.C. Deitemeyer, and N.B.H. Venable, 2014. Capitalizing on the daily time step of snow telemetry data to model the snowmelt components of the hydrograph for small watersheds, *Hydrological Processes*, 28(16), 4654-4668. https://doi.org/10.1002/hyp.10260

Fassnacht, S.R., et al., 2018. Distribution of snow depth variability, *Frontiers of Earth Science*, 12, 683–692. https://doi.org/10.1007/s11707-018-0714-z

Fu, P., and P.M. Rich, 2000. *The Solar Analyst 1.0 User Manual*, Helios Environmental Modeling Institute, LLC (HEMI).

Gleason, K., A. Nolin, and T. Roth, 2017. Developing a representative snow-monitoring network in a Forested Mountain watershed, *Hydrology and Earth System Sciences*, 21, 1137–1147. https://doi.org/10.5194/hess-21-1137-2017

Godsey, S.E., J.W. Kirchner, and C.L. Tague, 2014. Effects of changes in winter snowpacks on summer low flows: case studies in the Sierra Nevada, California, USA, *Hydrological Processes*, 28(19), 5048-5064. https://doi.org/10.1002/hyp.9943

Gray, D.M., and D.M. Male, 1981. *Handbook of Snow: Principles Processes, Management and Use*. Blackburn Press, Caldwell, New Jersey, 776 pp.

Grayson, R., G. Blöschl, A. W. Western, and T. A. McMahon, 2002. Advances in the use of observed spatial patterns of catchment hydrological response, *Advances in Water Resources*, 25(8–12), 1313–1334., https://doi.org/10.1016/S0309-1708(02)00060-X

Grayson, R.B., G. Blöschl, A.W. Western, and T.A. McMahon, 2002. Advances in the use of observed spatial patterns of catchment hydrological response, *Advances in Water Resources*, 25(8–12), 1313-1334. https://doi.org/10.1016/S0309-1708(02)00060-X

Grünewald, T., et al., 2013. Statistical modelling of the snow depth distribution in open alpine terrain, *Hydrology and Earth System Sciences*, 17, 3005–3021. https://doi.org/10.5194/hess-17-3005-2013

Hastie T, R. Tibshirani, 1987. Generalised additive model: Some applications, *Journal of the American Statisticians Association*, 82: 371–386

Hastings W.K., 1970 Monte Carlo sampling methods using Markov chains and their applications, *Biometrika*, 57(1): 97-109

Hiemstra, C.A, G.E. Liston, W.A. Reiners, 2006. Observing, modelling, and validating snow redistribution by wind in a Wyoming upper treeline landscape, *Ecological Modelling*, 197(1-2), 35-51. https://doi.org/10.1016/j.ecolmodel.2006.03.005

Hultstrand D.M., 2006. *Geostatistical Methods for Estimating Snowmelt Contribution to the Seasonal Water Balance in an Alpine Watershed*. Unpublished Master of Science Thesis, Watershed Science Program, Colorado State University, 130 pp

Hultstrand D, S.R. Fassnacht, and J. Stednick, 2006. Geostatistical methods for estimating snowmelt contribution to the alpine water balance. *Proceedings of the Annual Western Snow Conference*, (Las Cruces NM), 74: 149–154

Korfmacher, J.L. and D.M. Hultstrand, 2006. *Glacier Lakes Ecosystem Experiments Site hourly meteorology tower data*. Fort Collins, CO: U.S. Department of Agriculture, Forest Service, Rocky Mountain Research Station.

Kronholm, K. and K. Birkeland, 2007. Reliability of sampling design for spatial snow surveys, *Computers and Geosciences*, 33, 1097-1110.

Lapen, D.R. and L.W. Martz, 1996. An investigation of the spatial association between snow depth and topography in a Prairie agricultural landscape using digital terrain analysis, *Journal of Hydrology*, 184, 227-298.

López-Moreno J.I., D. Nogués-Bravo, 2005. A generalized additive model for the spatial distribution of snowpack in the Spanish Pyrenees, *Hydrological Processes,* 19, 3167–3176. https://doi.org/10.1002/hyp.5840

López-Moreno, J.I., and D. Nogués-Bravo, 2006. Interpolating snow depth data: a comparison of methods, *Hydrological Processes*, 20(10), 2217-232.

López-Moreno, J.I., J. Latron, and A. Lehmann, 2010. Effects of sample and grid size on the accuracy and stability of regression based snow interpolation methods, *Hydrological Processes*, 24, 1914–1928. https://doi.org/10.1002/hyp.7564

Liston, G.E., R.B. Haehnel, M. Sturm, C.A. Hiemstra, S. Berezovskaya, and R.D. Tabler, 2007. Simulating complex snow distribution in windy environments using Snow Tran-3D, *Journal of Glaciology*, 53 241-256. http://dx.doi.org/10.3189/172756507782202865

Luce, C. H., D.G. Tarboton, and K.R. Cooley, 1998. The influence of the spatial distribution of snow on basin-averaged snowmelt, *Hydrological Processes*, 12, 1671-1683.

Mayes Boustead, A.E., A.D. Hilberg, A.D. Shulski, and K.G. Hubbard, 2015. The Accumulated Winter Season Severity Index (AWSSI), *Journal of Applied Meteorology and Climatology*, 54(8), 1693-1712. https://doi.org/10.1175/JAMC-D-14-0217.1

Marofi, S., H. Tabari and H.Z. Abyaneh, 2011. Predicting Spatial Distribution of Snow Water Equivalent Using Multivariate Non-linear Regression and Computational Intelligence Methods, *Water Resources Management*, 25, 1417–1435 (2011). https://doi.org/10.1007/s11269-010-9751-4

McClung, D., and P. Schaerer, 1993. *The Avalanche Handbook,* The Mountaineers, Seattle, WA, 272 pp.

McKay, G.A. and D.M. Gray, 1981. The distribution of the snow cover, in: *Handbook of Snow* (edited by: Gray, D. and Hale, D.), Pergamon Press Canada Ltd., 153–190, 1981.

Meiman, J.R., 1968. Snow accumulation related to elevation, aspect and forest canopy, in *Snow Hydrology, Proceedings of Workshop Seminar*, Ottawa, Ontario, 35-47.

Molotch, N.P., M.T. Colee, R.C. Bales, and J. Dozier, 2005. Estimating the spatial distribution of snow water equivalent in an alpine basin using binary regression tree models: the impact of digital elevation data and independent variable selection, *Hydrological Processes*, 19(7), 1459-1479. DOI: 10:1002/hyp.5586.

Mott, R., V. Vionnet, and T. Grünewald, 2018. The Seasonal Snow Cover Dynamics: Review on Wind-Driven Coupling Processes, *Frontiers in Earth Science*, 6, 1- 25. https://doi.org/10.3389/feart.2018.00197

Musselman, R.C., 1994. *The Glacier Lakes Ecosystem Experiments Site*, Rocky Mountain Forest and Range Experiment Station, General Technical Report RM-249, 94 pp.

Pflug, J.M and J.D. Lundquist, 2020. Inferring Distributed Snow Depth by Leveraging Snow Pattern Repeatability: Investigation Using 47 Lidar Observations in the Tuolumne Watershed, Sierra Nevada, California, *Water Resources Research*, 56 (9), 1-17. https://doi.org/10.1029/2020WR027243

Pomeroy, J.W. and D.M. Gray, 1995. *Snowcover Accumulation, Relocation and Management*, National Hydrology Research Institute Science Report No. 7, Environment Canada, Saskatoon, 1995.

Razi MA, and k. Athappilly, 2005. A comparative predictive analysis of neural networks (NNs), nonlinear regression and classification and regression tree (CART) models, *Expert Systems with Applications*, 29, 65–74. https://doi.org/10.1016/j.eswa.2005.01.006

Revuelto, J., J.I. López-Moreno, C. Azorin-Molina, and S.M. Vicente- Serrano, 2014. Topographic control of snowpack distribution in a small catchment in the central Spanish

Pyrenees: Intra- and inter-annual persistence, *The Cryosphere*, 8, 1989–2006. https://doi.org/10.5194/tc-8-1989-2014

Roe, G.H, 2005. Orographic Precipitation, *Annual Review, Earth Planet Science,* 33, 645-671.

Stähli, M., J. Schaper, and A. Papritz, 2002. Towards a snow-depth distribution model in a heterogeneous subalpine forest using a Landsat TM image and an aerial photograph, *Annuals of Glaciology*, 34, 65–70. https://doi.org/10.3189/172756402781817923

Sturm, A., and A. Wagner, 2010. Using repeated patterns in snow distribution modeling: An Arctic example, *Water Resources Research*, 46, W12549, doi:10.1029/2010WR009434.

Tarboton, D.G. and C.H. Luce, 2006. *Utah Energy Balance Snow Accumulation Model (UEB)*, Computer model technical description and users guide, Utah Water Research Laboratory and USDA Forest Service Intermountain Research Station, 64 pp.

Vögeli, C., M. Lehning, N. Wever, and M. Bavay, 2016. Scaling Precipitation Input to Spatially Distributed Hydrological Models by Measured Snow Distribution, *Frontiers in Earth Science*, 4. https://doi.org/10.3389/feart.2016.00108

Whiting, J.M., and J. Kiss, 1987. Integration of digital terrain models into ground based snow and runoff measurements, *IAHS Publ*., 166: 375-387.

Willmott, C.T., 1982. Some comments on the evaluation of model performance, *Bulletin of the American Meteorological Society,* 63, 1309–1313.

Winstral, A., and D. Marks, 2002. Simulating wind fields and snow redistribution using terrain-based parameters to model snow accumulation and melt over a semi-arid mountain catchment, *Hydrological Processes*, 16, 3585-3603.

Winstral, A., K. Elder, and R.E. Davis, 2002. Spatial snow modeling of wind-redistributed snow using terrain-based parameters, *Journal of Hydrometeorology* 3(5), 524-538.

Wooldridge, G.L., R.C. Musselman, R.A. Sommerfeld, D.G. Fow, and B.H. Connell, 1996. Mean wind patterns and snow depth in an alpine-subalpine ecosystem as measured by damage to coniferous trees, *Journal of Applied Ecology* 33, 100-1088.

Yang H, P.R. Griffiths, and J.D. Tate, 2003. Comparison of partial least squares regression and multi-layer neural networks for quantification of nonlinear systems and application to gas phase Fourier transform infrared spectra, *Analytica Chimica Acta,* 489, 125–136. https://doi.org/10.1016/S0003-2670(03)00726-8

Zheng, Z., P.B. Kirchner, and R.C. Bales, 2016. Topographic and vegetation effects on snow accumulation in the southern Sierra Nevada: A statistical summary from lidar data, *The Cryosphere*, 10, 257–269. https://doi.org/10.5194/tc-10-257-2016

CHAPTER 4.0 - THE BEST PRECIPITATION ESTIMATES FOR A HYDROLOGIC MODEL BY COMBINING GAUGE AND RADAR DATA

4.1 Summary

Accurate estimation of the spatial and temporal distribution of rainfall is a crucial input into a surface water model, and for model calibration and evaluation. Typically, the number of rain gauges used to monitor rainfall is inadequate to resolve the spatial and temporal distributions over a watershed. When the measurement of rain falling in a watershed is based solely on rain gauges, these gauges are frequently located in convenient locations, which may not represent the entire watershed, and can lead to over- or under-estimation of runoff. Radar-estimated precipitation provides high spatial and temporal resolution, yet requires significant quality control and calibration before being useful for hydrologic modelling. Rain gauge data are combined with radar data to calibrate the rainfall rate.

In this study, four spatial precipitation estimates (inverse distance weighting (IDW), IDW-PRISM (Parameter-elevation Regressions on Independent Slopes Model), default radar, and gauge-adjusted radar) were used to generate high spatial and temporal resolution precipitation estimates for input into a hydrologic model to assess streamflow variability from the different precipitation inputs. Each input was used in the US Army Corps of Engineers Hydrologic Engineering Center Hydrologic Modeling System (HEC-HMS) model to examine precipitation uncertainty on simulated streamflow predictions in the 857 km^2 Alsea watershed. Initial Loss and Clark Transformation parameters were calibrated to observed streamflow from a 48-hour storm event using the gauge-adjusted radar precipitation dataset. The three remaining precipitation estimates were used as forcing datasets in the HEC-HMS model, showing that for this storm event, rainfall estimation gives rise to significant variability in streamflow predictions.

4.2 Introduction

Accurate hydrologic modelling requires good approximations of the spatial and temporal distribution of precipitation (Girons lopez *et al.*, 2015). Among the numerous input data to hydrologic models, precipitation measurements arguably have the most critical influence on the performance of a hydrologic model (Sik Kim *et al*., 2008; Ochoa-Rodriguez *et al.*, 2015). For over a century, hydrologists have tried to infer rainfall volume over a watershed through spatially interpolating point rainfall data from sparsely placed rain gauges (Thiessen, 1911). The number of rain gauges used to monitor precipitation is generally inadequate to resolve the spatial distribution of precipitation over a watershed (Ogden *et al.*, 2000; Moon *et al.*, 2004; Girons lopez *et al.*, 2015; Sivasubramaniam *et al.*, 2018) and are often too coarse of a temporal resolution (i.e., daily). Precipitation gauges are able to measure precipitation falling at a number of locations, but unable to estimate precipitation falling between the gauges. Typically, the spatial distribution of precipitation has been estimated by developing a spatial pattern based on rain gauge observations using interpolation, such as, Thiessen polygons, inverse distance weighting (IDW), or geostatistical techniques (Ogden *et al.*, 2000; Borga, 2002; Sharif *et al.*, 2002; Cole and Moore, 2008; Waleed *et al.*, 2009). Unfortunately, the spatial distributions inferred by these precipitation estimation techniques have limited connection with the actual patterns of precipitation.

Ground-based radar data have been used since the 1940's to estimate precipitation (Marshall and Palmer, 1948). Advancements in technology have made radar data a viable tool to improve the precipitation mapping between rain gauges (Brandes, 1975). With regards to precipitation monitoring, significant progress has been made over the last few decades, including

widespread increase in the use of weather radar rainfall estimates, generally provided at 1 km^2 resolution with a 5 – 10 min temporal scan. Radar data have been used to estimate precipitation at fine spatial and temporal resolutions (Sun *et al.*, 2000; Uijlenhoet, 2001; Vieux *et al.*, 2003; Ochoa-Rodriguez *et al.*, 2015), and can better capture the spatial variation of precipitation than rain gauge data in areas where rain gauges are sparsely distributed (Yang *et al.*, 2004; Segond *et al.*, 2007). Numerous studies have shown the improvements in flood estimation and flood forecasting using radar precipitation as the input data to hydrologic models (Kouwen, 1988; Pessoa *et al.*, 1993; Sun *et al.*, 2000; Ren *et al.*, 2003; Cole and Moore, 2008; Ochoa-Rodriguez *et al.*, 2015). Results are superior to those from techniques relying solely on precipitation gauges, particularly when gauge data are used to adjust the radar estimates (Fassnacht *et al.*, 1999; Sun *et al.*, 2000). Radar by itself has not proven to be a consistent estimator of actual precipitation amounts.

Most current radar-derived precipitation methods rely on a correlation between radar reflectivity (Z with units of $mm^6\ m^{-3}$) and precipitation rate (R with units of $mm\ h^{-1}$) in the form:

$$Z = aR^b \qquad \text{equation 4.1,}$$

where *a* is the "multiplicative coefficient" and *b* is the "power coefficient". Both *a* and *b* are directly related to the drop size distribution (DSD) and the drop number distribution (DND) within a cloud (Martner *et al.*, 2005).

Using gauge estimates of precipitation, Marshall and Palmer (1948) found $Z=200R^{1.6}$. The National Weather Service (NWS) currently uses a default Z-R relationship of $Z=300R^{1.4}$ to

estimate rain with their network of WSR-88D radars (NEXRAD) located across the United States, but it often produces highly variable and inaccurate results (Hunter, 2008). The variability in the results of the Z vs. R correlation is a direct result of differing DSD, DND, and air mass characteristics across the United States (Dickens, 2003; Adirosi *et al.*, 2015). The DSD and DND are determined by complex interactions of microphysical processes within a cloud that fluctuate seasonally, daily, regionally, and within the same cloud.

Radar data's greatest strength is the ability to resolve precipitation between the gauges, but lacks the accuracy to estimate precipitation magnitude (Ogden *et al.*, 2000). Merging radar and rain gauge data utilizes the strengths of each measurement technique while reducing their respective weaknesses (Moon *et al.*, 2004; Kim *et al.*, 2008). Radar data are used for the spatial distribution of precipitation, and precipitation gauge data are used to scale the magnitude of the spatial data often termed Gauge-Adjusted Radar Rainfall estimates (GARR) (Atlas *et al.*, 1997; Mousavi and Kouwen, 2003; Hultstrand *et al.*, 2008; Kim *et al.*, 2008; Waleed *et al.*, 2009; Hultstrand and Kappel, 2017). The result is a gauge-adjusted radar precipitation dataset that combines the spatial distribution of the radar and the scaling information of the gauge data (Fassnacht *et al.*, 2001; Hultstrand *et al.*, 2008; Hultstrand and Kappel, 2017).

The performance of distributed, physically-based hydrologic models depends heavily on the quality of the input data, especially precipitation (Sharif *et al.*, 2002; Ren *et al.*, 2003; Cole and Moore, 2008; Girons lopez *et al.*, 2015; Sirisena *et al.*, 2018). Hydrologic models ranging in complexity from the physically-based fully distributed to conceptual lumped models and their use depends upon the question being asked and the available input data. Ren *et al*. [2003] stated that radar precipitation estimates were far superior to rain gauge estimates as input into hydrologic models with Nash-Sutcliffe model efficiency of 83-93% for radar data compared to

27-69% for gauge data. Cole and Moore [2008] stated gauge-adjusted radar estimates are needed for any appreciable utility for flood modelling.

The purpose of this study is to evaluate the precipitation and runoff from a large rainfall event in the Alsea watershed in coastal Oregon USA, and use this information to determine the effect of different precipitation estimates on streamflow estimation. The specific objectives of this study are the following: (1) what are the spatial and temporal characteristics of different precipitation estimates; and (2) what are the implications of the precipitation estimates in modeled streamflow.

4.3 Study Site

The Alsea watershed above Tidewater, OR (USGS gauge number 14306500) is located within the Siuslaw National Forest, on the western Oregon coast. The Alsea watershed is 857 km^2 in size, ranges in elevation from 17 to 1,248 m with a mean basin elevation of 320 m (Figure 4.1). Average annual precipitation is approximately 2,068 mm, with 322 mm falling in November (Daly *et al.*, 2004; PRISM Climate Group, 2020). The watershed average 24-hour 2-year precipitation event is 104 mm and the 24-hour 100-year precipitation event is 193 mm (Schaefer *et al.*, 2008). These estimates are slightly lower than the older but official NOAA Atlas 2 values of 125 mm and 223 mm (Miller *et al.*, 1973).

The storm event analyzed for this paper is a 48-hour window from November 6 - 8, 2006. During this window, the Alsea watershed received an average of 138 mm of precipitation in a 48-hour period, a maximum point precipitation of 185 mm in a 48-hour period, and a maximum point precipitation of 170 mm in a 24-hour period. The maximum 24-hour gridded precipitation

within the Alsea watershed for this storm event is between the 2-year and 100-year 24-hour precipitation event (Schaefer *et al.*, 2008).

4.4 Data

A hydrometeorological spatial interpolation software, the Storm Precipitation Analysis System (SPAS), characterizes the spatial and temporal distributions of precipitation events (Parzybok *et al.*, 2008; Hultstrand *et al.*, 2008; Hultstrand and Kappel, 2017; Keim *et al.,* 2018; Brown *et al.*, 2020). The SPAS program was used to estimate hourly precipitation grids based on four spatial interpolation methods: i) IDW, ii) IDW-PRISM (Parameter-elevation Regressions on Independent Slopes Model), iii) default radar and iv) gauge-adjusted radar. Details on each of the four methods are described in the following sections. The four estimates of hourly precipitation were used as input into the US Army Corps of Engineers Hydrologic Engineering Center Hydrologic Modeling System (HEC-HMS) model. HEC-HMS is a physically-based hydrologic model that was developed by the US Army Corps of Engineers (Scharffenberg *et al.*, 2018).

4.4.1. Precipitation Gauge Data

Precipitation data were obtained from 48 recording rain gauges with hourly or daily temporal resolution over the entire storm period. Ten of these recording rain gages are located in or within 20 km of the Alsea watershed. This high density of gauges exists since the Alsea has been a research watershed for numerous decades (Chapman *et al.*, 1961; Hall and Stednick, 2008; Stednick, 2008; Segura *et al.*, 2020). Hourly gauge precipitation data were identified,

acquired, and quality controlled from the National Center for Environmental Information (NCEI, https://www.ncei.noaa.gov/) and the Remote Automated Weather Station (RAWS, https://raws.dri.edu/) networks. Precipitation from daily or event reporting locations were more abundant and were also identified, acquired and quality controlled from the NCEI and RAWS networks.

To increase the number of observations used for hourly interpolation, the daily and event reporting observations were converted to hourly estimated values based on the temporal distribution of precipitation at nearby hourly rain gauges (Parzybok *et al.*, 2008; Hultstrand *et al.*, 2008; Hultstrand and Kappel, 2017). To disaggregate (i.e., distribute) daily gauge data into estimated hourly values, official hourly reporting gauge data were first evaluated and quality controlled. Each hourly precipitation value was converted into a percentage that represents the incremental hourly precipitation divided by the total storm precipitation. A file was constructed for each hour for each gauge station that includes the latitude (x), longitude (y), elevation (elev), precipitation (R), reflectivity (Z) and the percent of precipitation (%R) for a particular hour. An IDW interpolation technique was applied to each of the hourly files. The result was a continuous grid with percentage values for the entire analysis domain, keeping the grid cells onto which the hourly gauge correctly estimates the observed/actual percentage. Since the percentages typically have a high degree of spatial autocorrelation (Daly *et al.*, 1994; Hunter and Meentemeyer, 2005; Hultstrand and Kappel, 2017), the spatial interpolation had skill in determining the percentages between gauges, especially since the percentages were somewhat independent of the precipitation magnitude (Schaake *et al.*, 2004). The end result was a grid for each hour that represented the percentage of the total storm precipitation that fell during that hour. After the hourly percentage grids were generated and quality-controlled, the hourly estimated timing at

each of the daily gauges was based on i) the daily gauge observation time, ii) daily precipitation amount and iii) the series of interpolated hourly percentages extracted from grids.

4.4.2. Streamflow Data

Streamflow data were acquired, and quality controlled for the Alsea River near Tidewater (gauge number 14306500) from the United States Geological Survey (USGS) National Water Information System (NWIS, https://nwis.waterdata.usgs.gov/nwis/sw) database. Daily streamflow has been archived since 1 October 1939, and 30-minute streamflow has been archived since 1 October 1986.

4.5 Methodology

4.5.1. IDW Precipitation Estimates

The hourly and hourly estimated precipitation data were spatially and temporally distributed based solely on the gauge data using an IDW algorithm (Isaaks and Srivastava, 1989):

$$\hat{z}(x_0) = \frac{\sum_{i=1}^{n} \frac{z(x_i)}{d_i^p}}{\sum_{i=1}^{n} \frac{1}{d_i^p}} \qquad \text{equation 4.2,}$$

where $\hat{z}(x_0)$ is the interpolated value, *n* is the number of sample points, $z(x_i)$ is the *i*th data value, d_i denotes the separation distance between the interpolated value and data value, and *p* denotes the weighting power. The IDW estimates for this study were derived as per Isaaks and Srivastava (1989) with a *p* value of 2 and are referred to as IDW estimates. An exponent of 2 is optimal in various applications (Fassnacht *et al.*, 2003a).

4.5.2 IDW-PRISM Precipitation Estimates

Climatology basemaps are independent grids of spatially distributed weather or climate variables that are used to govern the spatial patterns (Daly *et al.*, 1994; Daly *et al.*, 2004; Perica *et al.*, 2013; PRISM Climate Group, 2020). The National Weather Service (NWS) utilizes the "Mountain Mapper" methodology and Parameter-Elevation Regressions on Independent Slopes Model (PRISM) basemaps for quantitative precipitation estimates (QPE) (Daly *et al.*, 1994; Schaake *et al.*, 2004; Zhang *et al.*, 2011; Zhang *et al.*, 2014; Hultstrand and Kappel, 2017). The mountain mapper technique uses an IDW approach to estimate precipitation at ungauged locations from values at gauged locations while considering the climatology of precipitation at the gauged and ungauged locations (Schaake *et al.*, 2004). Mountain mapper methodology uses precipitation climatology such as PRISM mean monthly precipitation or the Hydrometeorological Design Studies Center (HDSC) NOAA Atlas 14 precipitation frequency grids (Perica *et al.*, 2013) to resolve orographic enhancement areas and micro-climates at a spatial resolution of 800 m. The PRISM methodology uses a weighted regression scheme to account for complex climate regimes associated with orography, rain shadows, temperature inversions, slope aspect, coastal proximity, and other factors (Daly *et al.*, 1994; Daly *et al.*, 2004;

PRISM Climate Group, 2020). NOAA Atlas 14 provide precipitation frequency climatologies with associated 90% confidence intervals and supplementary information on temporal distribution of heavy precipitation, analysis of seasonality and trends in annual maximum series data (Perica *et al.*, 2013). Basemap climatologies in complex terrain are often based on the PRISM mean monthly precipitation and/or NOAA Atlas 14 precipitation frequency grids given both resolve orographic enhancement areas and micro-climates in complex terrain. Basemaps climatologies of this nature in flat terrain are not as effective given the small terrain forced precipitation gradients. The Mountain Mapper method as per Schaake *et al.*, (2004) was applied in this study and is referred to as IDW-PRISM estimates.

4.5.3. Default Radar Precipitation Estimates

Level–II base reflectivity data were acquired from NCEI at a temporal resolution of 5 minutes, a spatial scale of approximately 1x1 km resolution, and with a precision of 0.50 Z. The SPAS tool performs radar data quality control algorithms (RDQC) to remove non-precipitation artifacts from base Level–II radar data and projects the data from polar coordinates to a Cartesian (latitude/longitude) grid (Hultstrand and Kappel, 2017). Non-precipitation artifacts include ground clutter, bright banding, sea clutter, anomalous propagation, sun strobes, clear air returns, chaff, biological targets, electronic interference and hardware test patterns (Lakshmanan and Valente, 2004; Lakshmanan *et al.*, 2014). The quality-controlled radar data were used as the raw radar reflectivity data across the watershed, that were subsequently adjusted to precipitation estimates.

The default radar dataset was computed by applying the NWS default Z-R relationship of $Z=300R^{1.4}$ to the raw quality-controlled radar reflectivity data. No further bias corrections were applied to these default radar estimates. The hourly precipitation estimates were derived by summing the sub-hourly scan-level precipitation grids.

4.5.4 Gauge-adjusted Radar Precipitation Estimates

The SPAS tool utilizes an iterative procedure for optimizing the *a* and *b* coefficients of the Z-R relationship each hour during the analysis period. For each hour, the algorithms determined if sufficient observed hourly precipitation data (minimum six stations) were available to compute a reliable Z-R relationship (Hultstrand and Kappel, 2017). If sufficient observed precipitation data were not available, then the Z-R relationship would adopt the previous hours Z-R relationship (if available) or apply a user supplied default algorithm, in this case $Z = 300R^{1.4}$. If sufficient precipitation data were available for an hour, they were related to the radar reflectivity data, and a least-squares power function was computer between the data points. The resulting *a* and *b* coefficients and the maximum estimated precipitation were subjected to several tests to determine if the Z-R relationship was acceptable. Once a mathematically optimized hourly Z-R relationship was determined, it was applied to the raw quality-controlled scan level Z-grid to compute initial precipitation estimates (in mm h^{-1}) at each grid cell over the extent of the radar data.

Spatial differences in the Z-R relationship exist across the radar domain due to differences in DSD, DND and/or poor radar coverage. To account for these local differences, SPAS computed spatial residuals, as per Fassnacht *et al*. (2003b), as the difference between the

precipitation estimates from the Z-R equation and the observed precipitation for each gauging station. To limit the impact of large anomalous residuals and promote a spatially smooth pattern, the residuals, also known as biases, were smoothed using a 3 by 3 block spatial filter. The final hourly precipitation grids were created by adding the initial precipitation estimate grid with the residual/bias grid, these precipitation estimates are referred to as gauge-adjusted radar estimates.

4.5.5 Hydrologic Modelling

The HEC-HMS model was developed by the US Army Corps of Engineers to simulate a variety of situations, including analyzing urban flooding, flood frequency, flood warning system planning, reservoir spillway capacity, and stream restoration (Scharffenberg *et al.*, 2018). HEC-HMS contains four main components: i) an analytical model to calculate overland flow runoff as well as channel routing, ii) an advanced graphical user interface that displays hydrologic system components with interactive features, iii) a system for storing and managing data, specifically large, time variable datasets, and iv) a means for displaying and reporting model outputs (Bajwa and Tim, 2002).

For this study, HEC-HMS was calibrated to the observed USGS streamflow data and the gauge-adjusted radar estimate dataset using HEC-HMS built in Optimization Manager interface. The HEC-HMS model was calibrated using deterministic model optimization, based on univariate-gradient search algorithm, involved adjusting initial parameter values so that the simulated results match the observed streamflow as closely as possible, as per Scharffenberg *et al.* (2018). For the Alsea watershed model, the Initial and Constant Loss method and the Clark method were selected for transforming the precipitation estimates into streamflow. The Initial

and Constant Loss method use two parameters: the initial loss and the constant loss values to define infiltration losses. Clark Unit Hydrograph model derives unit hydrographs by representing two critical process: translation and attenuation in the transformation of excess precipitation into runoff.

For the Initial and Constant Loss, the parameters of Initial Loss, Percent Impervious, and Constant Rate were estimated following US Army Corps of Engineers (2016) and adjusted through the HEC-HMS optimization method. For the Clark Unit Hydrograph, the parameters of Time of Concentration and Storage Coefficient were estimated following US Army Corps of Engineers (2016) and adjusted through the HEC-HMS optimization method. The deterministic optimization process was completed once the goodness-of-prediction estimates, "sum of absolute residuals" and "sum of squared residuals", provided the best value for each parameter adjusted. The "percent of error in peak" and "peak-weighted root mean square error" goodness-of-prediction indices were not used in the deterministic optimization.

4.6 Results

4.6.1. Precipitation

The gauge-adjusted estimated precipitation represents the true spatial (Figure 4.2) and temporal characteristics (Figure 4.3) and is considered as the reference for comparison. The gauge-adjusted estimated precipitation average volume on the watershed area was 138 mm and the maximum within the watershed 185 mm (Figure 4.2 and Table 4.1). Figure 4.5 compares accumulated maximum 24-hour estimated precipitation and the associated 24-hour average

recurrence interval (ARI). The gauge-adjusted maximum 24-hour ARI is 72-years with a watershed average of 14-years.

The uncalibrated default radar estimated precipitation created a spatial pattern that is not representative to the spatial (Figure 4.2) and temporal characteristics (Figure 4.3) of the reference gauge-adjusted radar precipitation. The uncalibrated default radar estimated precipitation significantly underestimated the precipitation from the storm. The uncalibrated default radar estimated precipitation average volume on the watershed area was 26% less than the reference gauge-adjusted radar precipitation volume and the maximum volume on the watershed area was 31% less than the reference gauge-adjusted radar precipitation (Figure 4.2 and Table 4.1). Figure 4.5 compares accumulated maximum 24-hour estimated precipitation and the associated 24-hour ARI. The uncalibrated default radar maximum 24-hour ARI is 17-years with a watershed average of 3-years. The uncalibrated default radar maximum 24-hour estimated precipitation significantly underestimated the precipitation from the storm. The uncalibrated default radar maximum 24-hour estimated precipitation average volume on the watershed area was 22% less than the reference gauge-adjusted radar precipitation volume and the maximum 24-hour volume on the watershed area was 27% less than the reference gauge-adjusted radar precipitation.

The IDW estimated precipitation created a spatial pattern that is similar to the spatial (Figure 4.2) and temporal characteristics (Figure 4.3) of the reference gauge-adjusted radar precipitation. The IDW estimated precipitation slightly underestimated the precipitation from the storm. The IDW estimated precipitation average volume on the watershed area was 3% less than the reference gauge-adjusted radar precipitation volume and the maximum volume on the watershed area was 6% less than the reference gauge-adjusted radar precipitation (Figure 4.2 and

Table 4.1). Figure 4.5 compares accumulated maximum 24-hour estimated precipitation and the associated 24-hour ARI. The IDW maximum 24-hour ARI is 53-years with a watershed average of 12-years. The IDW maximum 24-hour estimated precipitation slightly underestimated the precipitation from the storm. The IDW maximum 24-hour estimated precipitation average volume on the watershed area was 3% less than the reference gauge-adjusted radar precipitation volume and the maximum 24-hour volume on the watershed area was 6% less than the reference gauge-adjusted radar precipitation.

The IDW-PRISM estimated precipitation created a spatial pattern not representative the spatial (Figure 4.2) and temporal characteristics (Figure 4.3) of the reference gauge-adjusted radar precipitation. The IDW-PRISM estimated precipitation overestimated the precipitation from the storm. The IDW-PRISM estimated precipitation average volume on the watershed area was 12% more than the reference gauge-adjusted radar precipitation volume and the maximum volume on the watershed area was 22% more than the reference gauge-adjusted radar precipitation (Figure 4.2 and Table 4.1). Figure 4.5 compares accumulated maximum 24-hour estimated precipitation and the associated 24-hour ARI. The IDW-PRISM maximum 24-hour ARI is 160-years with a watershed average of 18-years. The IDW-PRISM maximum 24-hour estimated precipitation slightly overestimated the precipitation from the storm. The IDW-PRISM maximum 24-hour estimated precipitation average volume on the watershed area was 13% more than the reference gauge-adjusted radar precipitation volume and the maximum 24-hour volume on the watershed area was 24% less than the reference gauge-adjusted radar precipitation.

4.6.2. Mass Curves

Mass curves are plots of the temporal distribution and the magnitude of precipitation. Mass curves were extracted at three locations and for the basin average for each of the four precipitation estimates: i) the maximum precipitation location, ii) the basin outlet, iii) the basin average precipitation, and iv) the minimum precipitation location. The gauge-adjusted radar mass curves have a large difference in the magnitude; the overall timing is in good agreement. The maximum basin precipitation was 185 mm, the basin outlet was 183 mm, the average basin 138 mm, and the minimum basin precipitation was 106 mm (Figure 4.3a, Table 4.1). The default radar mass curves exhibit less variability in the magnitude; the overall timing is in good agreement. The maximum basin precipitation was 128 mm, the basin outlet was 101 mm, the average basin 102 mm, and the minimum basin precipitation was 71 mm (Figure 4.3b, Table 4.1). The IDW mass curves show little difference in the magnitude and the overall timing is in good agreement. The maximum basin precipitation was 174 mm, the basin outlet was 169 mm, the average basin 134 mm, and the minimum basin precipitation was 106 mm (Figure 4.3c, Table 4.1). The IDW-PRISM mass curves show little difference in the magnitude and the overall timing is in good agreement. The maximum basin precipitation was 178 mm, the basin outlet was 178 mm, the average basin 155 mm, and the minimum basin precipitation was 106 mm (Figure 4.3e, Table 4.1).

4.6.3. Observed Gauge Precipitation versus Predicted Precipitation

The overall fit between the total storm observed precipitation and estimated total storm precipitation at gauge locations were used to assess the overall fit of the gridded rainfall for each

of the four precipitation methods. The accuracy of the four precipitation estimates were quantified based on the following goodness-of-prediction estimates: the root mean square error (*RMSE*), the mean absolute error (*MAE*), the coefficient of determination (R^2), and the Nash-Sutcliffe Efficiency (NSE).

The gauge-adjusted radar total storm precipitation versus the observed precipitation correlation is extremely high; the R^2 is 0.998 and the NSE is 0.999 (Figure 4.6 and Table 4.2). The gauge-adjusted radar results have the best fit due to the nature of the spatial bias adjustment (residuals)accounting, which is an exact interpolator of the point but not representative between gauges. The default radar total storm precipitation versus the observed precipitation correlation is extremely poor; the R^2 is 0.168 and the NSE is -2.08 (Figure 4.6 and Table 4.2). The default radar results always underestimated the observed precipitation and provided the least accuracy of the four precipitation estimates. The IDW total storm precipitation versus the observed precipitation correlation is extremely high; the R^2 is 0.979 and the NSE is 0.979 (Figure 4.6 and Table 4.2). The IDW results have a great fit due to the nature of IDW, which is an exact interpolator of the point but not representative between gauges but still underperformed when compared to the gauge-adjusted precipitation estimates. The IDW-PRISM total storm precipitation versus the observed precipitation correlation is extremely high; the R^2 is 0.976 and the NSE is 0.974 (Figure 4.6 and Table 4.2). The IDW-PRISM run has a great fit due to the nature of IDW, which is an exact interpolator of the point but not representative between gauges, as is seen in the range of estimated precipitation values (Figure 4.2, Figure 4.3, and Table 4.2). The IDW-PRISM precipitation estimates underperformed compared to the gauge-adjusted precipitation estimates.

4.6.4. Hydrologic Modelling

The accuracy of the four precipitation estimates as input into HEC-HMS were quantified based on the following streamflow goodness-of-prediction estimates: *RMSE*, *MAE*, R^2, and NSE. For this study, HEC-HMS was calibrated to the observed streamflow data for and the gauge-adjusted radar precipitation estimates. Using the HEC-HMS calibrated parameters (Table 4.3), the model was forced by the three remaining precipitation estimates and results were used to quantify the variation in modeled streamflow. The observed maximum, average, and minimum streamflow was 472.9, 203.7, and 60.9 m^3/s, respectively. The observed cumulative total runoff for the Alsea watershed is 30.8 mm. Figure 4.4 shows the basin average precipitation used as input in to the Calibrated HEC-HMS model, the accumulation patterns illustrate the similarities in timing and magnitude of precipitation for the gauge-adjusted and IDW estimates and also illustrate significant differences in timing and magnitude of the default radar and IDW-PRISM estimates.

The runoff volume calculated for the gauge-adjusted radar precipitation estimates on average is 1.4% less than the average observed streamflow and the peak streamflow is 4.0% larger than the observed peak streamflow (Table 4.2). Although the peak discharge is 4% higher using the gauge-adjusted radar precipitation, the total runoff volume is 1.3% lower than the observed total runoff. The gauge-adjusted radar precipitation resulted in streamflow simulation with a slightly higher peak streamflow and an average slightly lower with the relatively excellent goodness-of-fit measures (Table 4.4) indicating a successful model calibration and a great reference dataset. The uncalibrated default radar estimated precipitation average streamflow is 31.5% less than the average observed streamflow and the peak streamflow is 33.2% lower than the observed peak streamflow (Table 4.2). The peak discharge is 33% lower using the

uncalibrated default radar estimated precipitation, the total runoff volume is 31.5% lower than the observed total runoff. The uncalibrated default radar estimated precipitation resulted in streamflow simulation that significantly lower in both peak, average and cumulative streamflow; and produced poor goodness-of-fit measures (Table 4.4). The IDW estimated precipitation average streamflow is 6.1% less than the average observed streamflow and the peak streamflow within 1% of the observed peak streamflow (Table 4.2). The total runoff volume is 6.2% lower than the observed total runoff. The IDW estimated precipitation resulted in streamflow simulation that slightly lower peak streamflow and an average slightly lower with the relatively good goodness-of-fit measures (Table 4.4) indicating a successful model calibration. The IDW-PRISM estimated precipitation average streamflow is 18.8% greater than the average observed streamflow and the peak streamflow is 30.8% greater than the observed peak streamflow (Table 4.2). The peak discharge is 30.8 greater using the IDW-PRISM estimated precipitation, the total runoff volume is 18.8% more than the observed total runoff. The IDW-PRISM estimated precipitation resulted in streamflow simulation that significantly overpredicted in both peak, average and cumulative streamflow; and produced poor goodness-of-fit measures (Table 4.4).

4.7 Discussion

The precipitation and streamflow data collected for the November 2006 storm event in the Alsea watershed, provided an opportunity to investigate the effect different precipitation estimates have on streamflow simulations for a typical large storm event (less than a 100-year ARI; Figure 4.5). This study provides quantitative information on the development of four different precipitation estimates, the calibration of a HEC-HMS model, and the resulting streamflow simulations as compared to observed streamflow.

Given the large variability in magnitude and timing of precipitation estimates (Figure 4.2; Figure 4.3; Figure 4.6; and Table 4.1), the results of this study highlight the significance of precipitation estimates used as input into hydrologic models (Sharif *et al.*, 2002; Ren *et al.*, 2003; Cole and Moore, 2008; Girons lopez *et al.*, 2015; Sirisena *et al.*, 2018). Goodness-of-fit measures performed on the observed precipitation data to the four estimated precipitation datasets show that the gauge-adjusted and IDW precipitation estimates resulted in the best representation of the observed precipitation (Ogden et al., 2000; Moon *et al*., 2004; Kim *et al*., 2008; Table 4.2). The default radar estimates showed significant underestimation of precipitation estimates while the default radar generated excessive precipitation estimates.

To place the precipitation estimates in a historical context, the four precipitation estimates were compared with Oregon's Department of Transportation (ODOT) 24-hour Regional Precipitation datasets gridded point precipitation ARIs (Schaefer et al., 2008). ARIs indicate the average time between events of a given magnitude when averaged over a long period (Lincoln 2014; Lincoln *et al*., 2017) and are frequently calculated for an event for a range of different durations, typically from hours to days. The ODOT contains Regional Precipitation datasets contains 24-hour precipitation estimates with recurrence intervals ranging from 1 to 1000 years. The precipitation frequency estimates are an expressed value reported with their corresponding 90% confidence intervals. As the ARIs increase, the confidence interval widths increase as well, resulting from variability in precipitation and the rare nature of extreme events. The annual exceedance probability (AEP), the probability that an event of the given magnitude will occur within any given year (one divided by ARI), is more commonly used to describe the rare nature of an event to the public (Lincoln *et al.,* 2017). Recent studies (Parzybok *et al.,* 2011; Keim *et al.,* 2018) have described rainfall totals in terms of both ARI and AEP to better define

the historical nature of a storm. For this study, the reference gauge-adjusted precipitation at the 24-hour duration (maximum occurred between November 6-8, 2006) had an ARI of 72-years (AEP is 0.014) and a watershed average ARI of 14-years (AEP is 0.071, Figure 4.5).

The HEC-HMS optimized parameters (Table 4.3) for the Initial and Constant Loss method and the Clark method were derived by calibrating the observed streamflow to the gauge-adjusted precipitation estimates. The final optimized parameters and are within the typical range to account for loss and transformation of excess precipitation into runoff (Scharffenberg *et al.*, 2018).

Streamflow simulations show a large degree of variability in the magnitude of peak streamflow and total streamflow volume (Figure 4.7; Table 4.9). As expected, the gauge-adjusted precipitation estimates resulted in the best overall streamflow simulation goodness-of-fit measures while the IDW, IDW-PRISM, and default radar precipitation estimates resulted in streamflow simulation goodness-of-fit rankings of second, third, and fourth best respectfully (Table 4.4). In particular, streamflow simulations using the gauge-adjusted radar method simulated the peak time and shape of hydrograph more accurately than the other methods. A result of the gauge-adjusted radar method utilizing both radar and gauge data to derive precipitation fields that represent the actual spatial and temporal characteristics of precipitation (Pessoa *et al.*, 1993; Sun *et al.*, 2000; Ren *et al.*, 2003; Cole and Moore, 2008; Hultstrand *et al.,* 2008; Ochoa-Rodriguez *et al.*, 2015). The IDW-PRISM precipitation estimates generated the second worst streamflow and goodness-of-fit estimates; these results can be attributed to excessive precipitation estimates driven by the basemap interpolation at higher elevation regions (Schaake *et al.*, 2004; Hultstrand and Kappel, 2017). The default radar precipitation estimates generated the worst simulated streamflow and goodness-of-fit estimates; these results can be

attributed to a drastic underestimate of precipitation resulting for raw uncalibrated radar (Dickens, 2003; Hunter, 2008; Adirosi *et al.*, 2015).

As shown in the is study, we found that different precipitation estimates have a considerable impact on streamflow simulation (Figure 4.6; Figure 4.7) with the greatest streamflow variability attributed to both the precipitation magnitude and timing. Although this study only investigated precipitation estimates for one storm event that was less than 100-year magnitude (Figure 4.5), the study further illustrates the importance of accurate spatial and temporal precipitation estimates in performing hydrologic model simulations (Sik Kim *et al*., 2008; Girons lopez *et al.*, 2015; Ochoa-Rodriguez *et al.*, 2015).

4.8 Conclusions

The four precipitation datasets for the Alsea watershed in Oregon are different in magnitude with varying spatial and temporal distributions across the study area. The gauge-adjusted radar estimates are of high quality and superior to the default radar, IDW, and IDW-PRISM estimates. The default radar estimates presented the largest deviation in magnitude and resulted in significant underestimation of storm total rainfall volume. The IDW estimates were the second best in regard to precipitation magnitude and goodness-of-fit measures but the spatial pattern was not representative since the rain gauges in and around the watershed are spaced far apart. The IDW-PRISM precipitation estimates resulted in overestimation of the storm total rainfall volume and generated a nonrepresentative spatial pattern anchored to the underlying terrain. The temporal characteristics within the Alsea watershed were similar for the three precipitation estimates that utilized gauge data (gauge-adjusted, IDW, IDW-PRISM) as compared

to the default radar. The default radar intensities were much lower as compared to the intensities of the estimates that included gauges.

The four precipitation datasets yield different simulated streamflows. The gauge-adjusted radar and IDW estimates both showed good agreement with the observed streamflow data, while the default radar estimates underestimated and the IDW-PRISM overestimated the observed streamflow. In terms best-fit statistic (NSE and R^2), the default radar and IDW-PRISM precipitation estimates were the poorest. Despite the low density of rain gauges in the Alsea watershed, simulations that included precipitation estimates that included gauge data showed a better agreement with observed streamflow as compared to streamflow simulations based on precipitation estimates that did not include gauge data.

4.9 Tables and Figures

Table 4.1. Gridded total storm precipitation statistics (mm) for the Alsea watershed for each of the four precipitation estimates.

	Gauge-Adjusted	Default	IDW	IDW-PRISM
Maximum	185	128	174	226
Average	138	102	134	155
Minimum	106	71	106	108
Outlet	183	101	169	178
StDev	18	14	19	25

Table 4.2. Total storm goodness-of-fit measures between the observed gauge data total storm precipitation (mm) and estimated gauge grid cell total storm precipitation (mm) for 42 gauge locations.

	Gauge-Adjusted	Default	IDW	IDW-PRISM
RMSE	1.872	89.56	7.414	8.157
MAE	0.793	76.32	1.983	3.574
R^2	0.999	0.168	0.979	0.976
NSE	0.999	-2.078	0.979	0.974

Table 4.3. Calibrated HEC-HMS parameters used with precipitation estimates to simulation streamflow.

Loss Rate	**Clark Transform**
Initial Loss = 9.60 mm (0.378 in)	Time of Concentration = 9.192 hours
Constant Rate = 4.013 mm/hr (0.158 in/hr)	Storage Coefficient = 14.44 hours

Table 4.4. Alsea basin observed and simulated streamflow statistics (m^3/s) and goodness-of-fit measures for four precipitation methods.

	Observed	Gauge-Adjusted	Default	IDW	IDW-PRISM
Cumulative (mm)	30.8	30.4	21.1	28.9	36.6
Maximum	472.9	491.7	315.9	469.9	618.7
Average	203.7	200.9	139.5	191.2	242.0
Minimum	60.9	60.9	60.9	60.9	60.9
RMSE	-	10.9	87.6	17.6	58.8
MAE	-	9.1	65.2	13.0	41.9
R^2	-	0.994	0.975	0.993	0.941
NSE	-	0.993	0.576	0.983	0.808

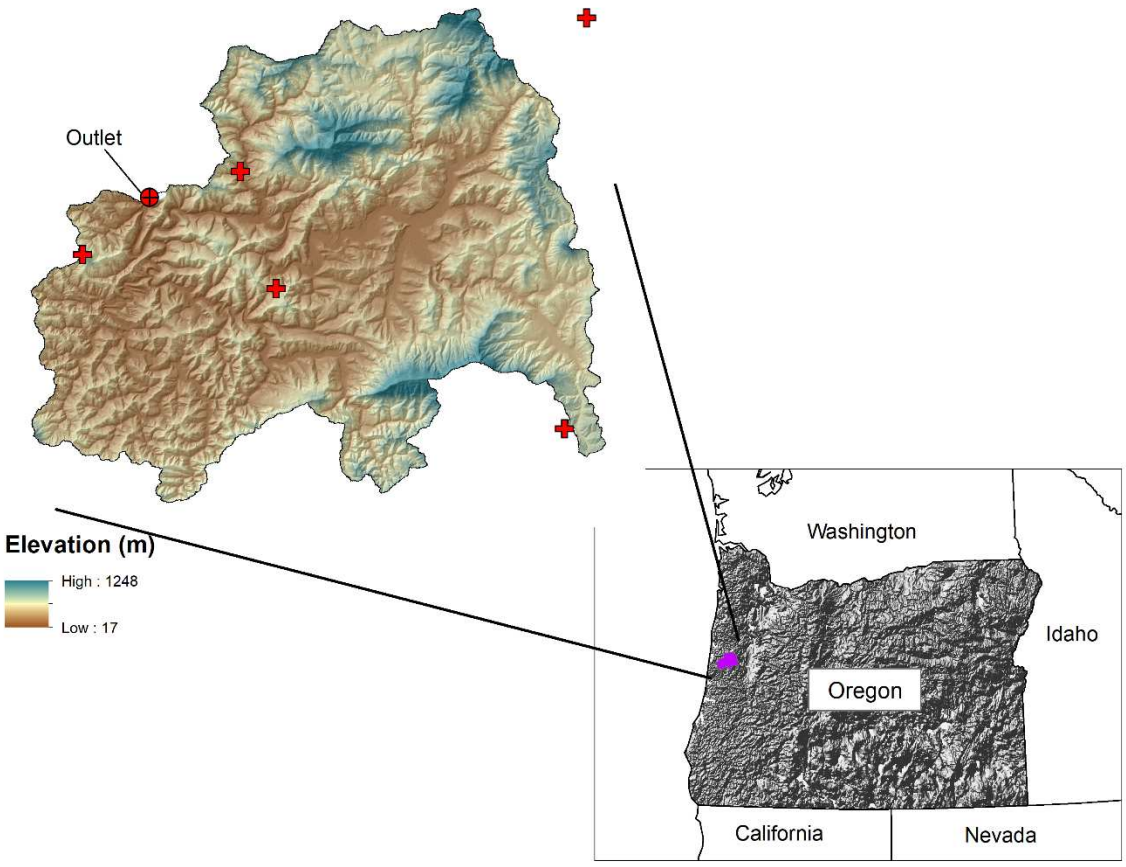

Figure 4.1. Study site map showing location of the Alsea watershed. Red circle is location of basin outlet and red plus symbols are precipitation gauges in the basin region.

a)

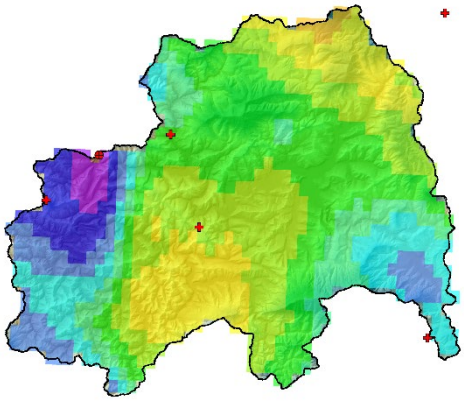

b)

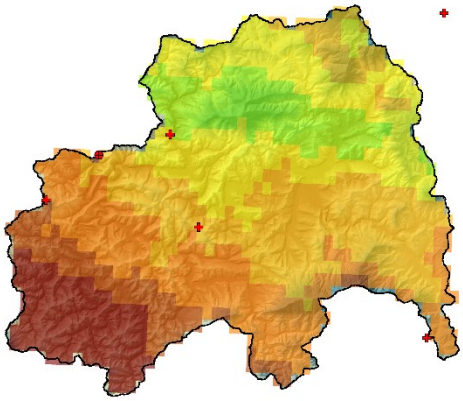

e)

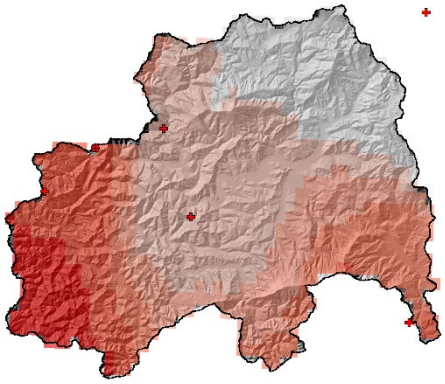

c)

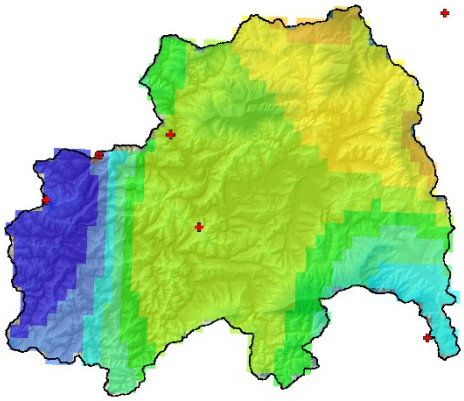

f)

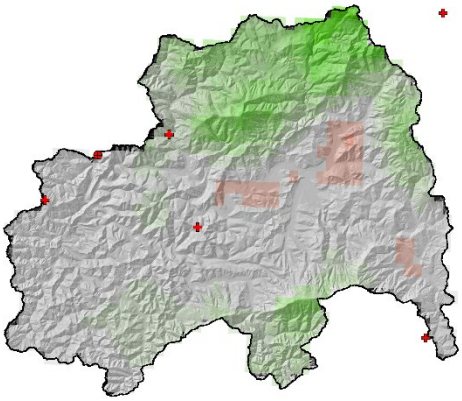

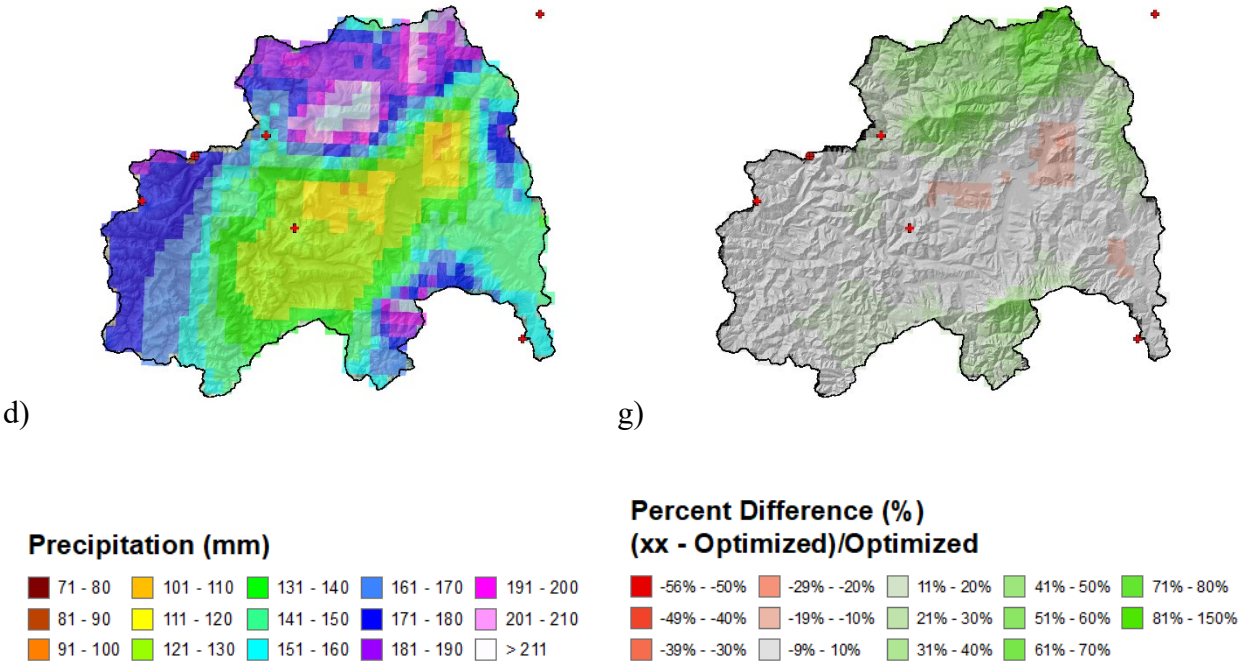

Figure 4.2. Spatial total storm precipitation patterns for a) gauge-adjusted radar reconstruction, b) default radar reconstruction, c) IDW reconstruction and d) IDW-PRISM reconstruction for the November 6 - 8, 2006 storm event. Percent difference from gauge-adjusted radar spatial pattern to e) default radar pattern f) IDW pattern and g) IDW-PRISM pattern. Red circle is location of basin outlet and red plus symbols are precipitation gauges in the basin region.

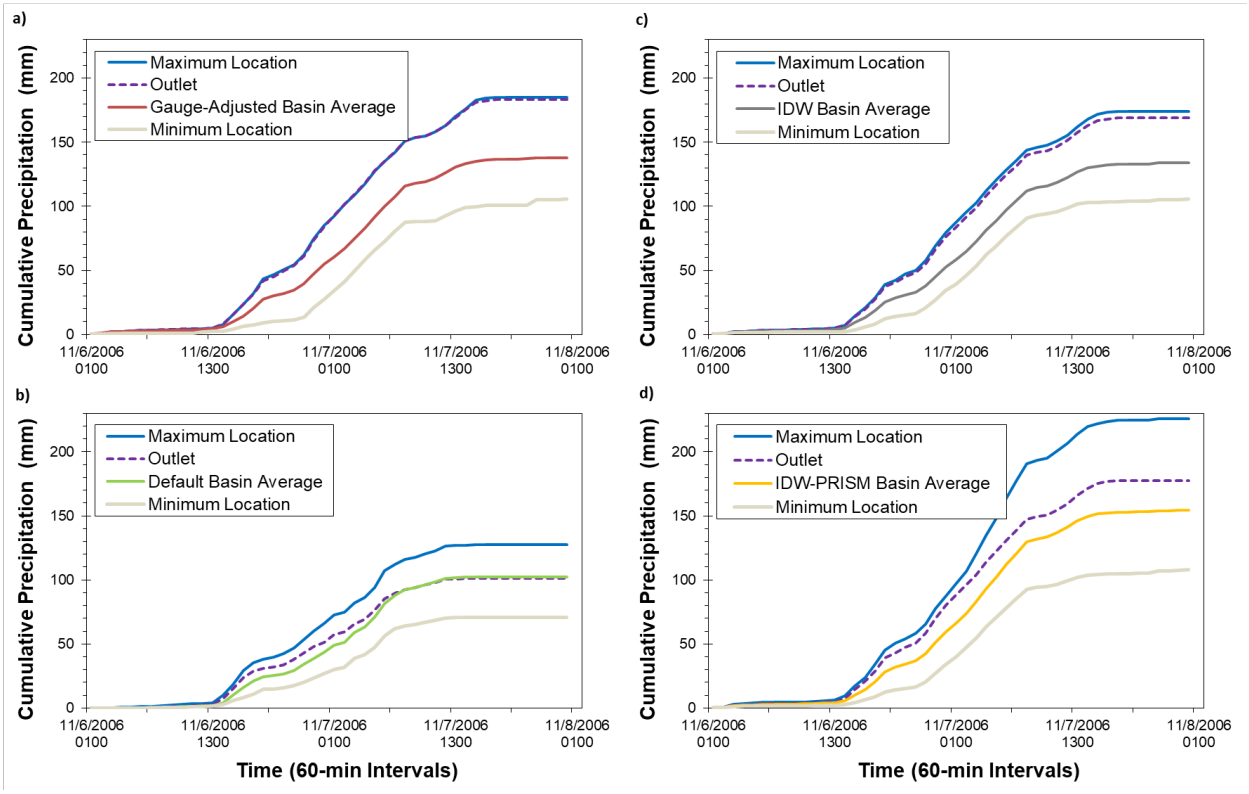

Figure 4.3. Hourly mass curve accumulated precipitation from 0100 PST 06 November to 0100 PST 08 November for a) gauge-adjusted radar reconstruction, b) default radar reconstruction, c) IDW reconstruction and d) IDW-PRISM reconstruction.

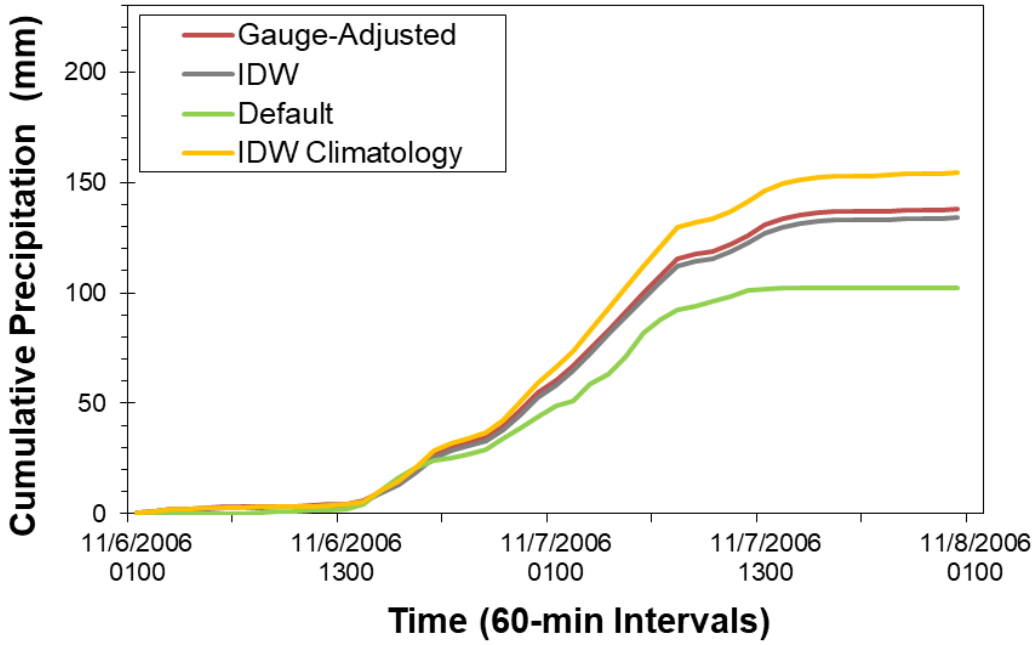

Figure 4.4. Hourly basin average mass curve accumulations used as input in to the calibrated HEC-HMS model to estimate to streamflow.

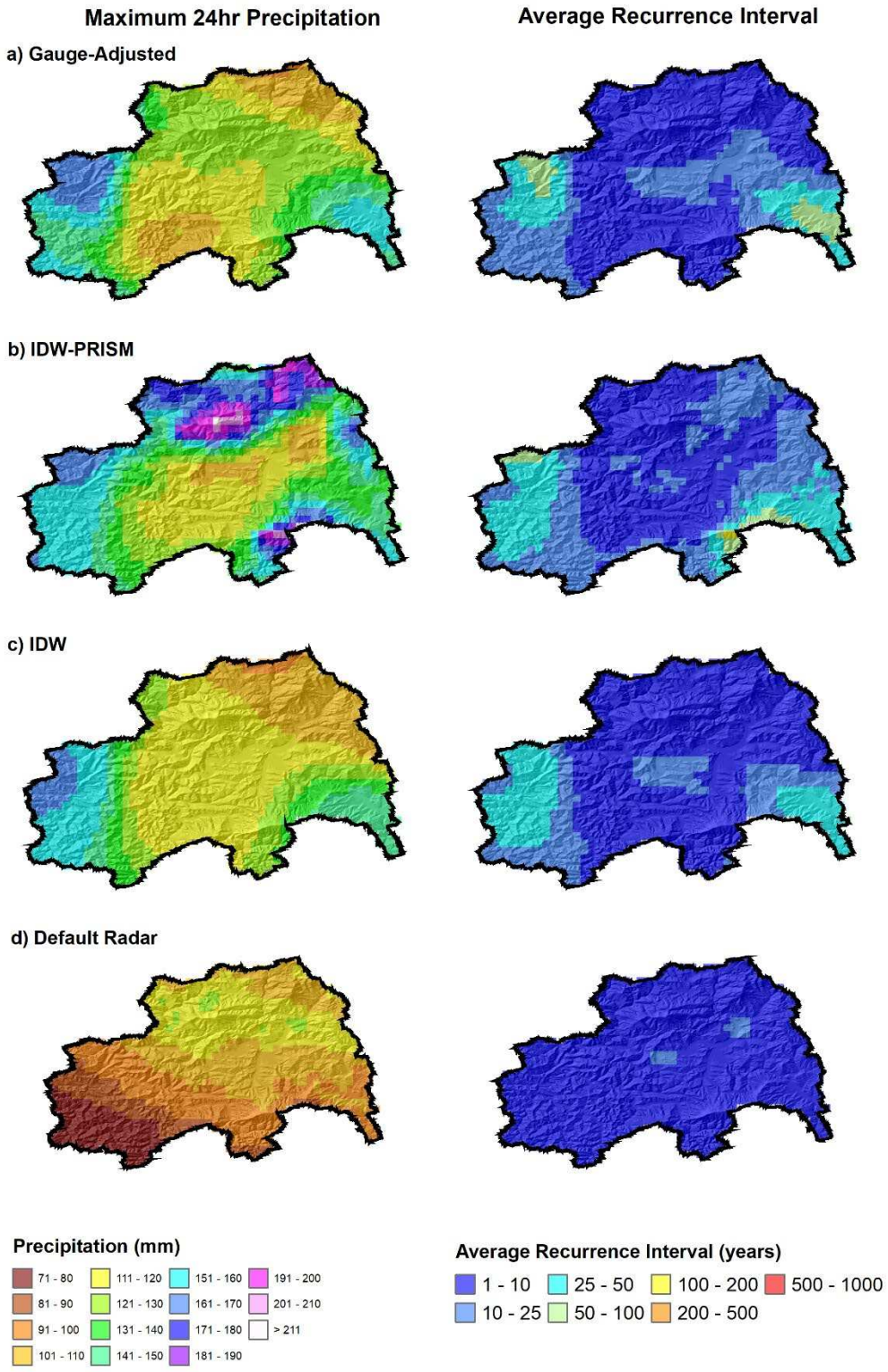

Figure 4.5. 24-hour maximum estimated precipitation and the associated 24-hour average recurrence interval for 6–8 November 2006 storm event for a) gauge-adjusted radar estimate, b) IDW-PRISM estimate, c) IDW estimate and d) default radar estimate.

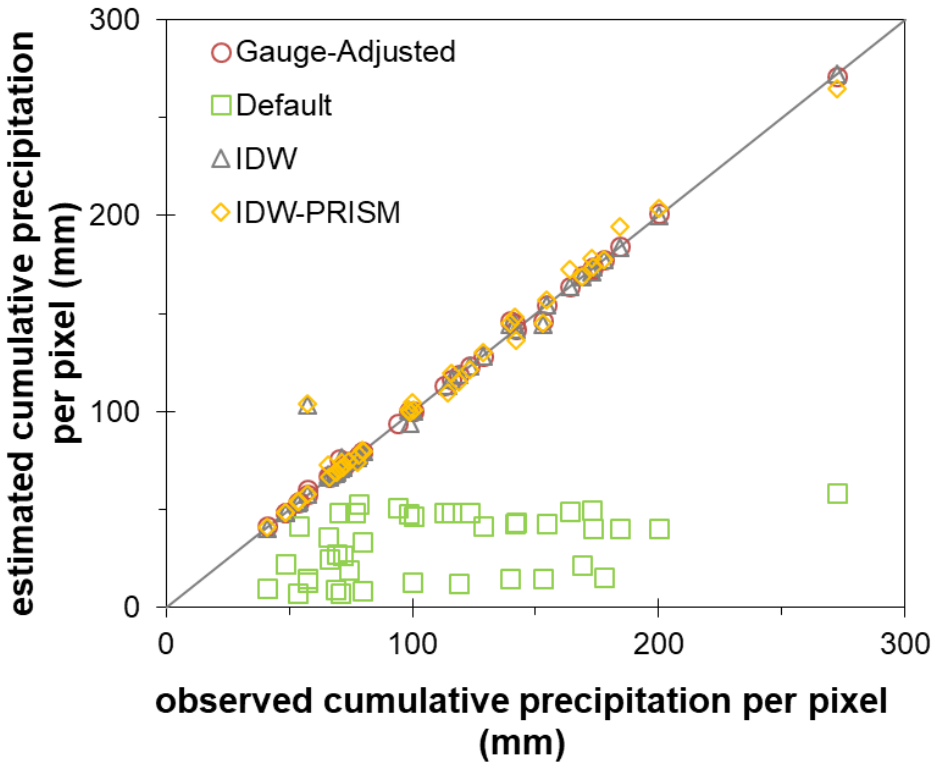

Figure 4.6. Fit between the observed total storm precipitation and estimated total storm precipitation at 42 gauge locations used to derive hourly and the total storm precipitation estimates. Black line represents a 1:1 fit.

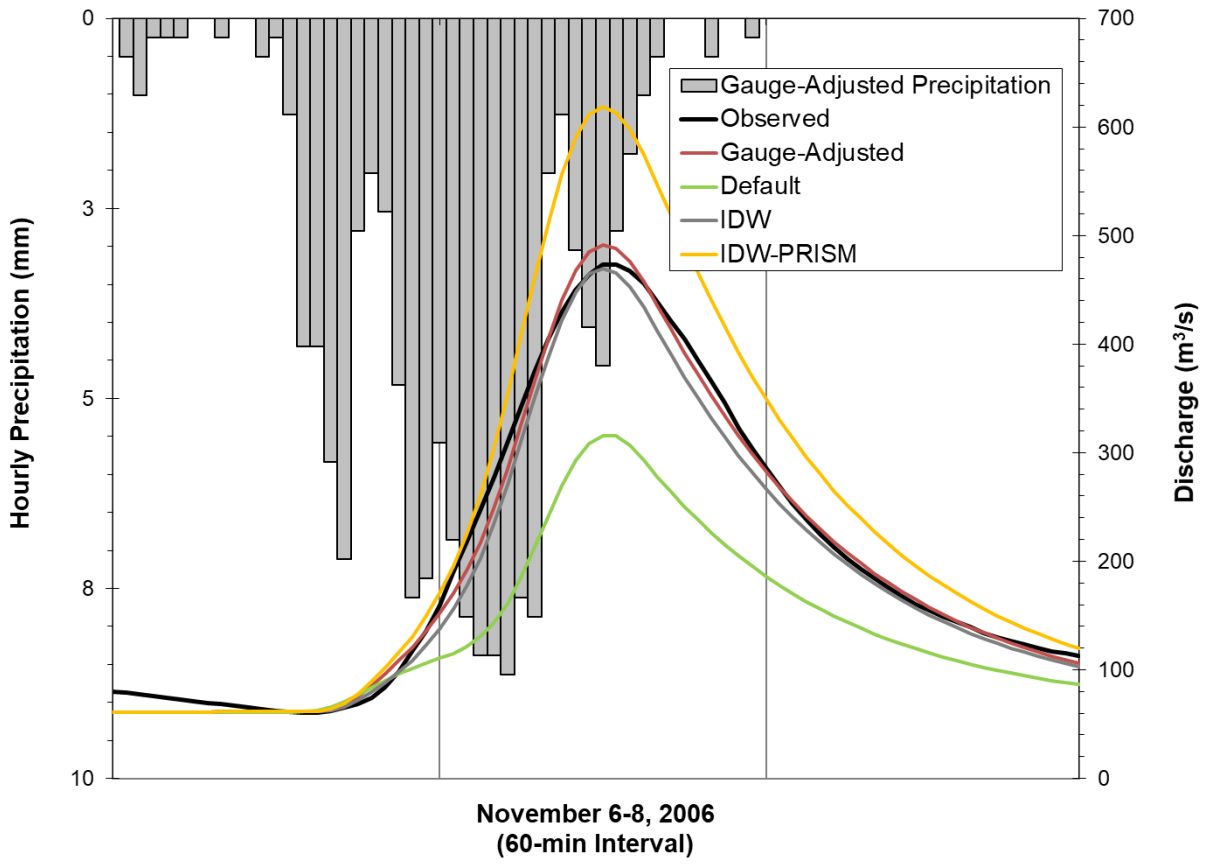

Figure 4.7. Streamflow modeled with the gauge-adjusted radar (red), default radar (green), IDW (grey), and IDW-PRISM (orange) average basin hourly precipitation grids. Gauge-adjusted hourly basin average precipitation is shown (grey) and observed USGS streamflow (black).

REFERENCES

Adirosi, E., Baldini, L., Roberto, N., Gorgucci, E., Gatlin, P., Tokay, A. 2015. Estimation of raindrop drop size distributions and their vertical profile using ground based disdrometer and FMCW vertically pointing radar. In: *1st URSI Atlantic Radio Science Conference (URSI AT-RASC)*, Las Palmas, Spain. https://doi.org/10.1109/URSI-AT-RASC.2015.7303070

Atlas, D., Ryzhkov, A., Zrnic, D. 1997. Polarimetrically tuned Z-R relations and comparison of radar rainfall methods. *Weather Radar Technology for Water Resources Management*, (eds Braga, B and Massambani O.) UNESCO Press, Paris, France, 3-67.

Bajwa, H.S., Tim, U.S. 2002. Toward immersive virtual environments for GIS-based floodplain modeling and visualization. In: *Proceedings of 22nd ESRI User Conference*, San Diego, TX, USA.

Borga, M. 2002. Accuracy of radar rainfall estimates for stream flow simulation. *Journal of Hydrology* 267, 26-39.

Brandes, E.A. 1975. Optimizing Rainfall Estimates with the Aid of Radar. *Journal of Applied Meteorology* 14, 1339-1345.

Brown, V.M., Keim, B.D., Kappel, W.D., Hultstrand, D.M., Peyrefitte, A.G., Black, A.W., Steinhilber, K.M. and Muhlestein, G.A. 2020. How Rare Was the August 2016 South-Central Louisiana Heavy Rainfall Event? *Journal of Hydrometeorology*, 21, 773–790, https://doi.org/10.1175/JHM-D-19-0225.1

Chapman, D.W., Corliss, J.F., Phillips, R.W., and Demory, R.L. 1961. *The Alsea Watershed Study*. Misc. Paper 110, Oregon State University, Agricultural Experimental Station, Corvallis, OR. 52pp.

Cole, S.J., Moore, R.J. 2008. Hydrological modelling using raingauge and radar-based estimator of areal rainfall. *Journal of Hydrology* 358, 159-181. https://doi.org/10.1016/j.jhydrol.2008.05.025

Daly, C., Gibson, W.P., Doggett, M., Smith, J., Taylor, G. 2004. Up-to-date monthly climate maps for the conterminous United States. *14th AMS Conf. on Applied Climatology*, 84th AMS Annual Meeting Combined Preprints, Seattle, WA.

Daly, C., Neilson, R.P., Phillips, D.L. 1994. A statistical-topographic model for mapping climatological precipitation for mountainous terrain. *Journal of Applied Meteorology* 33, 140-158.

Dickens, J. 2003. On the Retrieval of Drop Size Distribution by Vertically Pointing Radar. *American Meteorological Society 32nd Radar Meteorology Conference*, Albuquerque, NM, October 2003.

Fassnacht, S.R., Soulis, E.D., Kouwen, N. 1999. Algorithm application to improve weather radar snowfall estimates for winter hydrologic modelling. *Hydrological Processes* 13(18), 3017-3039. https://doi.org/10.1002/(SICI)1099-1085(19991230)13:183.0.CO;2-K

Fassnacht, S.R., Kouwen, K., Soulis, E.D. 2001. Surface temperature adjustments to improve weather radar representation of multi-temporal winter precipitation accumulations. *Journal of Hydrology* 253(1-4), 148-168. https://doi.org/10.1016/S0022-1694(01)00479-6

Fassnacht, S.R., Dressler, K.A., Bales, R.C. 2003a. Snow water equivalent interpolation for the Colorado River Basin from snow telemetry (SNOTEL) data. *Water Resources Research* 39(8), 1208. https://doi.org/10.1029/2002WR001512

Fassnacht, S.R., Soulis, E.D., Kouwen, N. 2003b. Radar precipitation for winter hydrological modelling. *Information from Weather Radar and Hydrological Modelling* (Proceedings IUGG 2003 Symposium HS02, Sapporo Japan, July 2003), IAHS 282, 35-42.

Girons lopez, M., Wennerström, H., Nordén, H., Seibert, J. 2015. Location and density of rain gauges for the estimation of spatial varying precipitation, *Geografiska Annaler: Series A, Physical Geography* 97(1), 167-179. https://doi.org/10.1111/geoa.12094

Hall J.D., Stednick J.D. 2008. The Alsea Watershed Study. In: *Hydrological and Biological Responses to Forest Practices* (ed. J.D. Stednick), Ecological Studies volume 199, Springer, New York, NY, p1-18.

Hultstrand, D.M., Parzybok, T.W., Tomlinson, E.M., Kappel, W.D. 2008. Advanced Spatial and Temporal Rainfall Analyses for Use in Watershed Models. In: *Proceedings of the Third Interagency Conference on Research in the Watersheds*, U.S. Geological Survey Scientific Investigations Report, Estes Park, CO, September 8-11, 2008.

Hultstrand, D.M., Kappel, W.D. 2017. The Storm Precipitation Analysis System (SPAS) Report. *Nuclear Regulatory Commission (NRC) Inspection Report* No 99901474/2016-201, Enercon Services, Inc., 95pp.

Hunter, R.D., Meentemeyer, R.K. 2005. Climatologically Aided Mapping of Daily Precipitation and Temperature. *Journal of Applied Meteorology* 44, 1501-1510.

Hunter, S.M. 2008. *WSR-88D Radar Rainfall Estimation: Capabilities, Limitations and Potential Improvements.* National Weather Service Forecast Office, Morristown, TN. http://nwafiles.nwas.org/digest/papers/1996/Vol20No4/Pg26-Hunter.pdf

Isaaks, E.H, and R.M. Srivastava, 1989. *An Introduction to Applied Geostatistics*. Oxford University Press, New York, 592 pp.

Keim, B.D., Kappel W.D., Muhlestein, G.A, Hultstrand, D.M., Parzybok, T.W., Lewis, A.B., Tomlinson, E.M., and Black A.W. 2018. Assessment of the Extreme Rainfall Event at Nashville, TN and the Surrounding Region on May 1-3, 2010. *Journal of the American Water Resources Associates*, 54(5), 1001-1010. https://doi.org/10.1111/1752-1688.12657

Kouwen, N. 1988. WATFLOOD: a Micro-Computer Based Flood Forecasting System Based on Real-Time Weather Radar. *Canadian Water Resources Journal / Revue canadienne des ressources hydriques* 13(1), 62-77. https://doi.org/10.4296/cwrj1301062

Lakshmanan, V., Valente, M. 2004. Quality control of radar reflectivity data using satellite data and surface observations. In: *20th International Conference on Inter. Inf. Proc. Sys. (IIPS) for Meteorology, Oceanography, and Hydrology*, American Meteorological Society, Seattle, CD-ROM, 12.2.

Lakshmanan, V., Karstens, C., Krause, J., Tang, L. 2014. Quality Control of Weather Radar Data Using Polarimetric Variables, *Journal of Atmospheric and Oceanic Technology* 31, 1234–1249. https://doi.org/10.1175/JTECH-D-13-00073.1

Lincoln, W.S. 2014. Analysis of the 15 June 2013 isolated extreme rainfall event in Springfield, Missouri. *Journal of Operational Meteorology* 2(19), 233–245. https://doi.org/10.15191/nwajom.2014.0219.

Lincoln, W.S, Thomason, R.F., Stackhouse, M., Schlotzhauer, D.S. 2017. Utilizing crowd-sourced rainfall and flood impact information to improve the analysis of the North Central Gulf Coast flood event of April 2014. *Journal of Operational Meteorology* 5,(3), 26-41. doi: http://doi.org/10.15191/nwajom.2017.0503.

Marshall, J.S., Palmer, W.M. 1948. The distribution of raindrops with size. *Journal of Meteorology* 5, 165-166.

Martner, B.E., Dubovskiy, V., Matrosov, S.Y. 2005. Z-R Relations from Raindrop Disdrometers: Sensitivity to Regression Methods and DSD Data Refinements. In: *32nd Radar Meteorology Conference*, Albuquerque, NM.

Miller, J.F., Frederick, R.H., Tracey, R.J. 1973. *Precipitation-Frequency Atlas of the Western United States, Volume X, Oregon*. U.S. Department of Commerce, National Weather Service, NOAA Atlas 2, Silver Springs, MD.

Moon, J., Srinivasan, R., Jacobs, J.H. 2004. Stream Flow Estimation Using Spatially Distributed Rainfall in the Trinity River Basin, Texas. *Transactions of the American Society of Agricultural Engineers* 47(5), 1445-1451. https//:doi.org/10.13031/2013.17624.

Mousavi, S., Kouwen, N. 2003. Coupling of MODFLOW and WATFLOOD in a hydrological modelling of a small watershed. *Information from Weather Radar and Hydrological Modelling* (Proceedings IUGG 2003 Symposium HS02, Sapporo Japan, July 2003), IAHS 282, 294-300.

Ochoa-Rodriguez, S., Wang, L.P., Gires, A., Pina, R.D., Reinoso-Rondinel, R., Bruni, G., Ichiba, A., Gaitan, S., Cristiano, E., Assel, J.v., Kroll, S., Murlà-Tuyls, D., Tisserand, B., Schertzer, D., Tchiguirinskaia, I., Onof, C., Willems, P., Veldhuis, M-C. 2015. Impact of Spatial and

Temporal Resolution of Rainfall Inputs on Urban Hydrodynamic Modelling Outputs: A Multi-Catchment Investigation. *Journal of Hydrology* 531(2), 389-407. http://dx.doi.org/10.1016/j.jhydrol.2015.05.035

Ogden, F.L., Sharif, H.O., Senarath, S.U.S., Smith, J.A., Baeck, M.L., Richardson J.R. 2000. Hydrologic analysis of the Fort Collins, Colorado, flash flood of 1997. *Journal of Hydrology*, 228(1-2), 82-100.

Parzybok, T.W., Hultstrand, D.M., Tomlinson, E.M., Kappel, W.D. 2008. High-Resolution Storm Rainfall Analysis for Use in Hydrologic Modeling: Storm Precipitation Analysis System (SPAS) and NEXRAD Weather Radar. *Hydrovision Conference*, Sacramento, CA. July 14-18, 2008.

Parzybok, T.W., Clarke, B., Hultstrand, D.M. 2011. Average recurrence interval of extreme rainfall in real-time. Earthzine. https://earthzine.org/average-recurrence-interval-of-extreme-rainfall-in-real-time-2/

Perica, S., Martin, D., Pavlovic, S., Roy, I., St. Laurent, M., Trypaluk, C., Unruh, D., Yekta, M., Bonnin, G. 2013. *NOAA Atlas 14 Volume 8 Version 2, Precipitation-Frequency Atlas of the United States, Midwestern States*. NOAA, National Weather Service, Silver Spring, MD.

Pessoa, M.L. Rafael, L.B., Earle, R.W. 1993. Use of weather radar for flood forecasting in the Sieve river basin: a sensitivity analysis. *Journal of Applied Meteorology* 32, 462-475.

PRISM Climate Group, 2020. PRISM Climate Data. Northwest Alliance for Computational Science & Engineering (NACSE), Oregon State University, Corvallis, Oregon, URL: http://www.prism.oregonstate.edu/, last accessed 23 March 2020.

Ren, L., Li, C., Wang, W. 2003. Application of Radar-Measured Rain Data in Hydrological Processes Modeling during the Intensified Observation Period of HUBEX. *Advances in Atmospheric Sciences* 20(2), 205-211. https://doi.org/10.1007/s00376-003-0005-8

Schaake, J., Henkel, A., Cong, S. 2004. Application of PRISM Climatologies for Hydrologic Modeling and Forecasting in the Western U.S. In: *18th Conference on Hydrology*, American Meteorological Society, Seattle, WA. https://ams.confex.com/ams/84Annual/techprogram/paper_72159.htm

Schaefer, M.G., Barker, B.L., Taylor, G.H., Wallis, J.R. 2008. *Regional Precipitation-Frequency Analysis and Spatial Mapping of 24-Hour Precipitation for Oregon*. Oregon State Department of Transportation Technical Report OR-RD-FHWA-08-05, January 2008. https://rosap.ntl.bts.gov/view/dot/21841

Scharffenberg, B., Bartles, M., Brauer, T., Fleming, M., Karlovits, G. 2018. Hydrologic Modeling System HEC-HMS – User's Manual, Version 4.3. U.S. Army Corps of Engineers, Institute for Water Resources, Hydrologic Engineering Center (CEIWR-HEC), Davis, CA, USA.

Segond, M., Wheater, H.S., Onof, C. 2007. The significance of spatial rainfall representation for flood runoff estimation: a numerical evaluation based on the Lee catchment, UK. *Journal of Hydrology* 347, 116-131.

Segura, C., Bladon, K.D., Hatten, J.A., Jones, J.A., Hale, V.C., Ice, G.G. 2020. Long-term effects of forest harvesting on summer low flow deficits in the Coast Range of Oregon. *Journal of Hydrology* 585, 124749. https://doi.org/10.1016/j.jhydrol.2020.124749.

Sharif, H.O., Ogden, F.L., Krajewski, W.F., Xue, M. 2002. Numerical simulations of radar rainfall error propagation, *Water Resources Research* 38(8), 1140. https://doi.org/10.1029/2001WR000525

Sik Kim, B., Kyung Kim, B., Soo Kim, H. 2008. Flood simulation using the gauge-adjusted radar rainfall and physics-based distributed hydrologic model. *Hydrological Processes* 22, 4400-4414. https://doi.org/10.1002/hyp.7043

Sirisena, T.S., Maskey, S., Ranasinghe, R., Babel, M.S. 2018. Effects of different precipitation inputs on streamflow simulation in the Irrawaddy River Basin, Myanmar. *Journal of Hydrology: Regional Studies* 19, 265-278. https://doi.org/10.1016/j.ejrh.2018.10.005

Sivasubramaniam, K., Sharma, A., Alfredsen, K. 2018. Estimating radar precipitation in cold climates: the role of air temperature within a non-parametric framework. *Hydrology and Earth System Sciences* 22(12), 6533-6546. https://doi.org/10.5194/hess-22-6533-2018

Stednick, J.D. 2008. The New Alsea Watershed Study. In: *Hydrological and Biological Responses to Forest Practices* (ed. J.D. Stednick), Ecological Studies volume 199, Springer, New York, NY, p115-121.

Sun, X., Mein, R.G., Keenan, T.D., Elliott, J.F. 2000. Flood estimation using radar and rain gauge data. *Journal of Hydrology* 239, 4-18.

Thiessen, A.H. 1911. Precipitation Averages for Large Areas. *Monthly Weather Review* 39(7), 1082-1084.

Uijlenhoet, R. 2001. Raindrop size distributions for radar reflectivity-rain rate relationships for radar hydrology. *Hydrology and Earth System Science* 5, 615-628.

U.S. Army Corps of Engineers 2016. *Hydrologic Modeling System (HEC-HMS) Quick Start Guide: Version 4.2*. U.S. Army Corps of Engineers, Institute for Water Resources, Hydrologic Engineering Center (CEIWR-HEC), Davis, CA, USA.

Vieux, B.E., Vieux, J.E., Chen, C., Howard, K.W. 2003. Operational deployment of a physics-based distributed rainfall-runoff model for flood forecasting in Taiwan. *Information from Weather Radar and Hydrological Modelling* (Proceedings IUGG 2003 Symposium HS02, Sapporo Japan, July 2003), IAHS 282, 251-257.

Waleed, A., Amin, M., Halim, G.A., Shariff, A., Aimrun, W. 2009. Calibrated Radar-Derived Rainfall Data for Rainfall-Runoff Modeling. *European Journal of Scientific Research* 30, 608-619.

Yang, D., Koike, T., Tanizawa, H. 2004. Application of a distributed hydrological model and weather radar observations for flood management in the upper Tone River of Japan. *Hydrological Processes* 18, 3119-3132.

Zhang, J., Howard, K., Langston, C., Vasiloff, S., Kaney, B., Arthur, A., Van Cooten, S., Kelleher, K., Kitzmiller, D., Ding, F., Seo, D., Wells, E., Dempsey, C. 2011. National Mosaic and Multi-Sensor QPE (NMQ) System: Description, Results, and Future Plans. *Bulletin American Meteorological Society* 92, 1321-1338. https://doi.org/10.1175/2011BAMS-D-11-00047.1

Zhang, J., Howard, K., Vasiloff, S., Langston, C., Kaney, B., Qi, Y., Tang, L., Grams, H., Kitzmiller, D., Levit, J. 2014. Initial Operating Capabilities of Quantitative Precipitation Estimation in the Multi-Radar Multi-Sensor System. In: *28th Conference on Hydrology*, American Meteorological Society, Atlanta, Georgia.

5.0 DISCUSSION

5.1 Details from the Individual Papers

Through a combination of field measurements, data collection, and modelling this dissertation applied scientific methods to build on and advance knowledge of four water balance components. With the goal to improve the hydrologic community awareness of water resources in terms of hydrologic uncertainty (Nearing and Gupta, 2018) and to improve water supply forecasting, water supply modelling, and design infrastructure. This dissertation is structured by the following questions examined in Chapters 2 through 4: (1) Can snowpack sublimation uncertainty be quantified, if so what variables are sensitive for snowpack sublimation estimates? (2) Can a snow depth measurement dataset be used to identify and model a snow depth distribution climatology, if so can the climatology be scaled to estimate snow depth distribution for different years within complex mountainous terrain? (3) What are the uncertainty and sensitivity that spatial rainfall data have on modeled streamflow? Chapters 2 through 4 of this dissertation evaluate and build on knowledge that are central to these overarching questions.

In Chapter 2, snowpack sublimation sensitivity was evaluated and quantified in a sub-alpine environment based on the bulk aerodynamic flux (BF) method. Sublimation measurements based on aerodynamic profile (AP) and eddy covariance (EC) require extensive meteorological measurements, typically limited to research facilities, whereas the BF method requires fewer meteorological measurements that are often available on standard operational meteorological monitoring networks. This evaluation of snowpack sublimation within mountainous terrain is particularly applicable for water balance modelling to properly account for instrumentation errors and what variables need the

greatest attention while performing snowpack sublimation computations. This study revealed snowpack sublimation losses, as a percent of annual total precipitation (14 to 65%), are generally greater when incorporating uncertainty analysis as compared to ranges stated in literature (21 to 52%). Results highlight how meteorological and related data that are used in models, such as in SnowModel with MicroMet (Liston and Elder, 2006), may have substantial impact on simulated datasets. These findings provide important considerations to evaluate sensor error, and related issues including discontinuity in measurements. For example, at the SNOTEL stations, they moved the temperature sensors without evaluating longterm impacts (Ma et al., 2019). Adequately quantifying and assessing the dynamic nature of snow surface roughness (Brock et al., 2006) showed the range of snow surface roughness (z_0) values for different locations, and Sanow et al. (2018) illustrated the differences in z_0 at one location based on snow accumulation and melt characteristics. As snow accumulates and melts, the distant from the sensors to the snow surface changes (z), and this must be incorporated into any sublimation computations. Ultimately, future studies should incorporate these considerations to provide a more robust and complete understanding of snowpack sublimation and benefit water resources investigations such as water supply forecasting, and water supply modelling in snow dominated regions.

In Chapter 3, 10-years of near peak snow depth measurements and General Additive Model (GAM) interpolation methods were combined with topographic parameters to estimate a climatological consistent snow depth pattern (CSDP) that is scaled based on a winter season index, i.e., the amount of snow in a particular winter. The identification and implementation of a repeatable and scalable snow depth distribution (Strum and Wagner, 2010) within complex mountainous terrain can provide an accurate estimation of the distribution which is imperative to accurately model snowmelt contributions. The snow depth distribution from GAMs were highly

correlated (r = 0.83; Chapter 3) between years providing confidence in the estimated CSDP. The derived winter season index (r^2 = 0.75; Chapter 3), based on the correlation between mean snow depth measurements to Brooklyn Lake SNOTEL SWE, was used to characterize the winter season accumulation based on the snow on the ground. This study identified a winter season scaling index (WSI), quantified snow depth pattern repeatability and applied the pattern based on the WSI for an alpine watershed. These results, based on measurements and interpolation methods, reveal individual year correlations within reported ranges with a mean correlation higher than Airborne Lidar Surveys (ALS) estimates (Pflug and Lundquist, 2020). The results confirm that snow depth distributions are a result of consistent interactions between the localized meteorology, in particular solar radiation, wind speed and direction, and terrain from year to year. Quantifying snow depth patterns can provide additional information for hydrologic models that utilize snow depth distribution patterns. This can aid in modelling ablation processes, as these dictate streamflow out of a system, estimating spatial snowpack sublimation, and simulating baseflow characteristics and groundwater recharge. A benefit of using snow depth estimates (Chapter 3) with estimates of density, as per some of the limitations outlined by López-Moreno et al. (2013) in measuring density in similar type areas, or using modeled density is to estimate SWE from spatially distributed snow depth (Painter et al., 2016). At finer resolution, these snow depth data could be used to evaluate snow surface characteristics which could help estimate snow surface roughness (z_0), which is used in sublimation modelling (Chapter 2). Future studies that take time to identify and develop repeatable and scalable snow depth patterns, whether through sample measurements, modelling, and/or ALS, should include uncertainty estimates, e.g.,Monte Carlo methods (Chapter 2 and Chapter 3), to provide a more robust and complete understanding of snow distribution variability and uncertainty through time to aid

water resource disciplines such as, water supply forecasting and water supply modelling used to design infrastructure in snow dominated regions.

In Chapter 4, four highly spatial and temporal rainfall datasets were estimated and used as input into a hydrologic model to quantify the sensitivity of precipitation on modelled streamflow. Results from hydrologic model simulations were compared to observed USGS streamflow to determine the variance in streamflow from the different forcing precipitation datasets. Hydrologic model evaluation for two of the four simulations showed satisfactory performance of mean and maximum streamflow, while the other two datasets resulted in poor performance with large differences in the mean and maximum streamflow. The temporal characteristics were similar for the three datasets that utilized gauge data, while the dataset based solely on radar had the lowest magnitude and smallest intensities. These results illustrate the need for precipitation data that have accurate spatial and temporal characteristics in order to use a physically-based streamflow model. Precipitation estimates are the most important input to hydrologic models for hydrologic calibration, verification, and forecasting (Vieux et al., 2004; Sirisena et al., 2018), and are among the most difficult to quantify spatially and temporally. For intense rainfall events, this is due to the high spatial variability (Ogden, 2000; Brogan et al., 2017) and the lack of measurements, while for snowfall (Smith et al., 2014; Reges et al., 2016), this is due in part to undercatch (Goodison et al., 1998; Kochendorfer et al. 2017). Inability to forecast, measure, or model the spatial and temporal magnitudes of precipitation will limit the analysis, interpretation of data, and attempts to model the hydrologic response. Streamflow data, observed or simulated, are used to perform frequency analysis, quantify water yields, and design flood retaining structures.

The research presented in this dissertation supports a theme that hydrology is a highly uncertain science (Montanari et al, 2009), and that the uncertainty is a result of our limited knowledge on the interacting physical and empirical methods used to model many of the hydrologic and meteorologic processes, a lack of data (Fassnacht, in review) and the requirement to interpolate/extrapolate from the data we have (e.g., Collados Lara et al., 2021), that are not representative (e.g., Fassnacht et al., 2012). This works shows that no single component of the water balance can be quantified at the watershed scale without substantial uncertainty. However, we can begin to quantify the uncertainty. Specifically, this research investigated the sensitivity and uncertainty of four of the main water balance components for a basin: snowpack sublimation (E_s), precipitation as snow (P_s), precipitation as rainfall (P_r) and streamflow(Q). Mean cumulative snowpack sublimation uncertainty was 41% with individual input parameter uncertainties in the range of 1 to 29%, and the top three variables (z varying with d_s, z_0, and RH; Chapter 2,) accounted for 74 to 84% of the cumulative sublimation uncertainty. Snow depth distribution patterns were highly repeatable (r = 0.83) and applied with a winter season index (r^2 = 0.75) provide accurate snow distribution estimates, even when limited data were available, i.e., the number of snow depth samples was small (Chapter 3). For the 10 sampling years, the simulated basin mean snow was within 15% of observed, with the extreme dry and wet years being within 5%. Annual estimates are dependent on labor intensive snow depth measurement collection efforts that depend on weather and safety concerns, as well as available field personnel, and require spatial modelling methods; these results show that the uncertainty of simulated snow distribution are relatively small (15%). The forcing precipitation dataset used in hydrologic models to estimate streamflow can have cumulative uncertainties in the range of 30 to

60%, with precipitation and streamflow mean and maximum uncertainties equal at 15 and 30% respectively (Chapter 4).

5.2 Implications

The findings of this study have important implications for hydrologic research and offer insight for future investigations. Future applications of water balance modelling, whether an open or closed system (Kampf et al., 2020), should account for the various hydrologic component uncertainties (Fassnacht et al., 2018). Hydrologic uncertainty, in terms of a water balance model, arises from numerous sources, such as input error, sampling error, instrumentation error, calibration accuracy, parameter sensitivity and parameter uncertainty. In this study, several approaches were investigated for analyzing the impact of parameter uncertainty. An overarching goal of hydrological studies is to determine streamflow, from understanding the function of systems to forecasting. The methods and applications to quantify uncertainty in components of the hydrology cycle work towards improving streamflow estimation and defining streamflow uncertainty, especially in unrelated basins (Hrachowitz et al., 2013). Here, a proposed approach is one that includes Monte Carlo simulation with stochastic and deterministic uncertainty analyses to identify components that have the greatest sensitivity to simulated streamflow estimates. This integrated approach will aid in the identification of significant, non-significant, and/or redundant components of the water balance model.

Future studies that deal with snowpack sublimation, snow depth distribution, precipitation, and streamflow will benefit from results presented in this dissertation. For example, investigation that model snowpack losses (Sexstone et al., 2016), spatial and temporal characteristics of snowpack, snowmelt, and precipitation (Liston and Elder, 2006) can contribute

to model parameterization. Studies that model spatial and temporal characteristics of precipitation (Daly et al., 1994), perform hydrologic model calibration and verification (Vieux et al., 2004) will have more robust results. Site-specific or regional studies (Hosking and Wallis, 1997) that perform rainfall and snowpack frequency analysis (Schaefer et al., 2008; Cho and Jacobs, 2020) or streamflow analysis (Sirisena et al., 2018) will both benefit and aid in critical designs for flood retaining structures (Cheng and AghaKouchak, 2014; Cho and Jacobs, 2020). The limitations and possible future investigations related to the work are presented below.

5.3 Limitations and Possible Next Steps

This dissertation used data collection and modelling of water balance components to provide advances related to the uncertainty in water balance studies and assist water resources decisions. While it also presents an opportunity for future investigations from this work, there are some limitations. In Chapter 2, a three year sample size limited the generalizability of the snowpack sublimation results. However, these three years were selected to represent the range of snowpack conditions within the available period of record, specifically a normal snowpack (2005), an above normal snowpack (2011), and a below normal snowpack (2012). Future research could estimate snowpack sublimation uncertainty for all available years of record. This could provide a more robust distribution of uncertainty estimates, yet the range of uncertainty was likely covered by the largest and smallest snowpack years investigated.

In Chapter 3, the accuracy of the CSDP may be influenced by the specific spatial interpolation model that was applied. However, the GAM interpolation method did produce highly correlated results, measurement spatial pattern to simulated spatial pattern, providing a

high level of confidence in the snow depth pattern. Future research could compare the empirically modeled snow depth patterns to results from a physically-based snow model (e.g., SnowModel, since component thereof was used near the study site; Hiemstra et al., 2002) to investigate pattern repeatability (Sturm and Wagner, 2010), and thus determine snow depth uncertainty estimates. This could include evaluating the distribution of sampling for the different years, such as focusing on how representative the last five sampling years were of the study site.

The precipitation evaluation and streamflow modelling in Chapter 4 examined one storm event and one basin which limited the generalizability of the precipitation and streamflow uncertainty results. However, the approximate 100-year rainfall event (Chapter 4) occurred in a well gauged basin, so this analysis deals with an important precipitation-runoff event for the basin. An assessment of individual events is common to understand the nature of the precipitation event and the resultant streamflow (e.g., Colle and Mass, 2000; Ogden et al., 2000; Brogan et al., 2017). Precipitation for one storm event was estimated based on four different interpolation methods, the sensitivity and uncertainty associated with different precipitation inputs into the hydrologic model were captured well. Future efforts could focus on different precipitation events with a range of precipitation recurrences. Expanding to additional basins is of interest to provide both refined local and regional uncertainty for precipitation inputs and effects on streamflow.

5.4 Future Opportunities

The methodology presented in Chapter 2 and Chapter 3 could be used in future investigations to evaluate parameterizations of other critical components for snowpack modelling

(Liston and Elder, 2006) and hydrological modelling (Ochoa-Rodriguez et al., 2015; Sirisena, 2018) applications. Also, snow modelling applications that utilize a fine grid resolution to simulate the processes driving snow distribution (e.g., snow redistribution by wind in alpine areas) or CSDPs, based on field measurement and ALS, may be particularly useful for model evaluation (e.g., Phillips, 2013; Pflug and Lundquist, 2020). Future research could evaluate the ability of snow model simulations to accurately characterize the spatial distribution of snow depth using detailed point measurements and ALS to infer model deficiencies based on errors in modeled snow depth.

The methodology presented in Chapter 4 could be used in future investigations to evaluate multiple precipitation estimates that are critical for streamflow model calibration and verification applications. Hydrologic models that utilize gridded datasets, compared to lumped models that use basin average data, to simulate streamflow may be particularly useful for model evaluation. Future research should take into account several precipitation estimates (e.g., gauge data, radar, satellite, reanalysis) as input into hydrologic models in order to accurately characterize the precipitation input uncertainties and modeled streamflow deficiencies. Incorporating Monte Carlo methods to account for precipitation dataset uncertainties will provide a suite of stochastic precipitation scenarios useful to estimate peak discharges with very low probability of occurrence (Felder and Weingartner, 2016).

Given that z of ds, RH, and z_o were estimated as a significant contribution of overall snowpack sublimation losses (e.g., Chapter 2), future research aimed at measuring these processes across multiple topographic locations could help to refine and improve the accuracy of estimated snowpack sublimation. In Chapter 3, near peak accumulation snow depth distribution was identified as being consistent year to year, topographic variables elevation, aspect, slope,

and maximum upwind slope controlled the snow distribution, future research should include these variables to refine and improve the accuracy of estimated snowpack distribution (Liston and Elder, 2006). Since different precipitation estimates provide a significant contribution of overall streamflow uncertainty (e.g., Chapter 4), future research that investigates multiple precipitation datasets should help to refine and improve the accuracy of estimated streamflow.

Lastly, future investigations should continue to pursue testing and improving water balance process representations within the hydrologic cycle; however, should also focus on the testing of the effectiveness of current model systems for water resources forecasting applications to evaluate potential deficiencies. For example, either the snow evolution model (Liston and Elder, 2006; Liston and Hiemstra, 2008) or the Utah Energy Balance Model (Tarboton and Luce, 2006) could be coupled with a hydrological model such as the US Army Corp of Engineers HEC-HMS and different precipitation forcing datasets to model water balance components to provide more robust and complete understanding on individual component uncertainties and propagated cumulative uncertainties. In the future, water resources management will likely benefit from the use of coupled physically-based models and Monte Carlo simulations that can account for snow processes such as redistribution and snow sublimation, account for different forcing precipitation datasets in order to quantify the spatial and temporal evolution and distribution of a water balance model.

5.5 Rational for Two Different Basins

The research of this dissertation focused on two mountain basins with different dominant precipitation inputs, specifically, rainfall and snowfall. In a snow dominant basin, the main source of precipitation inputs is in the form of snowfall; new snowfall accumulates to build the

snowpack during the winter season, storing water until spring temperatures increase, together with increased solar loading, to melt the snowpack. In a rain dominant basin, the main source of precipitation input is in the form of rainfall; rainfall has a direct impact on the basin streamflow and is not dependent on snowpack storage and melting. The two mountain basins, driven by rainfall and snowfall, were selected to estimate uncertainty of water balance components that are directly affect by the dominant precipitation type. Chapter 2 and 3 focused on a snow dominated watershed to capture the effects of snowpack sublimation and snowpack distribution in water balance modeling. In Chapter 4, we investigated a rain dominated basin and the direct effect on streamflow.

5.6 Scientific Method

The scientific method is a process of experimentation to ask and answer scientific questions. The scientific method typically consists of four steps: Observation, Hypothesis, Prediction, and Testing (Lee, 1992; Griffith, 2004; Schick and Vaughn, 2010). To me, the four steps seem limited and missing a few critical steps. I would define the scientific method in seven steps:

1) Problem or Question: develop a question or problem that can be solve through experimentation.
2) Observation and Research: make observations and perform research on problem or question.
3) Hypothesis: predict a possible outcome to the problem or question.

4) Experiment and Predictions: design a test or procedure to confirm or reject hypothesis.
5) Collect and Analyze Results: record data on what happened, modify procedure if needed.
6) Conclusion: review the data and check to see if hypothesis was correct.
7) Communicate the Results: present projects and results though presentations and journal submissions.

The most important feature of scientific method is the predictive power of the hypothesis, as tested though data analysis and experiments. In science disciplines, there is the possibility that new observations, experiments and/or technologies will conflict with the current theory. The entire procedure of scientific method is what makes science exciting, one can build on previous research to increase knowledge, or one can disprove a theory and diverge onto a new path. As new data, methods, and analysis procedures are developed, we can test against current data methods and theories.

In recent years, our society has been characterized by an unprecedented ability to produce, store, and analyze large amounts of data. With these data, the ability to process, analyze and extract useful information is important to gain additional process knowledge. Now, we have reached the point of creating a separate discipline, so-called Big Data (Succi and Coveney, 2019).

5.7 Big Data in Hydrology

Big Data build knowledge within and beyond science, enabling new, highly efficient ways to plan, conduct, disseminate and assess research (Nkiaka et al., 2016; Lange and Sippel, 2020). In the last few years, Big Data (BD), Machine Learning (ML), and Self Organizing Mapping (SOM) methods have created novel ways to produce, store, and analyze data. These new methods bring together computational, algorithmic, statistical and mathematical techniques to gain knowledge (Nkiaka et al., 2016; Lange and Sippel, 2020). With these data, questions such as "can we use large datasets to practice science to test scientific methods", "do these datasets change the way approach scientific methods", or "is there a blend of old and new methodologies that will help us build knowledge" can be asked. Big data are often associated with the idea of data-driven research (Succi and Coveney, 2019; Sabina, 2020), where learning happens through the accumulation of data and the application of methods to extract meaningful patterns from those data (Nkiaka et al., 2016).

For BD driven analysis, research tend to use data as their starting point, without relying on theoretical preconceptions, in contrast to theory-driven approaches where research consists of testing a hypothesis (Anderson, 2008). In principle, big data constitute the largest pool of data currently assembled and provide a starting point to search for hydrologic process interactions and correlations (Mayer-Schönberger and Cukier 2013). Crucial to data-driven approach credibility is the effectiveness of the methods used to extrapolate patterns from data and evaluate whether or not such patterns are meaningful, and what "meaning" may involve in the first place (Sabina, 2020).

In today's age, numerous data types are readily available (measured, modeled, simulated, probabilistic, machine learning, official, non-official) at one's fingertips, or a quick internet

search. The question we need to ask about these different data are how should we use them, which ones should we use, what scale or extent do they represent, can we combine multiple data (experimental, simulated, data driven, theoretical) to properly address specific scientific questions. Ultimately, uncertainty will always exist; the question is to what scale is acceptable, how can we reduce uncertainty, are big data driven correlations representative of the process and scale, and are they comparable to the scientific method?

5.8 Recommendations

Recommendations based on this dissertation are: 1) a need to assess uncertainty (Nearing and Gupta, 2018) so that we know what confidence we have in the deterministic numbers that our methods and models produce, 2) that uncertainty can be in various forms, including possible sensor error (Hultstrand and Fassnacht, 2018) or sensor bias (e.g., Ma et al., 2019), parameterization such as estimating the snowpack z_0 (e.g., Sanow et al., 2018), determination of consistent snowpack patterns (Sturm and Wagner, 2010; Chapter 3), spatial representivity of gauges (Fassnacht et al., 2003; Chapter 4), and 3) new data collection techniques, such as remote sensing tools (e.g., lidar becoming more operational or at least more prevalent in the context of hydrological monitoring; Painter et al., 2016) or the internet of things (Lettenmaier, 2017), and various modelling approaches (Dozier et al., 2016). However, we have much historical data and want to understand the past functioning of hydrological systems, even though non-stationarity is relevant (Milly et al., 2008) and impacts inter-annual patterns over longer time period (e.g., Fassnacht and Hultstrand, 2015).

Field measurements and instrumentation should accurately represent the physical properties of the hydrometeorological process being studied. In order to collect data that represent hydrometeorological process at the time of sampling, it is necessary to correctly locate and select equipment appropriate to site environments and study needs and use appropriate methods to make accurate field measurements. Calibration should be an ongoing requirement; this requirement will depend on the instrument technology and manufacturer recommendations. Instrument precision and accuracy should be measured periodically; precision and accuracy may vary, depending on the instrument used, sampling conditions, and sampling environment. In snow dominated basins, measurements of snow depth should be made, and it is recommended that snow depth sensors become a standard instrument on meteorological weather stations.

To investigate hydrologic uncertainty, two approaches could be taken within a Monte Carlo framework: (i) an analytical approach that considers in detail the potential sources of error and analyzes the nature of the component errors making use of available data, research results, and theoretical considerations, and (ii) an experimental approach that involves extensive comparative field studies (Dickinson, 1967; Montanari, 2007) and big data (Succi and Coveney, 2019). A combination of the analytical and experimental approaches would provide the best information on measurement and model errors of the hydrologic system. It is important that every hydrologic study consider at least one approach for studying uncertainty and the effect of uncertainty in that study.

REFERENCES

Anderson, C., 2008, “The End of Theory: The Data Deluge Makes the Scientific Method Obsolete”, *Wired Magazine*, 23 June 2008.

Brock, B., I. Willis, and M. Sharp, 2006. Measurement and parameterization of aerodynamic roughness length variations at Haut Glacier d’Arolla, Switzerland. *Journal of Glaciology*, 52(177), 281-297. https://doi.org/10.3189/172756506781828746

Brogan, D.J., P.A. Nelson, and L.H. MacDonald, 2017. Reconstructing extreme post-wildfire floods: a comparison of convective and mesoscale events. *Earth Surface Processes and Landforms*, 45(15), 2505-2522. https://doi.org/10.1002/esp.4194

Cheng, L., and A. AghaKouchak, 2014. Nonstationary Precipitation Intensity-Duration-Frequency Curves for Infrastructure Design in a Changing Climate. *Scientific Reports*, 4, 7093. https://doi.org/10.1038/srep07093

Cho, E., and J.M. Jacobs, 2020. Extreme Value Snow Water Equivalent and Snowmelt for Infrastructure Design Over the Contiguous United States. *Water Resources Research*, 56(10). https://doi.org/10.1029/2020WR028126

Collados-Lara A-J, S.R. Fassnacht, E. Pardo-Igúzquiza, and D. Pulido-Velazquez, 2021. Assessment of High Resolution Air Temperature Fields at Rocky Mountain National Park by Combining Scarce Point Measurements with Elevation and Remote Sensing Data. *Remote Sensing*, 13(1):113. https://doi.org/10.3390/rs13010113

Colle, B.A., and C.F. Mass, 2000. The 5–9 February 1996 Flooding Event over the Pacific Northwest: Sensitivity Studies and Evaluation of the MM5 Precipitation Forecasts. Monthly

Weather Review, 128(3), 593-617. https://doi.org/10.1175/1520-0493(2000)128<0593:TFFEOT>2.0.CO;2

Daly, C., Neilson, R.P., Phillips, D.L. 1994. A statistical-topographic model for mapping climatological precipitation for mountainous terrain. *Journal of Applied Meteorology* 33, 140-158. https://doi.org/10.1175/1520-0450(1994)033<0140:ASTMFM>2.0.CO;2

Dozier, J., E.H. Bair, and R.E. Davis, 2016. Estimating the spatial distribution of snow water equivalent in the world's mountains. *WIREs Water*, 3(3), 461-474. https://doi.org/10.1002/wat2.1140

Fassnacht, S.R. and M. Hultstrand, 2015. Snowpack variability and trends at long-term stations in northern Colorado, USA, *Proc. IAHS*, 371, 131–136. https://doi.org/10.5194/piahs-371-131-2015

Fassnacht, S.R., in review. A Call to: More Snow Sampling. Geosciences (submitted February 2021, geosciences-1131764)

Fassnacht, S.R., K.A. Dressler, and R.C. Bales, 2003. Snow water equivalent interpolation for the Colorado River Basin from snow telemetry (SNOTEL) data. *Water Resources Research*, 39(8), 1208. https://doi.org/10.1029/2002WR001512

Fassnacht, S.R., K.A. Dressler, D.M. Hultstrand, R.C. Bales, and G. Patterson, 2012. Temporal Inconsistencies in Coarse-scale Snow Water Equivalent Patterns: Colorado River Basin Snow Telemetry-Topography Regressions. *Pirineos*, 167, 167-186. https://doi.org/10.3989/Pirineos.2011.166008

Fassnacht, S.R., R.W. Webb, and M. Ma, 2018. Uncertainty in water resources: introduction to the special column. *Frontiers of Earth Science*, 12, 649–652. https://doi.org/10.1007/s11707-018-0737-5

Felder, G., and R. Weingartner, 2016. An approach for the determination of precipitation input for worst-case flood modelling. *Hydrological Sciences Journal*, 61(14), 2600-2609, https://doi.org/10.1080/02626667.2016.1151980

Goodison, B.E., P.Y.T Louie, and D. Yang, 1998. *WMO solid precipitation measurement intercomparison final report*, WMO Instruments and Observing Methods Report No. 67, WMO/TD No. 872.

Griffith, W.T., 2004. The Physics of Everyday Phenomena, fourth edition. McGraw Hill, New York, New York, 501 pp.

Hiemstra, C.A., G.E. Liston, and W.A. Reiners, 2002. Snow Redistribution by Wind and Interactions with Vegetation at Upper Treeline in the Medicine Bow Mountains, Wyoming, U.S.A., *Arctic, Antarctic, and Alpine Research*, 34:3, 262-273, DOI: 10.1080/15230430.2002.12003493

Hosking, J.R.M. and J.R. Wallis, 1997*: Regional frequency analysis, an approach based on L-moments*. Cambridge University Press, 224 pp

Hultstrand, D.M., and S.R. Fassnacht, 2018. The sensitivity of snowpack sublimation estimates to instrument and measurement uncertainty perturbed in a Monte Carlo framework. *Fronters of Earth Science*, 12, 728–738. https://doi.org/10.1007/s11707-018-0721-0

Kampf, S.K., et al., 2020. The case for an open water balance: Re-envisioning network design and data analysis for a complex, uncertain world. *Water Resources Research*, 56(6), e2019WR026699. https://doi.org/10.1029/2019WR026699Liston, G.E., and K. Elder, 2006. A distributed snow-evolution modeling system (SnowModel). *Journal of Hydrometeorology*, 7, 1259-1276. https://doi.org/10.1175/JHM548.1

Kochendorfer, J., et al., 2017. Analysis of single-Alter-shielded and unshielded measurements of mixed and solid precipitation from WMO-SPICE, *Hydrology and Earth System Sciences*, 21, 3525–3542, https://doi.org/10.5194/hess-21-3525-2017

Lange H., and S. Sippel, 2020. Machine Learning Applications in Hydrology. In: Levia D.F., Carlyle-Moses D.E., Iida S., Michalzik B., Nanko K., Tischer A. (eds) Forest-Water Interactions. *Ecological Studies (Analysis and Synthesis),* vol 240. Springer, Cham. https://doi.org/10.1007/978-3-030-26086-6_10

Lee, J., 1992. The education of hydrologists, *Hydrological Sciences Journal*, 37:3, 285-289.

Lettenmaier, D.P., 2017. Observational breakthroughs lead the way to improved hydrological predictions, *Water Resources Research*, 53(4), 2591-1597. https://doi.org/10.1002/2017WR020896

Liston, G. E., and K. Elder, 2006. A distributed snow-evolution modeling system (SnowModel). *Journal of Hydrometeorology*, 7(6), 1259-1276. https://doi.org/10.1175/JHM548.1

Liston, G.E., and C.A. Hiemstra, 2008. A Simple Data Assimilation System for Complex Snow Distributions (SnowAssim). *Journal of Hydrometeorology*, 9, 989-1004. https://doi.org/10.1175/2008JHM871.1

Ma, C., S.R. Fassnacht, and S.K. Kampf, 2019. How Temperature Sensor Change Affects Warming Trends and Modeling: An Evaluation Across the State of Colorado. *Water Resources Research*, 55(11), 9748-9764. https://doi.org/10.1029/2019WR025921

Mayer-Schönberger, V. and K. Cukier, 2013, Big Data: A Revolution that Will Transform How We Live, Work, and Think, New York: Eamon Dolan/Houghton Mifflin Harcourt.

Milly, P.C. et al., 2008. Stationarity is Dead: Whither Water Management?, *Science*, 319(5863), 573-574. DOI: 10.1126/science.1151915

Montanari, A., C.A. Shoemaker, and N. van de Giesen, 2009. Introduction to special section on Uncertainty Assessment in Surface and Subsurface Hydrology: An overview of issues and challenges. Water Resources Research, 45, W00B00, doi:10.1029/2009WR008471

Moreno, J.I., et al., 2013. Small scale spatial variability of snow density and depth over complex alpine terrain: Implications for estimating snow water equivalent, *Advances in Water Resources*, 55, 40-52. https://doi.org/10.1016/j.advwatres.2012.08.010

Nearing, G.S. and H.V. Gupta, 2018. Ensembles vs. information theory: supporting science under uncertainty. *Frontiers of Earth Science*, 12, 653-660. https://doi.org/10.1007/s11707-018-0709-9

Nkiaka, E., N.R., Nawaz, and J.C. Lovett, 2016. Using self-organizing maps to infill missing data in hydro-meteorological time series from the Logone catchment, Lake Chad basin. *Environmental Monitering and Assessment*, 188, 400. https://doi.org/10.1007/s10661-016-5385-1

Ochoa-Rodriguez, et al., 2015. Impact of Spatial and Temporal Resolution of Rainfall Inputs on Urban Hydrodynamic Modelling Outputs: A Multi-Catchment Investigation. *Journal of Hydrology*, 531(2), 389-407. http://dx.doi.org/10.1016/j.jhydrol.2015.05.035

Ogden F.L., et al., 2000. Hydrologic analysis of the Fort Collins, Colorado, flash flood of 1997, *Journal of Hydrology*, 228(1-2), 82-100. https://doi.org/10.1016/S0022-1694(00)00146-3

Pflug, J.M and J.D. Lundquist, 2020. Inferring Distributed Snow Depth by Leveraging Snow Pattern Repeatability: Investigation Using 47 Lidar Observations in the Tuolumne Watershed, Sierra Nevada, California. *Water Resources Research*, 56 (9), 1-17. https://doi.org/10.1029/2020WR027243

Painter, T.H., et al., 2016. The Airborne Snow Observatory: Fusion of scanning lidar, imaging spectrometer, and physically-based modeling for mapping snow water equivalent and snow albedo. *Remote Sensing of Environment*, 184, 139-152. https://doi.org/10.1016/j.rse.2016.06.018

Phillips M (2013). Estimates of sublimation in the Upper Colorado River basin. Unpublished Master of Science Thesis, Department of Atmospheric Science, Colorado State University, 57pp, < http://hdl.handle.net/10217/81052>

Reges, H.W., et al., 2016. CoCoRaHS: The Evolution and Accomplishments of a Volunteer Rain Gauge Network. *Bulletin of the American Meteorological Society*, 97(10) 1831-1846. https://doi.org/10.1175/BAMS-D-14-00213.1

Sabina, L, 2020. "Scientific Research and Big Data", The Stanford Encyclopedia of Philosophy (Summer 2020 Edition), Edward N. Zalta (ed.), URL =https://plato.stanford.edu/archives/sum2020/entries/science-big-data/

Sanow, J.E., et al., 2019. Geometric Versus Anemometric Surface Roughness for a Shallow Accumulating Snowpack. *Geosciences*, 8(12):463. https://doi.org/10.3390/geosciences8120463

Schick, T. and L. Vaughn, 2010. How to Think About Weird Things Critical Thinking for a New Age, sixth edition. McGraw Hill, New York, New York, 352 pp.

Sexstone, G.A., D.W. Clow, D.I. Stannard, and S.R. Fassnacht, 2016. Comparison of methods for quantifying surface sublimation over seasonally snow-covered terrain. *Hydrological Processes*, 30(19), 3373-3389. https://doi.org/10.1002/hyp.10864

Sirisena, T.S., S. Maskey, R. Ranasinghe, M.S. Babel, 2018. Effects of different precipitation inputs on streamflow simulation in the Irrawaddy River Basin, Myanmar. *Journal of Hydrology: Regional Studies* 19, 265-278. https://doi.org/10.1016/j.ejrh.2018.10.005

Smith, K.H., et al., 2014. Local observers fill in the details on drought impact reporter maps. *Bulletin of the American Meteorological Society*, 95, 1659–1662, doi:10.1175/1520-0477-95.11.1659

Sturm, A., and A. Wagner, 2010. Using repeated patterns in snow distribution modeling: An Arctic example, *Water Resources Research*, 46, W12549, doi:10.1029/2010WR009434

Succi S and P.V. Coveney, 2019. Big data: the end of the scientific method? *Philosophical Transactions Royal Publishing Society*, 377: 20180145. http://dx.doi.org/10.1098/rsta.2018.0145

Tarboton, D.G. and C.H. Luce, 2006. Utah Energy Balance Snow Accumulation Model (UEB), Computer model technical description and users guide, Utah Water Research Laboratory and USDA Forest Service Intermountain Research Station, 64 pp.

Vieux, B.E, Z. Cui, and A Gaur, 2004. Evaluation of a physics-based distributed hydrologic model for flood forecasting. *Journal of Hydrology*, 298(1-4), 155-177. https://doi.org/10.1016/j.jhydrol.2004.03.035

6.0 REFLECTIONS

6.1 Summary

My path through graduate school was non-traditional; I started my PhD graduate endeavor and dissertation research over 12-years ago. In this time, I have had numerous life experiences, such as a being a working professional, starting and growing a business, moving across the country several times, getting married, and being blessed with two wonderful children. These life experiences meant a traditional full-time graduate student was not an option for me. Over the years, life has become more of a balancing act, juggling professional, personal, and family schedules. I always knew I wanted to finish my dissertation and the research that I had started so many years ago.

I have always enjoyed academia, i.e., research, writing, presenting, and publishing. Although classified as a non-traditional graduate student, I started a niche hydrometeorologic business that is grounded on academic philosophies and methods I learned though my Masters and PhD experiences. The academic process and interactions with colleagues in my professional career where a large motivation for me to finish what I had started many years ago.

In my professional career, I apply scientific methods to operational research problems, identify methods, collect data, analyze data, publish results, and implement results that benefit hydrometeorologic communities and critical design infrastructure. This dissertation is an extension of my professional career, focused on quantifying spatial and temporal characteristics of extreme precipitation events, probable maximum precipitation, problem maximum snowfall, climate change, uncertainty analysis, and precipitation frequency analysis for federal, state, and local entities. As part of my working profession, I have had the honor to work closely with

numerous colleagues in federal agencies (NWS, HDSC, NOAA, FERC, NRC, ORNL, USACE, BIA, USGS, NRCS, USDA), all States Dam Safety programs, with State Climatologists (CO, NM, PA, NJ, LA, MA, NY, VI), and academia (LSU, CSU, TSU, Penn State).

Although classified as a non-traditional graduate student, I have academics infused within me through both graduate school and my career. These are being used to build and contribute new knowledge in the field of water resources through research, writing, presenting, and publishing. A fundamental finding that I have discovered about myself through this endeavor is that I enjoy academia, the structure, and the application of scientific processes in my professional and personal life.